Summer 2017

Mechanobiology of keratinocyte aggregate formation and its role in wound healing

Hoda Zarkoob
University of Iowa

Mechanobiology of Keratinocyte Aggregate Formation and Its Role in Wound Healing

by

Hoda Zarkoob

A thesis submitted in partial fulfillment
of the requirements for the Doctor of Philosophy
degree in Biomedical Engineering in the
Graduate College of
The University of Iowa

August 2017

Thesis Supervisor: Associate Professor Edward A. Sander

Graduate College
The University of Iowa
Iowa City, Iowa

CERTIFICATE OF APPROVAL

PH.D. THESIS

This is to certify that the Ph.D. thesis of

Hoda Zarkoob

has been approved by the Examining Committee for
the thesis requirement for the Doctor of Philosophy degree
in Biomedical Engineering at the August 2017 graduation.

Thesis Committee: _____
Edward A. Sander, Thesis Supervisor

_____
Michael Mackey

_____
John C. Selby

_____
M.L. Raghavan

_____
James Ankrum

TO MY BELOVED

PARENTS,

AND MY LOVELY HUSBAND

ACKNOWLEDGEMENTS

I would like to express my special gratitude and thanks to my advisor, Dr. Edward A. Sander for his guidance, support and imparting his knowledge and expertise in this study. I am also grateful to my committee members and co-authors for their valuable suggestions.

I would like to thank Dr. John Selby and Dr. Sathivel Chinnathambi for sharing their knowledge and insightful discussions on this work. Special thanks also go to all my lab mates for providing a friendly and supportive atmosphere.

I would like to extend my deepest gratitude to my father, mother, sister, and brothers, for their continued love, support, encouragement, and immense presence in my everyday life despite being far away around the world.

I am so grateful to a very special person, my dear husband, Hossein for his continued and unfailing love and support.

ABSTRACT

Wound healing is an intrinsic response to injury or disease that generally results in scarring. In skin, restoration of the barrier function after wounding is critically dependent on re-epithelialization. During re-epithelialization keratinocytes from the wound margin migrate over the wound bed, proliferate and re-differentiate to make an intact epidermis. Mechanical cues may play an important role in epidermal sheet formation and re-epithelization.

Here, polyacrylamide (PA) gels with tunable stiffness were used to study the potential contribution of mechanical properties of the wound bed in re-epithelialization. Live cell imaging and deformation tracking microscopy was performed on primary human keratinocytes maintained on soft (1.2 kPa) and stiff (24 kPa) PA gel substrates. The results of this study indicated that the formation of keratinocyte aggregates was significantly different on soft versus stiff polyacrylamide gels, with smaller spread contact area, increased migration velocities, increased rates of aggregate formation, and more cells per aggregate for keratinocytes cultured on soft gels versus stiff gels, respectively. The differences may be due to cell–cell mechanical signaling generated via local substrate deformations in the underlying substrate. These deformations were substantially larger for soft gels.

Broad-spectrum proteomics was performed to investigate which proteins were expressed differentially on soft and stiff PA gels. Protein lysates from soft and stiff samples were analyzed by LC-MS/MS (Q-Exactive). Expression of 56 proteins differed significantly between keratinocytes on soft and stiff substrate samples. The presence of serotransferrin, one of the most prominent protein candidate presented higher in the soft

samples, was confirmed using western blot. Further analysis needs to be conducted to investigate the rest of protein candidate in proteomics results.

The PA gel system was then used to explore the role that keratin intermediate filaments play in mechanosensing and force generation. Knock-out mouse keratinocytes that were missing certain keratins and their corresponding wild type controls demonstrated differences. Knock-outs were less spread out, had impaired actin formation, could not deform the substrate, and hardly made aggregates on soft substrates. These results revealed the importance of keratin intermediate filaments in keratinocyte mechanobiology.

In order to characterize keratinocyte mechanosensing, a needle was used to make controlled local mechanical deformations in soft PA gels in a defined distance from isolated single cells. Keratinocytes responded to needle-induced substrate displacements by changing direction, and migrating towards the needle. The inhibitors, Y27632 and blebbistatin were used to inhibit Rho kinase and myosin phosphorylation. Both Y27632 and blebbistatin impaired directed migration toward the needle.

Together my results reveal new insights on keratinocytes mechanobiology, which could help in the development of novel healing strategies.

PUBLIC ABSTRACT

A critical part of the cutaneous wound healing involves the re-establishment of the epidermis. During re-epithelialization, keratinocytes migrate across the wound bed to restore the epithelium. Although the process of re-epithelialization has been well-characterized, particularly in terms of biochemical factors, the role that mechanical factors play in this process remains unclear. I hypothesis that mechanical cues in the wound bed are important part of the re-epithelialization process. Here, I report on my investigation into this matter. My results indicated that substrate stiffness regulates keratinocytes morphology, migration speed, and the rate of aggregate formation. My results also highlighted the importance of keratin intermediate filaments in keratinocyte mechanobiological behavior. In addition, I found that keratinocytes are able to sense and respond to local mechanical deformations applied to the substrate. Together my results reveal new insights on mechanobiology of keratinocytes re-epithelialization.

TABLE OF CONTENTS

LIST OF TABLES

LIST OF FIGURES

NOMENCLATURE

APS	Ammonium persulfate
C-AM	Chloroacetamide
CHAPS	Dimethyl[3-(propyl]. azaniumyl}propane-1-sulfonate
DDA	Data dependent acquisition
DIC	Digital Image Correlation
DIC	Differential Interference Contrast
DR	Distance Rank
ECM	Extracellular Matrix
ERK	Extracellular-signal-related kinase
ESI	Electrospray ionization
FA	Formic acid
FAK	Focal Adhesion Kinase
HCD	Higher energy C-trap dissociation
HEKn	Human Epidermal Keratinocytes, neonetal
IF	Intermediate Filament
KO	Knock out
KSFM	Keratinocyte Serum Free Medium
LC-MS/MS	Liquid chromatography tandem mass spectrometry
LIMK	LIM Kinases
m/z	Mass-to-charge ratio; m = mass, z = charge

MAPK	Mitogen-activated Protein Kinase
MLC	Myosin Light Chain
MLC2	Myosin regulatory Light Chains
MPA	Mobile phase A
MPB	Mobile phase B
MS	Mass spectrum/Mass spectrometer
MS/MS (MS^2)	Tandem mass spectrum
MSC	Mesenchymal Stem Cell
MYPT1	Myosin Phosphatase Target subunit 1
PA	Polyacrylamide
PBS	Phosphate Buffered Saline
Q-Exactive	Hybrid quadrupole Orbitrap mass spectrometer
RC	Radius of Cooperativity
rCE	Relative collision energy
SDC	Sodium deoxycholate
SDS	Sodium dodecyl sulfate
SDS-PAGE	Sodium dodecyl sulfate polyacrylamide gel electrophoresis
TAZ	Transcriptional co-activator with PDZ-binding motif
TEAB	Triethyl ammonium bicarbonate
TECP	tris(2-carboxyethyl)phosphine
TFM	Traction Force Microscopy
TMT	Tandem Mass Tagging

w/v	Weight-to-volume ratio
WT	Wilde Type
YAP	Yes-associated Protein

Chapter I. INTRODUCTION

1.1 INTRODUCTION

Wound healing is an intrinsic response to injury or disease that generally results in scarring. It is estimated that $6.7 billion U.S. dollars is spent annually worldwide on wound care, and $4 billion in the U.S. alone on reducing scarring [1, 2]. Wound healing is a central part of any surgical procedures, as well as many injury/disease treatments. However, no clear strategies exist for optimizing the wound healing process and reducing scar. In cutaneous wound healing, restoration of the barrier function of skin is critically dependent on re-epithelialization. Here, keratinocytes are activated and migrate over the wound bed before differentiating and restoring an intact epithelium. Aberrant or delayed re-epithelialization observed in many different types of chronic wounds, like diabetic ulcers, not only increases the risk of infection and patient morbidity, but also correlates strongly with the severity of scarring [2, 3].

Different chemical and physical gradients direct cell migration in re-epithelialization. Until recently, the regulation of these processes were largely understood in terms of biochemical signals, but recent interest in the mechanobiology of tissues suggests that physical forces and mechanical cues from the wound bed may also play an important role in the healing process [4]. The dynamic evolving structure of the wound bed during the wound healing phases [5] further lead us to the possibility of the effect of mechanical properties of the wound bed in regulating re-epithelialization.

Mechanical properties of the wound bed could also play an important role in delayed re-epithelialization of chronic wounds, especially since a common feature of chronic wounds is a sclerotic, or stiffened, dermal extracellular matrix (ECM) present at the margins of wound bed [6, 7].

The central hypothesis of this thesis is that the mechanobiology of the wound site controls the rate and extent of re-epithelialization. Should this hypothesis hold true, then it follows that a greater understanding of this mechanobiology should allow one to design novel therapeutic interventions that could accelerate wound re-epithelialization and reduce scarring. These ideas could be particularly beneficial to the growing incidence of chronic wounds.

1.2 BACKGROUND INFORMATION

1.2.1 Skin Structure

Skin is the largest organ. It is critical to thermoregulation, fluid homeostasis, and immune surveillance. Human skin has two major layers: the dermis and epidermis (Figure 1). The dermis consists mainly of dense irregular connective tissue, composed primary of collagen I, type III, elastin and extrafibrillar matrix [8]. Fibroblasts, machrophages, and adipocytes are the three major cell types in the dermis. Fibroblasts are responsible for continued synthesis, degradation, and remodeling of extracellular matrix (ECM) [9]. The dermis is tightly connected to the epidermis through a basement membrane [10].

The epidermis is the outer most layer of the skin. It is a multi-layered structure consisting of a proliferative basal layer and several distinctive upper layers of differentiated keratinocytes at various stages of stratification [9]. The cells within and between layers are connected to each other via anchoring junctions called desmosomes and adherens junctions. Desmosomes connect to keratin intermediate filaments and adherans junctions connect to actin microfilaments. Both filaments are part of the cell cytoskeleton. The basal layer of keratinocytes also possesses keratin and actin connected to cell-matrix anchoring

junctions called hemidesmosmes and focal adhesions, respectively. Many of the blistering skin diseases, such as epidermolysis bullosa simplex, are caused by deficiencies in these anchoring junctions [9].

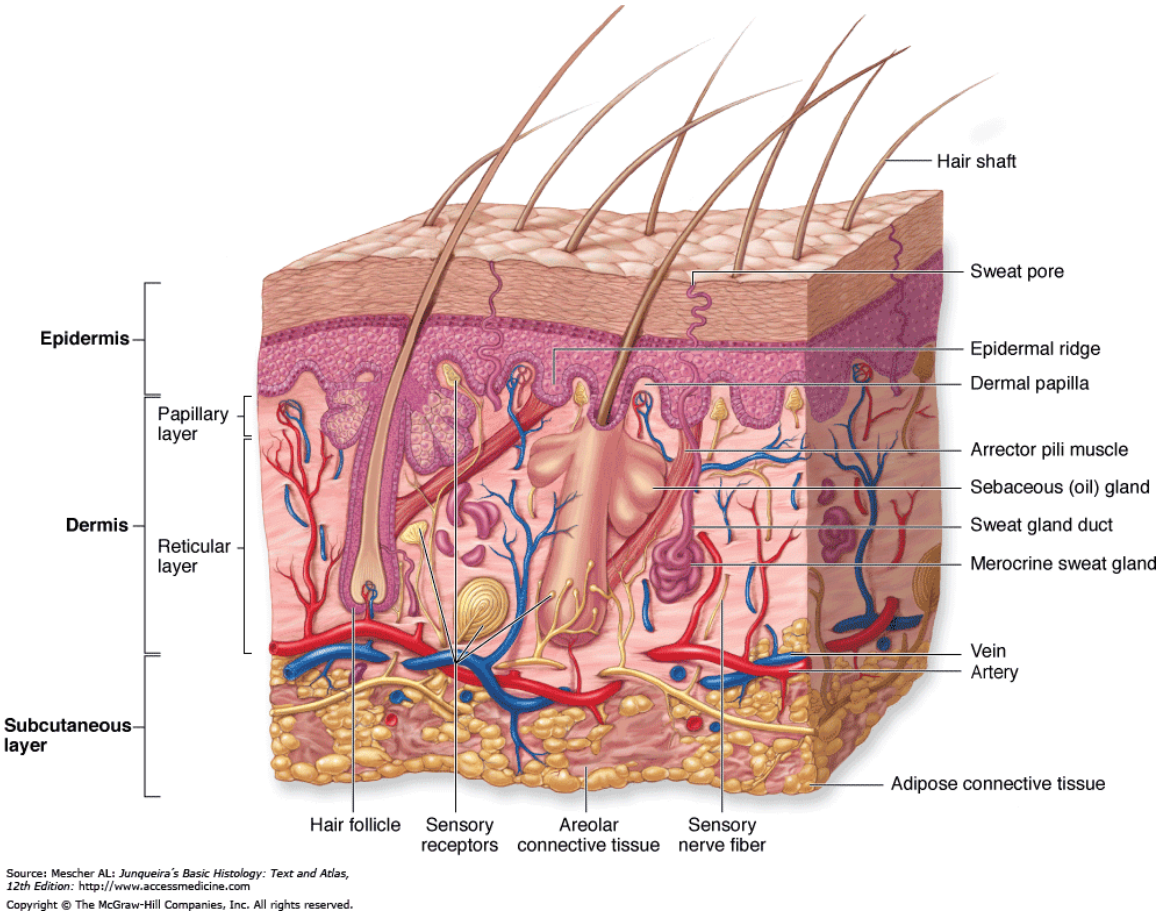

Figure 1. Skin anatomy [11]

1.2.2 Wound Healing

As soon as the skin injured several biochemical cascades are triggered to initiate the healing process. Wound healing happens in three over-lapping phases: 1) hemostasis and inflammation, 2) tissue formation (proliferation) and 3) maturation or remodeling [5] (Figure 2). Blood leakage into the wound bed after injury provides vasoactive factors, which trigger the activation of the clotting cascade [12]. The contact between collagen and platelets and the presence of thrombin and fibronectin induces the local release of cytokines

and growth factors, which in turn activate cells to migrate to the area of injury. In addition, a fibrin cloth forms that serves as a scaffold for invading cells, such as neutrophils, fibroblasts, and endothelial cells. The fibroblasts migrate into the wound, differentiate into myofibroblast and produce ECM proteins and contract the cloth. Myofibroblasts phenotypically are between fibroblast and smooth muscle cells. Unlike fibroblast, they express α-smooth muscle actin [13, 14]. Myofibroblasts are also distinctive from fibroblast because of their extensive cell-matrix adhesions, abundant intercellular adherents and gap junctions and bundles of stress fibers [15-17]. Although myofibroblast contraction has a beneficial effect in wound healing by narrowing the wound margin, excessive contraction causes the formation of undesirable contracture and scarring [18].

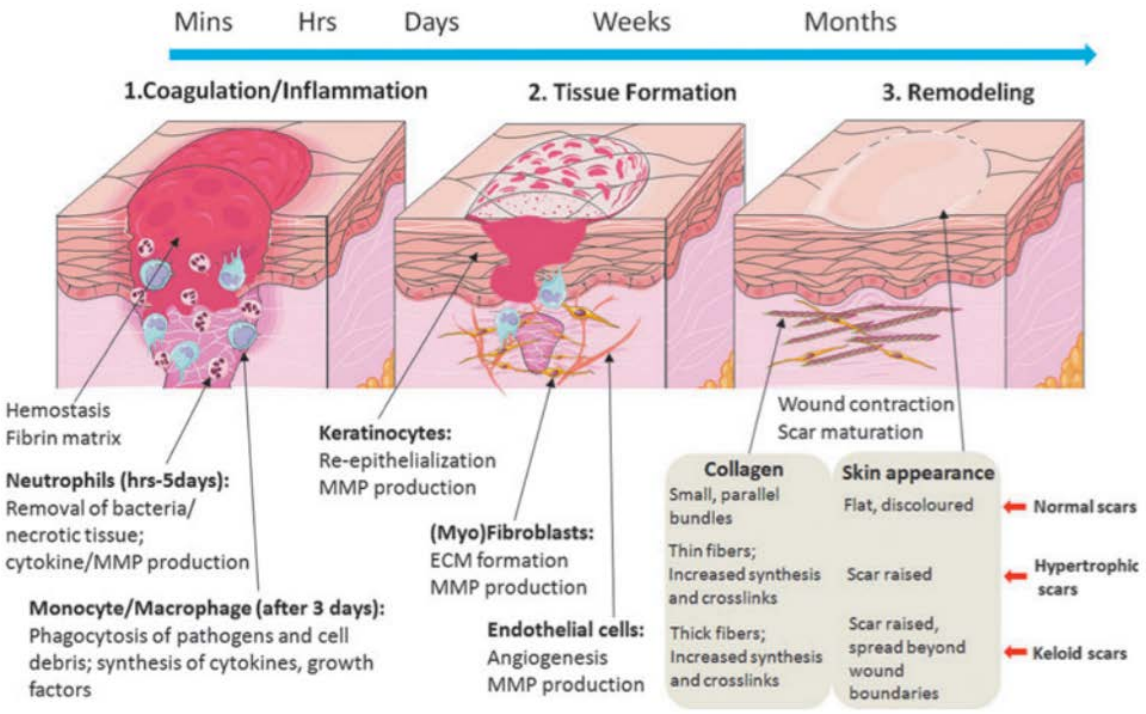

Figure 2. Three stages of wound healing [19]

A few hours after injury, keratinocytes also start to proliferate and migrate into the wound bed from wound edge or either from uninjured epithelial islands within the wound

[5], [2, 3, 20]. The re-epithelialization process primarily re-establishes the barrier function of epidermis [2, 3, 20].

The deposition of the collagen in the wound occurs in the maturation and remodeling phase. However, the composition of the wound changes dynamically over the three phases of wound healing. In early stages, it is predominantly composed of fibrin, fibronectin and thormbospondin I [21, 22]. Subsequently collagen becomes the predominant scar protein [5]. The granulation tissue possess about 30 % type III collagen, whereas in the mature scar type III collagen decrease to 10% [23-25].

The structure of the collagen matrix also changes with time. Collagen in normal dermis has a basket weave-like pattern, whereas in the scar thinner collagen fibers are arranged parallel to the skin [5]. These thinner collagen fibers gradually thicken after wounding and organize along the stress lines of the wound concurrent with the increase in the tensile strength of the wound [26]. The wound has just 3% of its final strength after the first week [24], and 20% after the 3 weeks [27]. After 3 months it regains approximately 80% of the strength of unwounded skin, with no further increase thereafter [27]. Along with strength, the stiffness of the wound bed also changes over time. It has been reported that the elastic modulus of the granulation tissue from a rat increased from 18.5 kPa on day seven to 29.4 kPa on day nine post-wounding [28]. No comparable data appears to exist for human wounds.

1.2.3 Mechanical Interaction of Cells with Their Substrate

The mechanical interplay between a cell and a substrate has been shown to be an essential regulator of many important cellular processes, including cell shape, migration, and differentiation [29-32]. For example, in a seminal study by Engler *et al.*, it was found

that modulating the stiffness of polyacrylamide (PA) gels induced mesenchymal stem cells (MSCs) to display phenotypic markers associated with the cells that inhabit tissues of comparable stiffness. Specifically, soft gels produced neuronal markers, intermediate gels produced skeletal muscle markers, and stiff gels produced bone markers on the MSCs [33]. Recently, several studies have shown substrate-stiffness-dependent behaviors in epithelial cells that affect their proliferation, migration, and differentiation [29, 30, 32, 34].

As the substrate stiffness increases, cell spread area and cell traction forces exerted on the substrate typically increase [31, 35-37]. For example, it was reported that fibroblasts on stiff substrate generate more stress fibers compared to fibroblasts on soft substrate [38].

How cells sense the substrate stiffness and how they translate it into cellular signals remains poorly understood. Recently, the importance of integrin-mediated components for mechanosensing has emerged [39]. Cells interact mechanically with their substrates through integrins [40]. Integrins are the main transmembrane receptors for ECM proteins. They connect the ECM to the cell's cytoskeleton, specifically via the actin microfilaments. An increase in substrate stiffness recruits more integrin proteins to the site of adhesion, which in turn activates more focal adhesion kinase (FAK). The increase in FAK activity also stimulates the Rho/ROCK (Rho kinase) pathway. Rho is a family of small GTPases that activate Rho kinase (ROCK), which in turn regulates myosin light chain (MLC) phosphorylation. Phosphorylated MLC is necessary for engagement of actomyosin generated intracellular tension [41].

Rho/ROCK, and actin microfilaments seem to play important role in cell mechanobiology [42, 43]. Intermediate filaments (IFs) are also known to play an important role in the mechanics of epithelial sheets [9]. For keratinocytes, the primary intermediate

filaments of interest are the keratins. Keratins consist of heterotypic pairs of type I (K9–28) and type II (K1–K8 and K71–K80) keratin chains that connect the cytoskeleton to other cells through desmosomes or to the ECM through hemidesmosomes. Their principal function is thought to be mechanical in that they provide mechanical support to the cell and that they maintain the integrity of the epidermis and dermal-epidermal junction [9]. Keratins may also play an important role in other mechanical contexts similar to those of actin filaments, but the potential for this functionality remains under explored. Some recent reports in the literature suggest that there is communication between focal adhesions and hemidesmosomes [44-46]. Of particular interest, is the potential mechanosensing role of the hemidesmosome integrin protein, α6β4, which is canonically linked to keratin IFs [32, 47-49]. This protein appears to be a key regulator of keratinocyte migration in re-epithelialization, as well as in the invasion of carcinoma cells [48-51]. The potential association of this integrin with actin filaments has also been suggested [45, 50, 52].

Other mechnosensitive proteins and pathways may be involved in cell fate decisions and keratinocyte differentiation including mitogen-activated protein kinase (MAPK)/extracellular-signal-related kinase (ERK) [29], and Hippo pathway/YAP-TAZ [53]. There is also evidence that Src/p130Cas [39, 54] plays a role in keratinocytes mechanosensing as well [55].

1.2.4 Traction Force Microscopy

Various methods have been developed to measure cell traction forces for both single cells and multiple cells, including cell-populated collagen gels [56], substrate wrinkling [57], and micro pillar arrays [58]. The most commonly used technique is cell traction force microscopy (CTFM) [59]. It is among the most efficient and reliable methods

for measuring traction forces in 2D [60]. The basic idea for CTFM, suggested by Dembo and Wang (1999), is to measure substrate displacements by tracking fluorescent beads embedded in a linear elastic substrate. With knowledge of the substrates material properties, the traction force required to deform the substrate can be estimated [59, 61].

The elastic material that has been widely used for CTFM, is polyacrylamide gel (PA). PA gel is a synthetic polymer which formed tunable elastic gels. It has been reported that cells can sense long distances through the thickness of the gel, such that a rigid substrate underneath a PA gel could the effective stiffness that a cell senses [62]. According to Maskarinec *et al.* study, having a 100 μm thick polyacrylamide layer is enough to ensure that the substrate does alter the perceived stiffness of the gel [63]. PA gels are also commonly used to characterize relationships between cell traction forces and substrate stiffness because their mechanical properties can easily be manipulated, and the gels can be covalently coated with various ECM proteins. The method of preparing PA gel is discussed in Wang and Pelham [64]. To conduct CTFM the displacement field of the substrate is computed by comparing the spatial configuration of embedded fluorescent beads in images taken while the cell is attached to the substrate (i.e., the "force-loaded" image) and when the cell is detached (i.e., the "null force" image). Digital Image Correlation (DIC) techniques are often used in order to find the correlation between "null force" and "force-loaded" images [32, 65] (Figure 3). To compute the displacements of each point in null force image, a square subset of pixels centered at the desired point is chosen and cross-correlated to the adjacent locations in the force-loaded image. The matching procedure is completed by searching for the location of the peak of the correlation coefficient distribution. This peak corresponds to the local displacement [65].

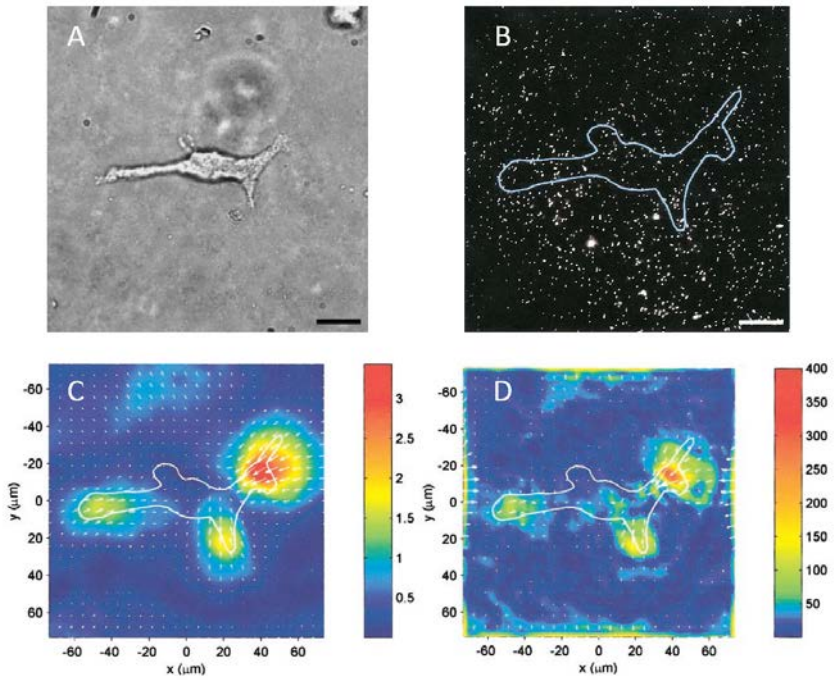

Figure 3. Traction Force Microscopy, A) The phase contrast image of a cell attached to PA gel substrate, B) Fluorescent image if the same field of view as in A, The displacement field computed from the 2 fluorescence images, force-loaded and null-force, D) The traction field computed from the displacement field. Scale bar, 20μm [66]

Once the displacement field is obtained, the traction forces are determined using either the Boussinesq solution [59, 61, 66], inverse finite element methods [63, 67], or through other means.

1.3 THESIS HYPOTHESIS

The central hypothesis of this thesis is that the mechanobiology of the wound site controls the rate and extent of re-epithelialization. In order to test this hypothesis, I produced an experimental platform that provides flexibility for modifying the various mechanical attributes of the substrate and allows for quantification of keratinocyte behavior in response to these mechanobiological cues. I used this system to accomplish the following specific aims:

Aim 1: Test the hypothesis that keratinocyte aggregate formation is dependent on substrate stiffness using PA gels. Keratinocyte behaviors, such as migration speed, aggregate formation, and cytoskeletal structure and the formation of anchoring junctions will be assessed over a 24-hour period on soft and stiff gels.

Aim 2: Identify proteins and genes that change due to substrate stiffness, by repeating the same keratinocyte aggregate formation experiments in Aim 1, in order to detect the proteins involved in keratinocytes mechanotransductive pathways.

Aim 3: Test the hypothesis that keratin intermediate filaments play an essential role in controlling keratinocyte mechanosensing and aggregate formation by repeating Aim 1 with wild-type and keratin-muted keratinocytes. The role of keratin intermediate filaments on keratinocyte mechanosensing will be investigated using mouse keratin-free knock out and wild-type keratinocytes using similar methods as in Aim 1. Keratinocytes aggregates will also be investigated in order to further ascertain the role keratin filaments play in force generation and aggregate formation.

Aim 4: Investigate the response of keratinocytes to local mechanical perturbation. Apply different drugs to inhibit various parts of the Rho/ROCK mechanosignaling pathway and to determine the cells response to local mechanical deformations.

Successful completion of these aims will improve our understanding of the role of mechanobiology in wound healing. In addition, it will give us new insights to the mechanobiology of cell-ECM interactions, cell-cell mechanical signaling, and their connection with Rho/ROCK pathway during keratinocyte migration and aggregate formation.

Chapter II. SUBSTRATE STIFFNESS AFFECTS HUMAN KERATINOCYTE AGGREGATE FORMATION

(The content of this chapter is published in ref. [32] with “Substrate Stiffness Affects Human Keratinocyte Colony Formation” title)

2.1 INTRODUCTION

The human epidermis, composed of its principle cell type, the keratinocyte, plays an important role in the barrier function of skin, essential to the physiologic processes of water homeostasis, photoprotection from UV-induced damage, and immune surveillance [68]. Central to its biomechanical function, the epidermis is endowed with the ability to regenerate following a variety of different pathophysiological insults. Keratinocyte migration, proliferation, and stratification during the process of wound healing represent the body's attempt to restore the complex organization and function of the tissue [69, 70]. This organization is critically dependent on the arrangement of interconnecting desmosomes, adherens junctions, focal adhesions, hemidesmosomes, and transcellular intermediate filament networks. These and other cytoskeletal proteins are responsible for the biomechanical properties of the epidermis. Coupled with fibroblast-mediated repair and reorganization of the dermal extracellular matrix (ECM), investigations focused on enhancing our understanding of the mechanobiological process of wound healing represent an important and ongoing topic of active research.

Under normal physiologic conditions *in vivo*, keratinocytes at the wound margins must form cell-matrix adhesions in order to migrate, proliferate, and reform a continuous epithelial barrier spanning the zone of damaged tissue. The extracellular matrix (ECM) that keratinocytes are in contact with throughout this process – clinically referred to as granulation tissue – is dynamic in both composition and structure. By necessity, the ability of keratinocytes to sense and respond to changes in such a dynamic mechanical environment must play an integral role in the process of wound healing and the structure-function relationships that develop within the epidermis post-tissue repair [71]. Past works

have shown that keratinocyte force generation, morphology, migration, and differentiation *in vitro* can be modulated via changes in the elasticity (or stiffness) of the culture substrate, geometric constraints on cell shape and spreading, the physical dimensionality of the culture system (2D versus 3D), and the biochemical specificity of extracellular matrix proteins available for the formation of adhesive contacts [29, 72-75].

More recently, researchers have explored the mechanobiology of monolayer epithelial sheets via traction force microscopy experiments that probe the migratory behaviors of Madin-Darby canine kidney epithelial cells during the attempted closure of geometrically prescribed defects both internal and external to the boundaries of the monolayer [76-78]. As a fiducial model of epithelial sheet mechanics, these studies provide novel insight into the potential behavior of keratinocytes within the context of wound healing. Collectively, however, these studies are focused on the movements of a monolayer epithelial sheet, and not the behaviors of individual cells during the initial formation of the sheet. Although not universally recognized as a mechanism of re-epithelialization, it is conceivable that individual keratinocyte migration, proliferation, and aggregate formation may play a role in the re-epithelialization of large wounds *in vivo*. Moreover, individual keratinocyte migration, proliferation, and aggregate formation may also represent the primary mechanism by which liquid spray-applied keratinocyte cell-based therapies contribute to the enhanced re-epithelialization of chronic human venous ulcers observed in some clinical trials [79, 80]. Arguably, experiments that assay the migration, proliferation, and differentiation of individual keratinocytes during the process of re-epithelialization will not only increase our understanding of the physiology of wound healing, but they will also aid in the development and optimization of cell-based wound care therapies of the future.

Towards this end, the purpose of this study was to investigate the role of substrate elasticity (stiffness) on keratinocyte aggregate formation *in vitro* during the process of nascent epithelial sheet formation as triggered by the calcium switch model of keratinocyte culture [81-83]. In this culture model, normal epidermal keratinocytes maintained in a proliferative monolayer state under low calcium concentrations (0.05-0.1 mM) are induced to form stable cell-cell junctions and stratify by increasing the calcium concentration of the culture media (1.2-1.8 mM). Using a combination of time-lapse differential interference contrast microscopy and substrate displacement tracking microscopy, I monitored cell migration characteristics, rates of aggregate formation, cytoskeleton/cell morphology, and cell-generated substrate deformations for keratinocytes cultured on both soft (nominal 1.2 kPa) and stiff (nominal 24 kPa) polyacrylamide (PA) gels coated with covalently attached pepsin digested type I collagen and embedded with fluorescent microspheres, before, during, and after a calcium switch. In these experiments, keratinocytes cultured on soft PA gels migrated at increased velocities, produced substantially larger substrate displacements, and colonized faster via more cooperative cellular behaviors than did keratinocytes cultured on stiff PA gels. I hypothesize that the differences in aggregate formation observed in these experiments could be due to durotactic cell-cell signaling generated via local substrate deformations which appear to correlate with the increased expression of β4 integrin within keratinocytes positioned along the periphery of the evolving cell aggregate.

2.2 MATERIAL AND METHODS

2.2.1 Cell Culture

Neonatal human epidermal keratinocytes (HEKn) (Invitrogen, Carlsbad, CA) were cultured in keratinocyte serum free medium (KSFM) (Invitrogen) supplemented with 1%

penicillin–streptomycin and 0.1% amphotericin-B in a humidified incubator maintained at 37 °C and 95%/5% air/CO_2. The baseline concentration of calcium in this supplemented medium is 0.09 mM, designated here as Low Ca^{2+} medium. High Ca^{2+} medium, with a calcium concentration of 1.2 mM, was created by adding $CaCl_2$ to KSFM medium supplemented with penicillin-streptomycin and amphotericin-B as noted above. HEKn were initially plated and passaged in Low Ca^{2+} medium using standard tissue culture polystyrene flasks. Passage 3 keratinocytes were used for all experiments.

2.2.2 Polyacrylamide Gels

The polyacrylamide (PA) gels used in these experiments were prepared using a modified version of the protocol described by Pelham and Wang [31]. Briefly, glass coverslips (40-mm circular No. 1½, Warner Instruments, Hamden, CT, and 12-mm circular No. 1, Fisher brand, Fischer Scientific, Pittsburgh, PA) were cleaned and etched with a 50:50 hydrochloric acid and methanol solution [84]. 40 mm coverslips were used for time-lapse imaging experiments and 12 mm coverslips were used for immunofluorescence studies. After washing, coverslips were activated with 0.1 N sodium hydroxide (Fisher Scientific), 100% 3-aminopropyltrimethyoxysilane (Sigma-Aldrich, St. Louis, MO), and 0.5% glutaraldehyde (Fisher Scientific). To fabricate either a soft or stiff PA gel, respectively, I combined 250 µL and 625 µL or 940 µL and 750 µL of acrylamide and bis-acrylamide using stock solutions of acrylamide monomer (40% w/v, Bio-Rad, Hercules, CA) and bis-acrylamide (2% w/v, Fisher Scientific) that had been passed through a 0.2 µm filter. In a separate mixture, I added 100 µL of 0.5 µm diameter fluorescent microspheres (FluoSpheres® Ex/Em 580/605 nm, Life Technologies, Grand Island, NY), to either 3,392.5 µL (soft gels) or 3,180 µL (stiff gels) of deionized water, sonicating each

solution for 15 minutes. The microsphere solutions were then added to their respective soft or stiff acrylamide/bis-acrylamide mixtures. Using a vortex mixer, I then added 7.5 µl of N,N,N',N' tetramethylethylenediamine (TEMED) (Fisher Scientific) to each acrylamide/bis-acrylamide/microsphere solution, immediately followed by a 15 minute vacuum degas. Finally, 25 µL of 10% ammonium persulfate (APS) (Fisher Scientific) was added to each acrylamide/bis-acrylamide/microsphere/TEMED solution in order to initiate polymerization. For my time-lapse imaging experiments, 20 µL of either fully combined acrylamide/bis-acrylamide/microsphere/TEMED/APS solution was pipetted onto the surface of an inactivated Rain-X (ITW Global Brands, Houston, TX) treated glass microscope slide cut to measure 15 mm x 15 mm. An activated 40 mm cover glass slip was then placed on top of the liquid bead, in effect forming a thin liquid film between the microscope slide and cover glass. My immunofluorescence specimens were prepared in a similar fashion, using 10 µL of either fully combined acrylamide/bis-acrylamide/microsphere/TEMED/APS solution, an uncut but inactivated Rain-X treated glass microscope slide, and activated 12 mm coverslips. After allowing the samples to polymerize for 15 minutes at room temperature, the Rain-X treated coverslips were removed. The resultant time-lapse and immunofluorescence specimens consisted of approximately 60-100 µm thick PA gels incorporated with fluorescent microspheres predominantly localized to the free surface of the gel. Upon completion of this initial fabrication sequence, all PA gel specimens were washed with phosphate buffered saline (PBS) and placed in sterile deionized water overnight on an orbital shaker to remove any unreacted residual acrylamide and bis-acrylamide.

In order to facilitate keratinocyte attachment for my calcium switch experiments, pepsin digested type I collagen was covalently attached to the surface of both soft and stiff PA gels using a protocol modified from Pelham and Wang [31]. Briefly, sulfosuccinimidyl 6 (4-azido-2-nitrophenyl-amino) hexanoate (sulfo-SANPAH) (Thermo Scientific, Waltham, MA) was dissolved in DMSO (0.25 w/v) and then diluted in 50 mM 4-(2-hydroxyethyl)-1-piperazineethanesulfonic acid (HEPES) (adjusted to pH = 8.5) to a final concentration of 0.2% v/v. The solution was added to the surface of each PA gel and placed under a UV light (Lamp XX-20BLB; 365 nm, 115 V, 20 W, Fisher Scientific) for five minutes. Samples were then washed with HEPES and a fresh mixture of sulfo-SANPAH and HEPES was added to the gel surface. Samples were then exposed to UV light for an additional five minutes. After a final HEPES wash, 100 µg/ml of pepsin digested type 1 collagen (PureCol® Advanced Biomatrix, San Diego, CA) was added to the surface of each PA gel and allowed to incubate at room temperature for two hours. Unbound collagen was removed by rinsing the gels with PBS. PA gel substrates were sterilized under UV light (254 nm) in the biosafety cabinet for 15 minutes prior to initiating cell culture. Though not directly measured, the nominal moduli for the soft and stiff PA gels used in this work were assumed to be 1.2 kPa and 24 kPa, respectively, as my gel formulations were nearly identical to those measured previously [66, 85].

2.2.3 Time-Lapse Live Cell Imaging

Time-lapse live cell images were acquired with a Nikon Eclipse Ti inverted microscope equipped with a perfect focus system, wide-field epifluorescence and differential interference contrast (DIC) microscopy capabilities, a DS-Qi1 Nikon CCD camera, and a ProScan II motorized stage, all driven by NIS Elements software. DIC

images for my cell tracking, counting, and classification analyses were obtained with a CFI Plan Apo 10x DIC objective (NA=0.45), as were the fluorescent images used in my substrate deformation tracking analysis (cf. Section 2.6). Inside the biosafety cabinet, a PA gel was placed in a temperature-controlled perfusion chamber (RC-31A, Warner Instruments). The keratinocytes were then plated onto the gel at a density of 4,000 cells/cm^2 in Low Ca^{2+} medium (cf. Section 2.1). Within 15 minutes, the chamber was mounted onto the microscope stage, the temperature was stabilized at 37 °C, and time-lapse imaging was initiated. Keratinocytes were allowed to attach and reach a relative equilibrium for three hours before the calcium concentration of the medium was increased from Low Ca^{2+} to High Ca^{2+} via a syringe pump attached to the chamber. High Ca^{2+} medium was introduced to the chamber at a rate of 0.02 ml/min. The moment that the syringe pump was activated was designated as t = 0. The syringe pump was turned off at t = 50 minutes to ensure that at least two volume changes of the medium had occurred within the chamber. Time-lapse images were collected for a total of 24 hours, after which, the experiment was terminated via introduction of trypsin to the perfusion chamber. For each discrete observation time, t, DIC and fluorescent (Ex/Em 545/620 nm) image pairs were acquired at four overlapping visual fields on the PA gel. Of these four fields, the field with a keratinocyte count closest to 30 cells at time t = 0 was selected for use in the data analyses detailed in sections 2.4, 2.5, and 2.6. The time interval between images in my experiments was set at two minutes as a compromise between the need to minimize the keratinocytes' exposure to light (i.e., phototoxicity) and the need to minimize microsphere displacement tracking errors arising from large microsphere movements between subsequent image pairs. To ensure repeatability, three replicate experiments were performed on each type of PA gel substrate

(n = 3 soft gels, n = 3 stiff gels). In addition, in order to provide some context for keratinocyte behavior in the absence of High Ca^{2+} medium, the experiment was repeated once on each substrate (n = 1 soft gel, n = 1 stiff gel) with exactly the same conditions except that Low Ca^{2+} medium was perfused through the chamber (starting at t = 0) instead of High Ca^{2+} medium.

2.2.4 Cell Classification and Counting

In order to differentiate between single cell and collective cell behaviors, keratinocytes observed in each acquired DIC image were classified as belonging to one of three groups: (i) single cells- individual keratinocytes lacking definitive cellular contacts along the entire periphery of its cell membrane; (ii) cell couples- two juxtaposed keratinocytes with a definitive area of mechanical contact formed by the apposition of their respective cell membranes; and (iii) aggregates- three or more juxtaposed keratinocytes with multiple definitive areas of contact formed by the apposition of their respective cell membranes. In this classification scheme, cell couples were distinguished from aggregates due to the possibility that cell couples could represent either a dividing cell or a transient cell-cell contact. The number of single cells, cell couples, and aggregates were counted at every hour of the experiment. Regardless of their would-be classification, keratinocytes intersecting the border of each DIC image were excluded from the counts due to the uncertain presence of cell-cell contacts outside the field of view.

2.2.5 Cell Tracking

Cell migration was hand-tracked using the Manual Tracking plugin for ImageJ (National Institutes of Health, Bethesda, MD). The migratory path of a single keratinocyte i at time t in a DIC image was determined by clicking on the center of the cell nucleus and

following it frame-by-frame until the cell reached the border of the field of view or until the keratinocyte joined a cell pair or aggregate. In this manner, an array of position vectors was created for the tracked keratinocyte. The process was repeated for all individual keratinocytes observed within the DIC image field. Although the time-lapse between DIC images was constant across all of my experiments, the total number of image frames counted for a given keratinocyte varied greatly, i.e., I could not control whether or not the keratinocyte being tracked remained within the field of view, nor could I control how quickly or slowly a keratinocyte being tracked joined a cell pair or aggregate.

Several parameters associated with keratinocyte migration and aggregate formation were calculated from the hand-tracked position vectors. First, the average instantaneous speed, , of cell i was calculated as, where N is total number of image frames counted for the keratinocyte being tracked, and is the instantaneous velocity vector for cell i, calculated as, where is the time-lapse interval between frames. A small number of cells (approximately 5% to 10% per frame) that left the image within the first 15 frames (i.e., 30 minutes) of the experiment were excluded from analysis in order to negate any effect the shear stress generated by the active flow of High Ca^{2+} medium into the perfusion chamber may have imposed on the initial migratory behaviors of the keratinocytes.

Second, an *ad hoc* ordinal distance rank (DR) was calculated for each single keratinocyte present in the field at time t = 0. To calculate this metric, I started with a single keratinocyte of interest at t = 0 and ranked the remaining keratinocytes in the visual field by order of the magnitude of their respective internuclear separation distances with the cell closest to the keratinocyte of interest being labeled with a rank of 1. All keratinocytes present within the field were rank ordered, regardless of whether or not they were present

as single cells, couples, or aggregates. Tracking keratinocytes forward in time, I then identified the rank of the cell that ultimately joined the original keratinocyte of interest to form a couple or aggregate. The ranking and tracking process was repeated for each single keratinocyte present within the DIC image at time t = 0.

Third, an *ad hoc* analysis I term the radius of cooperativity (RC) was calculated for each keratinocyte couple or aggregate present in my DIC images. To calculate this metric, I constructed a circle of radius, RC, centered on a keratinocyte couple or aggregate observed within the visual field. I then counted all cellular entities (single cells, couples, or aggregates) that migrated into the circle, including entities in contact with only the peripheral margin of the circle. Tracking these entities forward in time, I then calculated the percentage of entities initially localized to within the circle that ultimately joined the aggregate or couple under analysis. The calculations were repeated for each aggregate or couple formed within the DIC image during the course of the experiment.

2.2.6 Substrate Displacement Tracking

Substrate displacements generated by keratinocyte tractions on PA gels were measured by tracking the displacements of fluorescent microspheres embedded in my PA gels using a modified version of a template matching digital image correlation algorithm [65] applied to the fluorescent images collected during live time-lapse cell imaging. The algorithm, which uses normalized cross-correlation with an optimized sub-pixel displacement algorithm and local neighborhood smoothing, was applied to subsequent pairs of fluorescent microsphere images associated with times t and t-Δt. Embedded microsphere positions noted at the initialization of the experiment, i.e., just after cell seeding but prior to cell attachment, were used as the reference, or undeformed

configuration of the gel. Note that in this version of the algorithm, the sub-pixel displacements were calculated using the algorithm proposed by Chan and Nguyen [86]. All displacement tracking and visualization was done in MATLAB (Mathworks, Natick, MA). In adjunctive studies to my major time-lapse cell imaging experiments, I attempted to perform simultaneous cell tracking and counting analyses and substrate displacement tracking using a CFI Plan-Apo 20x DIC objective (NA = 0.75) combined with a 1.5x magnifier. Although the higher magnification proved useful for resolving small substrate displacements on stiff gels (cf. Section 3.2), the smaller field of view impaired my ability to conduct cell counting and tracking analyses. As a compromise, all major experiments were performed using a 10x objective (cf. Section 2.3). Lastly, note that for reasons to be discussed in Section 3.2, measured substrate displacements were not used to calculate/estimate the associated cellular tractions as is typically done in a traction force microscopy (TFM) experiment [87].

2.2.7 Immunofluorescence

In a separate but parallel set of experiments, keratinocytes were cultured in Low Ca^{2+} on both soft and stiff PA gels that were fabricated on 12 mm coverslips for immunofluorescent labeling of either actin microfilaments and E-cadherin; keratin intermediate filaments and desmoplakin; integrins β1 and β4; or involucrin. Labeling was performed in accord with protocol modified from Zamansky [81] and Selby [88]. After seeding and allowing the cells to equilibrate for three hours, the calcium levels of the culture medium were increased to High Ca^{2+} for selected specimens. At times t = 0 minutes, 1 hour, 4 hours, and 24 hours following the calcium switch, keratinocytes were removed from culture and fixed with either cold (-20 °C) methanol for 10 minutes (actin and E-

cadherin; keratin and desmoplakin) or 4% paraformaldehyde at room temperature for 1 hour (β1 and β4; involucrin). Samples in which the calcium concentration was initialized and maintained at 0.09 mM throughout culture (Low Ca^{2+}) were also removed from culture and fixed at 0 and 24 hours. Fixative was then removed and the samples were washed with PBS. Samples that were fixed with 4% paraformaldehyde were further permeablized with 0.5% Triton-X for 5 minutes and washed in PBS for 10 minutes. All samples were then blocked for 30 minutes with either 10% normal goat serum or 10% normal donkey serum and incubated at 37 °C using the following antibody combinations: (i) a 1:100 dilution of rabbit anti-cytokeratin polyclonal antibodies (#BT-571, Biomedical Technologies, Ward Hill, MA) and a 1:100 dilution of mouse anti-desmoplakin I + II monoclonal antibodies (#AB16434, Abcam); (ii) a 1:100 dilution of mouse anti-actin monoclonal antibodies (#MAB1501R, EMD Millipore, specific for both globular and filamentous actin) and a 1:100 dilution of rabbit anti-E cadherin monoclonal antibodies (#AB40772, Abcam); (iii) a 1:100 dilution of goat anti-integrin β1 polyclonal antibodies (#SC6622, Santa Cruz Biotechnology) and a 1:100 dilution of mouse anti-human CD104 (i.e., integrin β4) monoclonal antibodies (#555722, BD Pharmingen); and (iv) a 1:500 dilution of mouse anti-involucrin monoclonal antibodies (#AB68, Abcam). Anti-involucrin antibodies were allowed to incubate for 2 hours at 37 °C as opposed to the 1-hour incubation used for the other antibody combinations. Following incubation, samples were treated with a second blocking step in either 10% normal goat serum or 10% normal donkey serum for a period of 20 minutes. Finally, the coverslips were incubated for 30 minutes at 37 °C with a 1:100 dilution of the corresponding secondary antibodies: goat anti-rabbit IgG antibodies (#A-11034, Invitrogen Corporation), goat anti-mouse IgG antibodies (#A-11031, Invitrogen

Corporation), donkey anti-goat IgG H&L antibodies (#AB150129, Abcam), or donkey anti-mouse IgG antibodies (#A10036, Life Technologies). Between each step in the process, all samples were washed with PBS. Finally, coverslips were mounted onto microscope slides with Prolong® Gold Antifade Mountant with DAPI (Life Technologies) in order to visualize keratinocyte nuclei. Immunofluorescence images were acquired using a Nikon Eclipse Ti inverted microscope with a 20x CFI Plan Apo DIC objective and a 1.5x magnifier.

2.2.8 Statistical Analysis

Statistical significance ($p < 0.05$) was determined by performing either Student's t-tests when comparing two groups or analysis of variance (ANOVA) when comparing multiple groups. All statistical analysis was done in MATLAB.

2.3 RESULTS

2.3.1 Kinematics of Keratinocyte Migration and Aggregate Formation

Differences in keratinocyte behavior and aggregate formation as a function of substrate stiffness and exposure to Low Ca^{2+} (0.09 mM) and High Ca^{2+} (1.2 mM) medium were assessed by imaging and tracking keratinocyte migratory behaviors on pepsin digested type I collagen coated soft and stiff PA gels. Over the 24-hour observation period, several behavioral differences were observed.

First, keratinocytes were significantly more spread out on stiff substrates compared to soft. Significant differences in spread areas between keratinocytes on soft and stiff substrates in my Low Ca^{2+} control experiments were observed for all analyzed time points (Table 1). For example, at t = 2 hours, the average area of a single keratinocyte maintained in my Low Ca^{2+} control experiments on soft versus stiff gels was 535 ± 315 μm2 (n = 18)

and 3,189 ± 2,119 µm2 (n = 16), respectively. In my High Ca^{2+} experiments, a two-way ANOVA suggests that keratinocyte spread area is a function of both time and substrate stiffness, with increased spread areas on stiff compared to soft substrates, and a general trend of decreasing spread areas with duration of culture for both types of substrate (Table 1). In comparing differences between spread areas in High Ca^{2+} and Low Ca^{2+} experiments, I did find that the calcium switch had an effect on spread area during the first several hours of culture on soft gels (but not stiff gels), but the significance was lost at later time points.

With regard to migration velocities (Table 2), in Low Ca^{2+} medium, keratinocytes were 30% faster on soft gels, with an average instantaneous velocity of 1.13 ± 0.25 µm/min compared to 0.86 ± 0.27 µm/min on stiff gels ($p < 0.005$). Velocities remained virtually unchanged upon exposure to High Ca^{2+} medium (1.11 ± 0.41 µm/min on soft gels and 0.85 ± 0.39 µm/min on stiff gels) across all time points, demonstrating that keratinocyte speed was not affected by the calcium switch.

Table 1. Keratinocyte spread areas

Condition		**Cell Area ($x10^3$ µm^2)**						
		0 hr	1 hr	2 hr	4 hr	8 hr	16 hr	24 hr
Low Ca^{2+}	*Soft*	0.96 ± 0.64	1.06 ± 0.52	0.54 ± 0.32	0.62 ± 0.37	0.51 ± 0.22	0.74 ± 0.41	0.42 ± 0.13
	Stiff	3.23 ± 1.31	3.54 ± 1.71	3.19 ± 2.12	2.33 ± 1.27	2.57 ± 1.83	2.08 ± 1.44	2.15 ± 1.58
High Ca^{2+}	*Soft*	1.41 ± 0.85	1.55 ± 1.05	0.96 ± 0.73	0.96 ± 0.73	0.96 ± 0.87	0.57 ± 0.21	0.56 ± 0.13
	Stiff	3.17 ± 1.59	2.76 ± 1.56	2.94 ± 2.02	2.58 ± 2.09	1.99 ± 1.02	1.99 ± 1.37	1.85 ± 1.50

Table 2. Keratinocyte migration and aggregate forming metrics

Measurement	**Low Ca^{2+}**		**High Ca^{2+}**	
	Soft	**Stiff**	**Soft**	**Stiff**
Keratinocyte Speed (µm/min)	1.13 ± 0.25	0.86 ± 0.27	1.11 ± 0.41	0.85 ± 0.39
Duration of Cell Engagement (min)	53 ± 99	100 ± 120	152 ± 155	219 ± 157
$t_{50\%}$ (min)	-	-	57.3 ± 22.7	162.7 ± 74.9
t_{first} (hr)	-	-	4.5 ± 2.7	11.7 ± 5.5
Distance Rank (DR)	-	-	2.6 ± 2.8	5.7 ± 5.5
RC – 125 µm (% of cells that attached)	-	-	77.8 ± 4.9	51.7 ± 12.1
RC – 175 µm (% of cells that attached)	-	-	64.8 ± 2.8	40.3 ± 10.9

In contrast, the process of aggregate formation was dependent on the switch to High Ca^{2+} medium (Table 2, Table 3, and Figure 4). On both types of PA gel, pairs of keratinocytes in Low Ca^{2+} medium frequently came into contact with each other, but they did not form permanent attachments, and they ultimately disengaged from each other on time scales ranging from a few minutes to several hours over the 24-hour observation period. The duration of engagement (Table 3), though not significantly different ($p = 0.1454$), was generally shorter on soft gels (average of 53 ± 99 minutes, median 23 minutes) than on stiff gels (average of 100 ± 120 minutes, median 46 minutes). Changing to High Ca^{2+} medium triggered the keratinocytes to join aggregates that were marked by the formation of more permanent cell adhesions, consisting of both desmosomes (Figure 8) and adherens junctions (Figure 8). This process unfolded in a dynamic substrate-dependent manner, with keratinocytes joining and sometimes releasing from each other until the majority of cells in the field were associated with couples or aggregates. On soft gels, the number of single keratinocytes in a field quickly decreased from an average of 24.3 ± 4.7 cells (or $87.6\% \pm 13.6\%$ of total cells in the field) at $t = 0$ hours to 3.7 ± 2.5 cells ($10.8\% \pm 7.8\%$) at $t = 24$ hours (Table 3). The number of single keratinocytes on stiff gels did not decrease as quickly or to the same extent (31.0 ± 5.3 to 6.0 ± 4.0 cells or $97.7\% \pm 4.0\%$ to $21.5\% \pm 12.2\%$ over the same range). A two-way ANOVA indicated that the number of single cells was dependent on both time and substrates stiffness ($p < 0.001$), whereas the average total number of keratinocytes per visual field for the soft and stiff gels remained statistically constant throughout the duration of the experiment at 32.1 ± 4.7 cells and 29.8 ± 5.7 cells, respectively ($p = 0.57$).

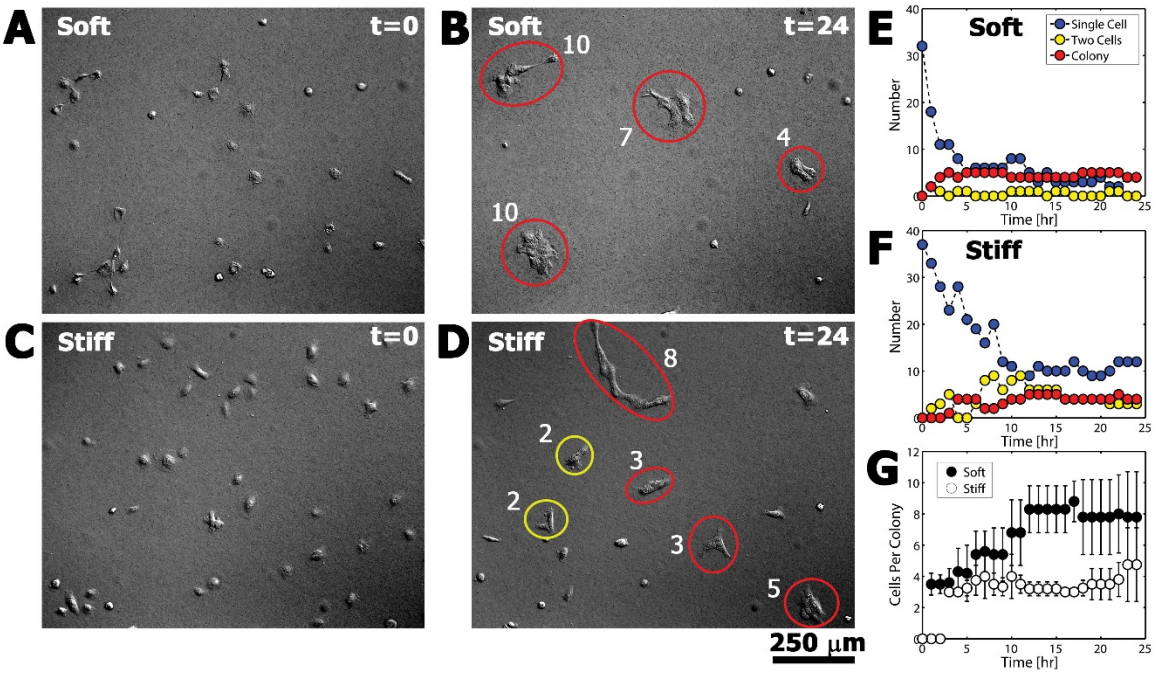

Figure 4. Representative DIC images showing differences in aggregate formation on soft and stiff PA gels at t = 0 hours (A,C) and t = 24 hours (B,D). At each hour the number of single cells, couples (yellow ellipses), and aggregates (red ellipses) was determined (E,F), along with (G) the number of cells per aggregate (colony) (number adjacent to each ellipse).

In High Ca^{2+}, when two keratinocytes joined together on a soft gel, the couple that formed generally did not last long (152 ± 155 minutes, median 88 minutes) because either the cells released from each other and continued on as single cells or other cells quickly joined the couple to form an aggregate. In contrast, keratinocytes on stiff gels formed couples that endured longer (219 ± 157 minutes, median 198 minutes). The number of couples did not change significantly over time on either gel (Table 3). There was, however, a significant dependence on substrate stiffness ($p < 0.001$), with roughly twice as many couples found on stiff gels (3.3 ± 1.0 couples, or 21.7% ± 5.8% of the total cells) as were found on soft gels (1.5 ± 0.3 couples, or 10.6% ± 2.8%). It should be noted that a small number of couples (n = 3 on soft gels, n = 4 on stiff gels) persisted for the duration of the experiment and were excluded from these calculations.

Table 3. Keratinocyte classification and counts

Condition		Measurement	Time 0 hr	1 hr	2 hr	4 hr	8 hr	16 hr	24 h
High Ca^{2+}	Soft	No. Single	24.3 ± 4.7	19.0 ± 1.7	13.3 ± 4.0	9.7 ± 1.5	7.3 ± 1.5	4.7 ± 2.1	3.7 ± 2.5
	(n = 3)	No. Couples	0.7 ± 1.2	1.7 ± 0.6	1.7 ± 0.6	1.7 ± 0.6	1.3 ± 1.2	1.7 ± 0.6	1.7 ± 0.6
		No. Aggregates	0.7 ± 0.6	1.7 ± 0.6	3.0 ± 1.0	2.3 ± 1.5	4.3 ± 1.2	4.0 ± 0.0	4.7 ± 1.2
		No Cells per Aggregate	2.0 ± 1.7	3.2 ± 1.4	3.3 ± 1.2	5.1 ± 2.6	4.9 ± 2.2	6.3 ± 3.3	6.1 ± 3.2
	Stiff	No. Single	31.0 ± 5.3	26.3 ± 6.1	24.0 ± 3.6	21.3 ± 5.9	12.3 ± 6.6	7.7 ± 2.1	6.0 ± 4.0
	(n = 3)	No. Couples	0.3 ± 0.6	1.7 ± 1.5	2.7 ± 0.6	2.3 ± 2.1	5.3 ± 3.5	2.3 ± 1.5	3.0 ± 2.0
		No. Aggregates	0.0 ± 0.0	0.3 ± 0.6	0.7 ±0.6	2.0 ± 1.7	3.3 ± 1.5	3.3 ± 0.6	3.0 ± 1.0
		No Cells per Aggregate	0.0 ± 0.0	1.0 ± 1.7	2.3 ± 2.1	3.2 ± 0.4	3.4 ± 0.5	4.0 ± 1.3	5.2 ± 2.3
Low Ca^{2+}	Soft	No. Single	28	28	23	21	23	22	25
	(n = 1)	No. Couples	0	0	2	3	0	0	0
		No. Aggregates	0	0	0	0	1	0	0
		No Cells per Aggregate	0	0	0	0	3	0	0
	Stiff	No. Single	21	22	21	20	20	20	22
	(n = 1)	No. Couples	2	0	0	0	1	2	3
		No. Aggregates	0	1	1	0	0	1	1
		No Cells per Aggregate	0	3	3	0	0	4	4

The vast majority of keratinocytes on both types of PA gel ultimately formed aggregates, with significantly more aggregates (3.8 ± 1.0 versus 2.9 ± 1.3, $p < 0.001$) and more cells per aggregate (5.4 ± 1.2 and 3.6 ± 1.2, $p < 0.001$) forming on soft rather than stiff gels, using keratinocyte counts averaged over the duration of the experiment (Figure 4). At the conclusion of the experiment (t = 24 hours), the same trends were observed with 4.7 ± 1.2 aggregates versus 3.0 ± 1.0 aggregates and 6.1 ± 3.2 cells per aggregate versus 5.2 ± 2.3 cells per aggregate observed on soft versus stiff gels, respectively. Aggregates also formed faster on soft gels. Two metrics were used to characterize the rate of aggregate formation (Table 2). First, the average time, first, required for the first aggregate to form (excluding aggregates already formed at t = 0) was calculated. It was found that the first aggregate formed faster (but not significantly, $p = 0.08$) on soft gels (57.3 ± 22.7 minutes) than on stiff gels (162.7 ± 74.9 minutes). The second metric calculated was the average time, t50%, required for at least 50% of the keratinocytes in the image to associate with an

aggregate. This time also was shorter on soft compared to stiff gels at 4.5 ± 2.7 hours and 11.7 ± 5.5 hours, respectively, though again, not significantly ($p = 0.1115$).

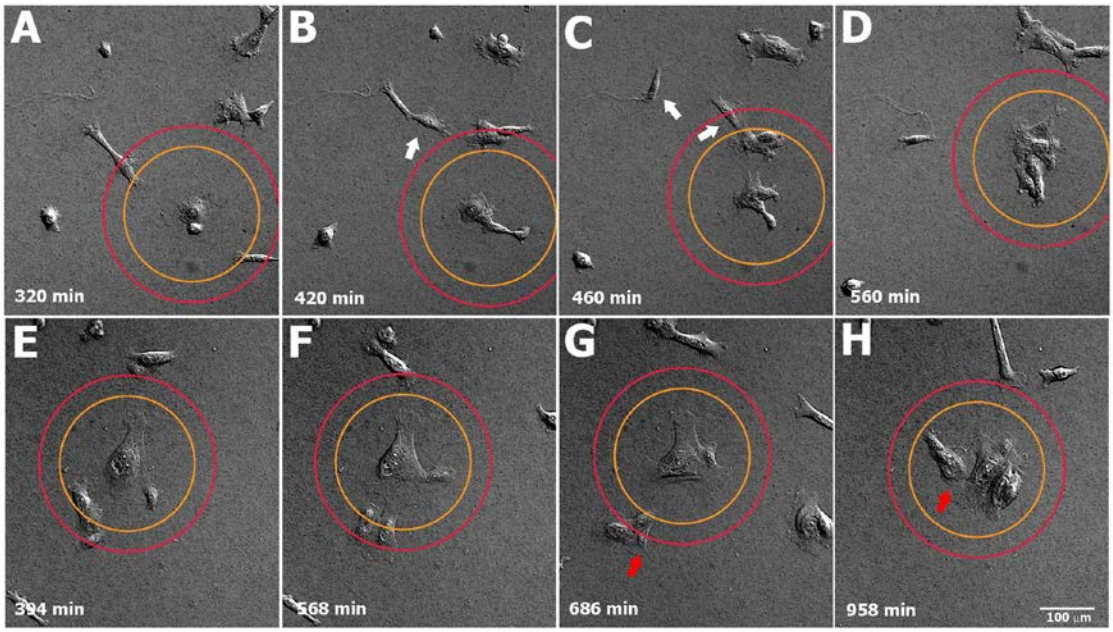

Figure 5. Representative images showing single keratinocytes, couples, and aggregates entering the radius of cooperativity (RC) for radii of 125 µm (orange circle) and 175 µm (red circle) on soft (A-D) and stiff PA gels (E-F). The couple/aggregate analyzed in each example is indicated by an asterisk. On the soft gel (A-D), an approaching couple (white arrow) crosses the inner & outer RC at t = 320 min in close proximity to a small aggregate (red arrow) that just touches the outer RC. As the aggregate migrates into the inner RC at t = 420 and t = 460 min, keratinocytes of the first couple disengage from one another (two separate white arrows). One cell eventually exits the outer RC and the other cell merges with the entering aggregate (red arrow) to join the central aggregate (asterisk) at time t = 560 min. On a stiff gel (E-H), a small aggregate (red arrow) is present at the inner RC, and a cell couple (white arrow) is present at the outer RC at t = 394 min. The couple eventually exits both RC (leaving the field of view) without joining the central couple of interest (asterisk), while the small aggregate (red arrow) temporarily moves away from the couple of interest at t = 568 min and t = 686 min before finally merging with it at t = 958 min to form a small aggregate.

In general, keratinocytes did not always form couples or aggregates through mechanical contacts with their closest neighboring cells, an unexpected behavior that was particularly evident for cells cultured on stiff gels. To quantify this difference in keratinocyte behavior observed during the process of aggregate formation on soft versus stiff substrates, I defined an *ad hoc* analysis termed the distance rank (DR). When ranked ordered by the magnitudes of their respective internuclear separations, keratinocytes cultured on stiff gels formed couples or aggregates with neighboring cells that had an

average distance rank (DR) of 5.7 ± 5.5, median rank of 4, compared to an average DR on soft gels of 2.6 ± 2.8, median rank of 2 (Table 2).

In addition to the ordinal DR metric, I performed a second *ad hoc* analysis, termed the radius of cooperativity (RC), in an attempt to correlate the length scale of a cell with the degree of cooperativity in aggregate formation characterized by keratinocytes cultured on soft versus stiff substrates. Based on observed cell spread areas at time t = 0 (Table 1) for High Ca^{2+} conditions, I estimated nominal cell diameters (assuming circular spread areas) of ~40 μm and ~60 μm for keratinocytes cultured on soft and stiff substrates, respectively. Then, assuming a stiffness-independent mean nominal cell diameter of ~50 μm and hence a nominal cell couple diameter of ~100 μm, RC analysis was performed for radii of 125 μm and 175 μm, or ~1.5 and ~2.5 nominal cell diameters, respectively, from the peripheral margin of a hypothetical cell couple of interest (Table 2, Figure 5). Keratinocytes joined with 77.8% ± 4.9% of the cellular entities (single cells, couples, or aggregates) present within a 125 μm RC on soft gels, compared to 51.7% ± 12.1% for the same 125 μm RC on stiff gels ($p < 0.03$). Similarly, keratinocytes joined with 64.8% ± 2.8% of the cellular entities present within a 175 μm RC on soft gels, compared to 40.3% ± 10.9% for the same 175 μm RC on stiff gels ($p < 0.019$).

2.3.2 Substrate Displacements during Aggregate Formation

In addition to keratinocyte morphology and kinematics, differences in substrate deformations were also observed between keratinocytes cultured on soft versus stiff substrates. Under both High Ca^{2+} and Low Ca^{2+} conditions, keratinocytes cultured on stiff PA gels generated very small substrate displacements, as monitored by tracking the positions of embedded fluorescent microspheres. The single largest tracked displacement

using a 10x objective was 1.6 μm- a value below the estimated 2.7 μm algorithm measurement error at this magnification. Consequently, the microsphere displacements on stiff gels at this magnification were treated as effectively zero, and no further quantitative analysis was conducted. Adjunctive experiments performed on a stiff PA gel using a 20x objective with a 1.5x magnifier resulted in an average maximum displacement per time point of 1.39 ± 1.93 μm (0.62 μm estimated algorithm error), with 2.29 μm representing the single largest maximum displacement measured over the 24-hour duration of the experiment. These observations confirmed that small but measureable substrate displacements were generated by keratinocytes cultured on stiff substrates. However, at this magnification the field of view was markedly reduced, and ultimately deemed too restrictive for assessing collective keratinocyte behaviors during the process of aggregate formation.

For keratinocytes cultured on soft gels maintained in Low Ca^{2+} conditions as controls, microsphere displacements were much higher, but did not vary much over the 24-hour time course (Figure 6). The overall average microsphere displacement was 4.2 ± 2.6 μm, with 17.9 μm representing the single largest microsphere displacement tracked. Under High Ca^{2+} conditions, keratinocytes generated microsphere displacements that were not only higher, but they also increased with duration of culture and in parallel with nascent epithelial sheet formation (Figure 6, Figure 7). Average displacements ranged from 8.7 ± 5.7 μm at t = 0 hours to 19.4 ± 21.2 μm at t = 24 hours. Here, the single largest displacement tracked was 113.5 μm, occurring at t = 24 hours.

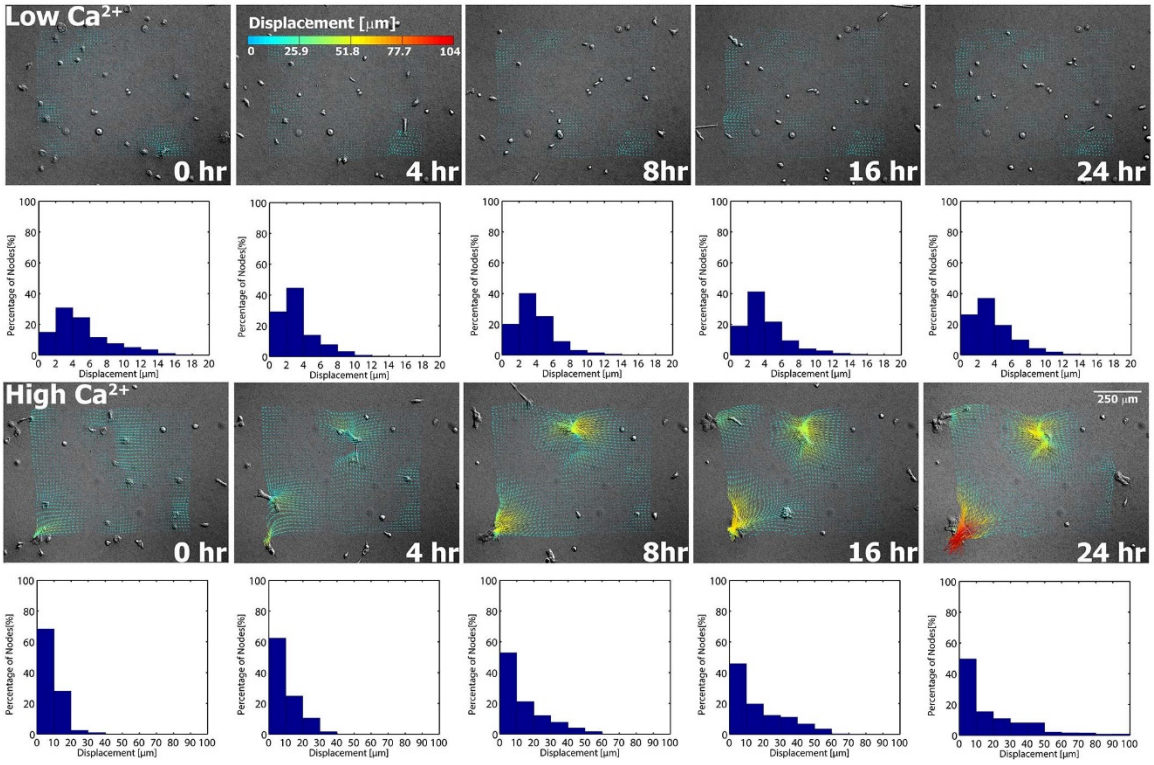

Figure 6. Cell tractions deform soft PA gels in a manner that is dependent on the calcium concentration of the culture medium and the extent of keratinocyte aggregate formation. Substrate displacements are determined by tracking microsphere displacements in Low Ca^{2+} and High Ca^{2+} experiments at the indicated time points (cf. Section 2.6). Displacements increase with time under High Ca^{2+} conditions, correlating with the extent of keratinocyte aggregate formation. Note the difference in the range of x-axis displacements indicated on the histograms associated with the Low Ca^{2+} and High Ca^{2+} measurements.

Two important experimental factors precluded quantitative traction force microscopy (TFM) analysis in my study, namely: (i) limitations in the detection and tracking of substrate displacements for my extremes in substrate stiffness, and (ii) the ill-defined and dynamic nature of the boundary conditions required to solve the inverse problem of calculating cell tractions from measured substrate displacements. With regards to the former, the soft and stiff formulations of my PA gels were not optimized for TFM analysis: substrate displacements observed in my stiff gels were so small that they fell within the uncertainty of my tracking algorithms, while the extremely large displacements observed in my soft gels invalidate many of the assumptions inherent to most forms of TFM analysis (infinitesimal strains and a linear elastic continuum).

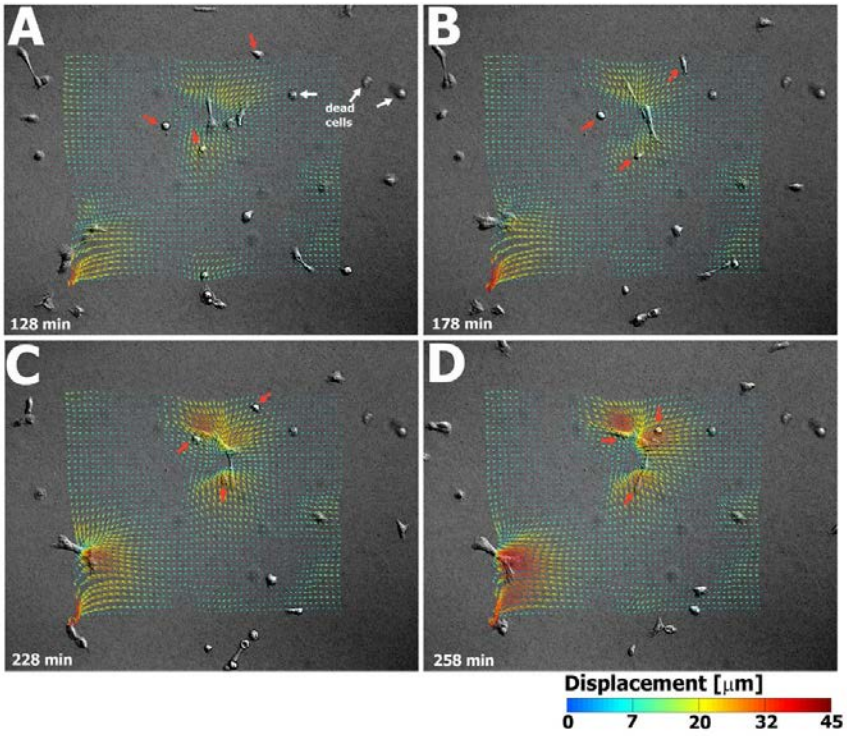

Figure 7. Selected frames show that in High Ca^{2+} conditions, keratinocyte aggregates forming on soft PA gels generate large substrate displacements that appear to draw single keratinocytes inward towards a forming aggregate. Dead cells are indicated by white arrows. The relative positions of three selected individual keratinocytes are indicated by red arrows at all four time points with respect to a forming aggregate (indicated by an asterisk).

With regards to boundary conditions, note that keratinocytes were free to migrate in and/or out of the optical field of view throughout the 24-hour duration of my experiment. Thus, not only are the cellular tractions present at the boundaries of my observation window spatially uncertain, they are also temporally variable. These technical issues will be addressed in future work by using smaller cell numbers, more focused fields of view with higher power objectives, and TFM analysis that employs a large deformation formulation [89].

2.3.3 Keratinocyte Cytoskeletal Morphology

Immunofluorescent labeling of actin microfilaments, keratin intermediate filaments, desmoplakin (component of desmosomes), and E-cadherin (component of

adherens junctions) within keratinocytes cultured on both soft and stiff PA gels revealed differences in cytoskeletal organization that were consistent with the dynamic cell morphologies observed in my time-lapse DIC images (Figure 8, Figure 9). In Low Ca^{2+} conditions (t = 0 hours), keratinocytes on both soft and stiff substrates assumed a predominantly rounded morphology, with cells on stiff substrates exhibiting a notably increased degree of cell spreading. Spindled morphologies were also observed, with an increased number density on soft compared to stiff substrates. With respect to my time-lapse DIC images, small rounded keratinocytes were observed to migrate over the surface of both types of gel, occasionally transitioning into an elongated spindled morphology before eventually condensing back into a rounded morphology and resuming their migratory behaviors. This type of transitional morphologic behavior, though present, was relatively uncommon on stiff gels. Following 24 hours of culture in Low Ca^{2+} conditions, the number of keratinocytes adopting a small rounded-up morphology was dramatically increased on soft compared to stiff substrates.

For both substrate types under Low Ca^{2+} conditions, focal actin concentrations were noted at the cell peripheries, with thicker actin fibers indicative of stress fibers more clearly visualized in keratinocytes cultured on stiff substrates across all time points. At baseline (t = 0 hours, Low Ca^{2+}), keratin intermediate filaments formed networks that centrifugally extended from a perinuclear cage-like structure. Following the calcium switch, microfilament organization within keratinocytes cultured on soft PA gels changed rapidly, marked by the formation of lamellipodial- and pseudopodial-like structures at t = 1 hour. At t = 24 hours following the calcium switch, cell-cell adherens junctions were formed

between keratinocytes within aggregates on both soft and stiff substrates, as marked by the punctate/linear staining of E-cadherin (Figure 9).

Within this same time frame, keratin intermediate filaments reorganized to form highly integrated networks that spanned multiple cell-to-cell contacts within aggregates cultured on both soft and stiff substrates. These networks were associated with the formation of cell-cell desmosomes, as marked by the punctate staining pattern of desmoplakin (Figure 8). Desmoplakin staining appeared more prominent on stiff versus soft substrates at t = 4 hours, suggestive of an increased rate of desmosome assembly.

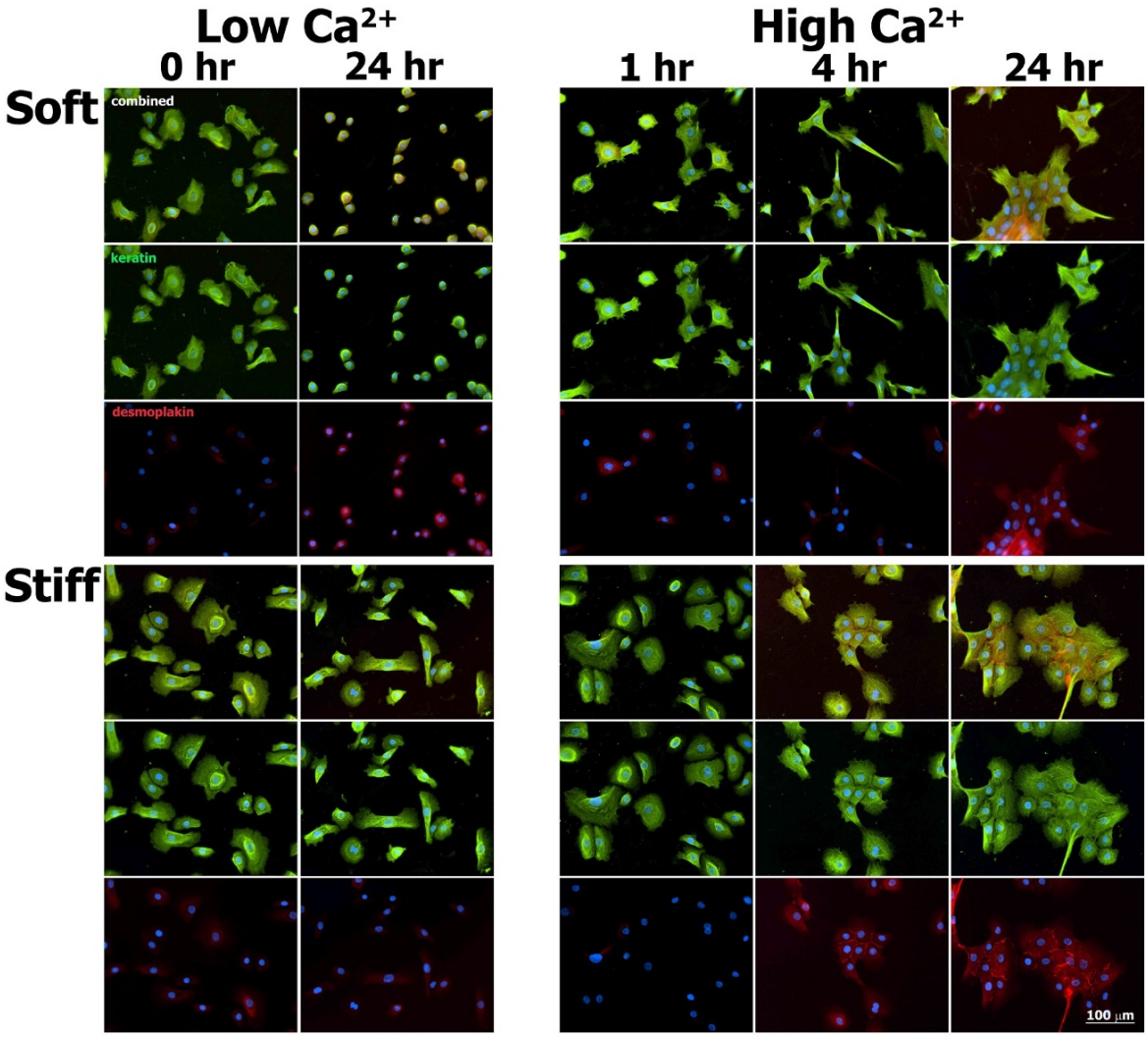

Figure 8. Immunofluorescence images of keratin intermediate filaments (green), desmoplakin (red), and nuclei (blue) in normal human epidermal keratinocytes culture for select times on soft and stiff PA gels exposed to both Low Ca^{2+} and High Ca^{2+} conditions.

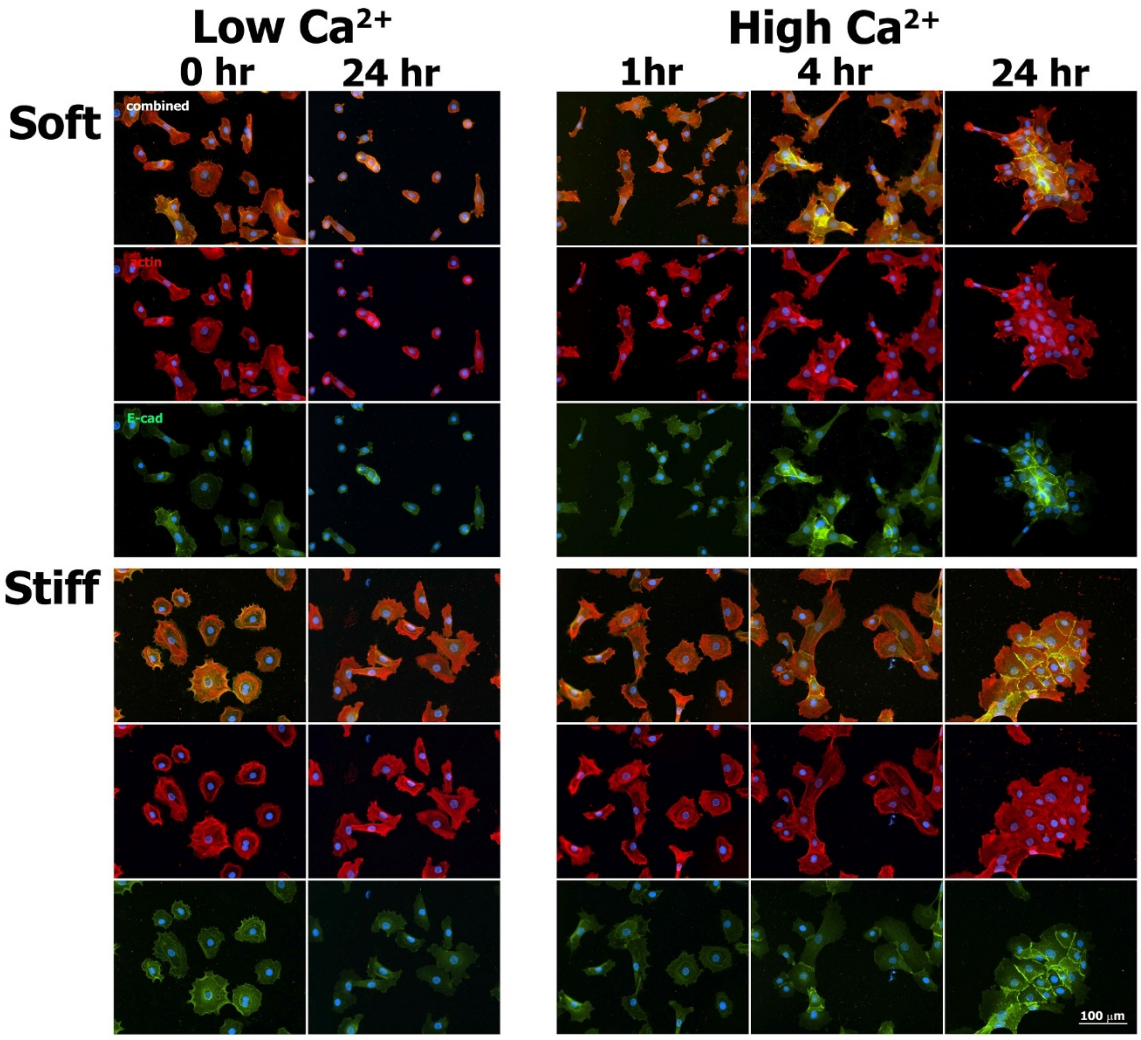

Figure 9. Immunofluorescence images of actin (red), E-cadherin (green), and nuclei (blue) in normal human epidermal keratinocytes culture for select times on soft and stiff PA gels exposed to both Low Ca^{2+} and High Ca^{2+} conditions.

Interestingly, keratinocytes found along the periphery of aggregates cultured on soft substrates exhibited a spindled morphology with visible lamellipodial- and pseudopodial-like microfilament structures, suggestive that aggregates on soft substrates are more actively seeking mechanical contact(s) with neighboring cells or aggregates in order to incorporate them into the evolving epithelial sheet. Similar pseudopodial-like extensions were also observed in some single keratinocytes that were in close proximity to a nearby aggregate. By correlation, in my time-lapse DIC images (Figure 10), single keratinocytes

on soft gels were frequently observed to extend pseudopodial-like structures that were directed towards the aggregate it was attempting to join. In contrast to these findings, keratinocytes present along the periphery of aggregates cultured on stiff substrates exhibited a more rounded morphology with little to no evident formation of pseudopodial-like microfilament structures. As noted in my DIC images, keratinocytes on stiff substrates frequently did not join an aggregate via directed orthogonal movements, but rather seemed to merge with its eventual aggregate via an increasingly tangential approach (Figure 10).

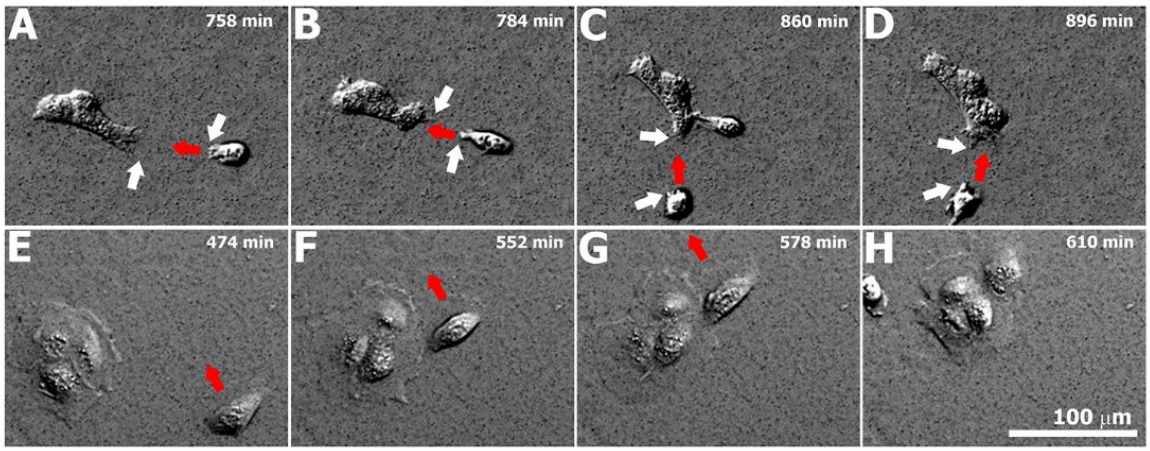

Figure 10. The characteristics of aggregate formation differ on soft (A-D) and stiff (E-H) gels. On soft gels (A-D), small pseudopodial-like projections (white arrows) extend outward from both the approaching cell (indicated by an asterisk) and its eventual cell of contact (indicated by number sign) within the aggregate. The approaching cell migrates directly (velocity vector indicated by red arrows) towards its contact cell in a process that appears to be mediated by these pseudopodial-like extensions. On stiff gels (E-H), pseudopodial-like projections were not observed between merging keratinocytes during the process of aggregate formation. Rather, migrating keratinocytes (asterisk) often approached their eventual cell of contact within an aggregate (number sign) via an almost tangential pathway, as can be seen by the velocity vectors (red arrows) indicated for the approaching keratinocyte labeled in (E), (F), and (G) that eventually joins the aggregate shown in (H).

In order to explore possible differences in cell-matrix adhesive contacts under various experimental conditions, immunofluorescence experiments (Figure 11) were performed by co-labeling for β1 integrin, a component of focal adhesion contacts, and β4 integrin , a component of hemidesmosomes *in vivo* and hemidesmosome-like contacts *in vitro* [90]. Under Low Ca^{2+} conditions, some staining of β1 integrin was observed over 24 hours of culture, whereas β4 integrin was diffusely expressed throughout the cytoplasm

without any definitive foci of staining along the cell-matrix interface. After 24 hours of culture under High Ca^{2+} conditions, punctate foci of β1 integrin staining were observed in all keratinocytes belonging to an aggregate, independent of a given cell's position within the aggregate and independent of the stiffness of the PA gel. Staining for β4 integrin remained cytoplasmically diffuse in cells cultured on stiff PA gels. At t = 24 hours following the calcium switch, punctate staining of β4 integrin along the cell-matrix interface appeared within keratinocytes positioned along the periphery of aggregates cultured on soft substrates. This staining pattern was not observed within aggregates cultured on stiff gels.

Lastly, the average internuclear spacing of keratinocytes within aggregates cultured under High Ca^{2+} conditions on soft substrates was diminished compared to the internuclear spacing of cells on stiff substrates. In some instances, this reduction in spacing might be due to the local three-dimensional stratification and differentiation of keratinocytes within the aggregate, as can be inferred from partially overlapping DAPI-stained nuclei (Figure 8, Figure 9, soft substrate, t = 24 hours). In order to evaluate whether substrate-dependent keratinocyte differentiation played a role in the aggregate-forming behavior observed in my experiments, I also evaluated involucrin expression (a keratinocyte-specific differentiation marker [82] across select time points of culture under both Low Ca^{2+} and High Ca^{2+} conditions (Figure 13).

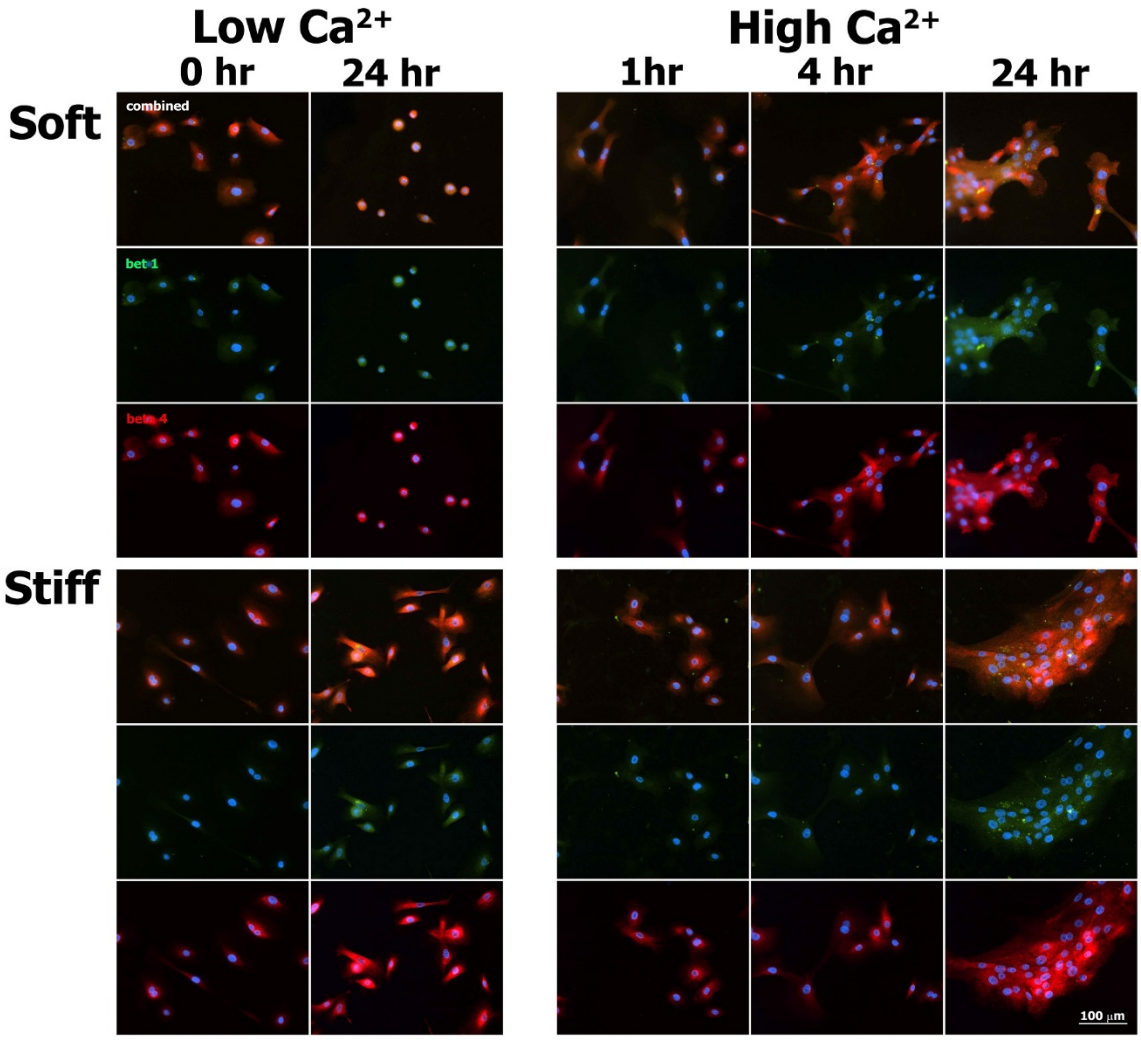

Figure 11. Immunofluorescence images of β4 (red), β1 (green), and nuclei (blue) in normal human epidermal keratinocytes culture for select times on soft and stiff PA gels exposed to both Low Ca^{2+} and High Ca^{2+} conditions.

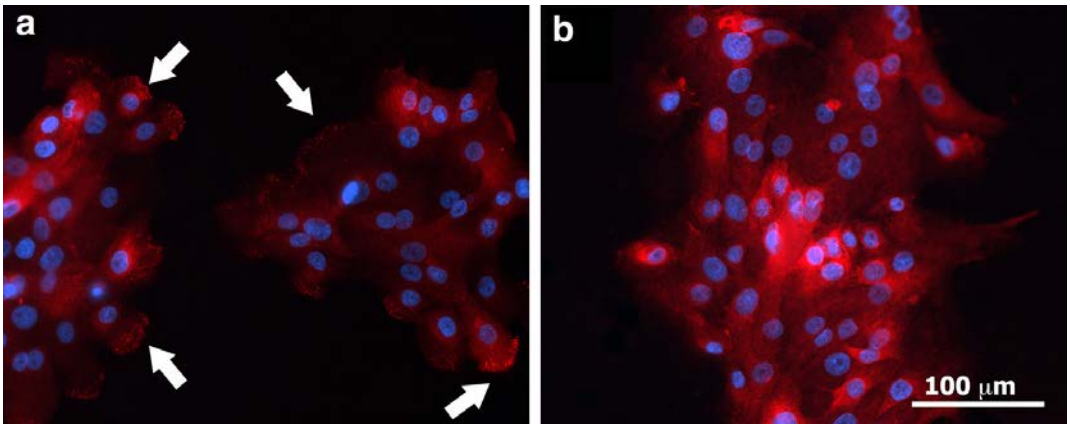

Figure 12. Immunofluorescence images of β4 (red) and nuclei (blue) in normal human epidermal keratinocytes cultured for 24 hr in High Ca^{2+} conditions on (a) soft and (b) stiff PA gels. White arrows highlight areas of punctate staining observed in peripheral keratinocytes within aggregates cultured on soft gels.

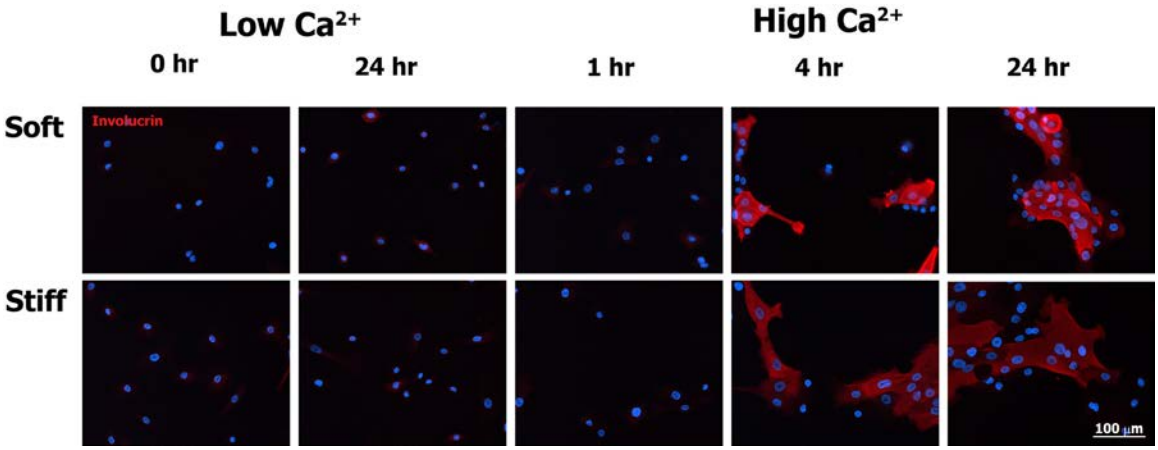

Figure 13. Immunofluorescence images of involucrin (red) and nuclei (blue) in normal human epidermal keratinocytes culture for select times on soft and stiff PA gels exposed to both Low Ca^{2+} and High Ca^{2+} conditions.

Under Low Ca^{2+} conditions, positive staining for involucrin was noted at t = 24 hours for a very small subset of cells cultured on both soft and stiff PA gels. At t = 4 and t = 24 hours following the calcium switch, positive involucrin staining was observed within keratinocytes cultured on both soft and stiff gels, with staining primarily localized to cells positioned within the center and stratified layers of each given aggregate. Involucrin staining was notably absent from peripheral cells of the aggregate and keratinocytes

migrating as single cells. No definitive differences in involucrin staining were noted between soft and stiff gels.

2.4 DISCUSSION

In qualitative agreement with Pelham's and Wang's seminal observations of the migratory behaviors of 3T3 fibroblasts and rat kidney epithelial cells (NRK-52E) [31], my experiments showed that normal human epidermal keratinocytes exhibit smaller spread areas but increased migration velocities when cultured on soft as opposed to stiff substrates. When compared to normal human keratinocytes cultured on type I collagen attached to an *in vitro* "observation chamber" (1.2 ± 0.7 μm/min; exact substrate material not specified), my observed migration velocities are strikingly similar in magnitude [91]. In quantitative agreement with the experiments performed by Trappmann *et al*. [29], I observed similar keratinocyte spread areas on my nominal 1.2 kPa soft PA gels compared to their 0.5 kPa PA gels. Additionally, the transient spindled morphologies I observed in keratinocytes cultured on my soft gels were also observed by Trappmann *et al*. in keratinocytes cultured on their 2 kPa gels.

Collectively, the effects of substrate stiffness on spread areas and migration velocities that I observed in my keratinocyte studies are in agreement with prior studies that utilized cells of both parenchymal and mesenchymal origin. Some have argued that these general observations can be attributed to the weak/unstable nature of focal contacts associated with cells cultured on soft substrates [31, 92]. Interestingly, for fibroblasts, the apparent dependence on bulk substrate stiffness seems to disappear when cells are cultured on fibrous matrix [93]. Trappmann *et al*. have reported a similar finding with cultured

keratinocytes, proposing that cells respond to feedback from the mechanical tethering of individual near-field matrix fibers as opposed to any bulk mechanical property of the substrate [29]. More recently, Wen *et al*. have reported that the differentiation of adipose-derived and bone marrow-derived stromal cells is regulated by matrix stiffness in a manner that is independent of protein tethering [94]. Given the apparent discrepancies among these various studies, I pose that the mechanobiological mechanism by which keratinocytes sense and respond to perturbations in their mechanical environment remains an open question ripe for further investigation.

Although the migration rates of fully-formed keratinocyte sheets have been observed to be dependent on substrate stiffness [73], to the best of my knowledge, my work represents the first studies that have documented the effect of substrate stiffness on the migration velocities of individual human epidermal keratinocytes. Wang *et al*. cultured HaCaT epidermal cells (an immortalized human keratinocyte cells line) on polydimethylsiloxane (PDMS) substrates that were 16 kPa, 20 kPa, and 200 kPa in nominal stiffness. Using what is often referred to as a scratch assay, they found that a fully-formed keratinocyte sheet migrates to close an artificially created defect in the sheet at a faster rate when cultured on stiffer (200 kPa) versus softer substrates (16 kPa). In contrast, my study found that keratinocyte velocities were faster on soft (nominal E = 1.2 kPa) as opposed to stiff (nominal E = 24 kPa) PA gels. Furthermore, other researchers have observed that the proliferation/growth of fully-formed epithelial sheets *in vitro* (Madin-Darby canine kidney epithelial cells) is effectively independent of substrate stiffness [78]. These apparent contradictions can possibly be explained by more careful consideration of the collective number of cell-cell and cell-matrix contacts present, in addition to consideration of the

biochemical milieu the keratinocytes are exposed to at the time the observations are made, i.e., it is possible that the effect of substrate stiffness depends on whether or not one assays (i) individual keratinocytes during their initial attempts at aggregate formation (nascent epithelial sheet formation) versus (ii) keratinocytes incorporated into a fully-developed epithelial sheet (associated with fully-formed cell-cell desmosomes and adherens junctions) versus (iii) keratinocytes within a fully-developed but physically damaged epithelial sheet surrounded by cytokines and other paracrine signals released from adjacent damaged cells.

As gleaned from my time-lapse DIC images, the process of aggregate formation involves a number of dynamic and interrelated mechanobiological phenomena that make precise quantification of keratinocyte behavior difficult: individual cells, couples, and aggregates are moving both towards and away from each other via cell-matrix tractions imposed on their underlying substrate, all the while forming transient and sometimes permanent cell-cell junctions in an attempt to form a nascent epithelial sheet. To begin to quantify some of the collective behaviors that are more qualitatively apparent to the eye of the observer, I developed two *ad hoc* analyses, termed the distance rank (DR) and the radius of cooperativity (RC). Both DR and RC provide an indication of how close keratinocytes need to be to a forming aggregate in order to join that aggregate, and both metrics suggest that keratinocyte that keratinocytes cultured on soft PA gels form aggregates in an increasingly cooperative process compared to the process of aggregate formation observed for keratinocytes cultured on stiff PA gels.

A cooperativity-like phenomenon has been qualitatively observed by other groups, specifically Guo *et al*. [95], where they observed the spontaneous formation of tissue-like

"spheroids" in both fibroblasts and NRK-52E epithelial cells cultured on soft substrates (nominal E = 2.49 kPa). In a similar fashion, Reinhart-King *et al*. observed that individual endothelial cell migration becomes restricted when endothelial cells are cultured in close proximity to other cells on substrates with nominal stiffness ranging between 2.5 kPa and 5.5 kPa [96]. With their migration velocities restricted, endothelial cells exhibit increasing cell-cell contact events that may represent a nidus for tissue formation. In their work, Rheinhart-King *et al*. postulated that this form of tissue genesis may arise via cell-cell mechanical communication that occurs through local substrate displacements. In essence, this type of behavior can be interpreted as a form of durotaxis [35] where cells sense changes in perceived substrate elasticity due to the deformations induced in the substrate (a non-linear elastic material) by the tractions exerted from neighboring cells.

The results of my study are also in agreement with the idea of durotactic cell-cell signaling generated via local substrate displacements, specifically, the enhanced cooperativity of nascent epithelial sheet formation that I observed in keratinocytes cultured on soft substrates (Figure 7). Under High Ca^{2+} conditions, keratinocyte aggregates produced large substrate displacements, the magnitude of which increased temporally in correlation with the number of cells integrated into a given aggregate. Surprisingly, in comparing integrin expression between cells cultured on soft versus stiff substrates, I found a distinct difference in the expression of the β4 integrin subunit, specifically, the localization of β4 to the cell-matrix interface within keratinocytes positioned along the periphery of aggregates on soft PA gels. *In vivo*, the α6β4 integrin (i.e., hemidesmosome) mechanically couples the keratin intermediate filament system to the basement membrane [90]. *In vitro*, true ultrastructurally complete hemidesmosomes have not been demonstrated

in primary keratinocyte cultures [90], and in my experiments, I did not perform any IF for co-staining of β4 integrin and keratin to see if these proteins also co-localized to the periphery of my cell aggregates. However, recent work has suggested that α6β4 integrin also plays a role in the regulation of keratinocyte migration via signaling through Rac1 to the actin-severing protein cofilin present within the lamellipodia of a motile cell [97, 98]. In other words, α6β4 integrins can interact (indirectly and possibly directly) with the microfilament network as opposed to being strictly confined to adynamic mechanical contacts with the keratin intermediate filament network. Thus, it is conceivable that the presence of β4 integrin in peripheral keratinocytes within aggregates forming on soft gels is associated with the large substrate displacments generated by these aggregates, though with respect to the results presented here, I can only speculate as to whether this association is one of correlation or causality.

It is important to note that presence of a soft substrate alone cannot account for the enhanced aggregate formation observed in my High Ca^{2+} experiments. If it did, then one might expect enhanced aggregate formation to occur in my Low Ca^{2+} control experiments, but this was not the case. I also considered whether the increase in calcium concentration associated with my High Ca^{2+} medium could in some way contribute to the differences in aggregate formation observed in my experiments via a direct effect on integrin function. Integrin binding is dependent on the presence of extracellular divalent cations, with preference for magnesium and manganese over calcium [99]. Changes in the concentration of extracellular Mg^{2+} and Ca^{2+} have been shown to differentially influence β1 integrin-associated keratinocyte adhesion and migration on type I collagen, with calcium having a mild inhibitory effect at concentrations lower than 2 mM and a more prominent inhibitory

effect at calcium concentrations greater than 2 mM [100, 101]. Following the calcium switch to High Ca^{2+} medium, it is conceivable that the formation of cadherin-mediated cell-cell contacts occurs at the expense of diminished integrin functionality, as changes in cell-cell and cell-matrix contacts are both a cause and consequence of keratinocyte differentiation. Whatever role calcium-induced changes in integrin function might play in the process of keratinocyte aggregate formation, the keratinocytes cultured on both my soft and stiff gels would be affected equally. Thus, the observed differences in cooperativity should be due primarily to the effect of substrate stiffness.

Incorporating all of my observed experimental findings, I hypothesize that the enhanced cooperativity of aggregate formation (nascent keratinocyte sheet formation) observed in my soft gel experiments arises in the following fashion. First, increased calcium concentrations in my High Ca^{2+} experiments enable the formation of stronger cell-cell adhesive contacts (adherens junctions and desmosomes) that maintain intercellular adhesion within an evolving aggregate. Second, as cell-cell tension increases within an evolving aggregate, cell-substrate tractions along the perimeter of the aggregate are increased in order to maintain mechanical equilibrium. Third, local substrate displacements- associated with the localization of β4 integrin and its direct or indirect interactions with the microfilament network- develop at the periphery of the aggregate in response to the increased tractions exerted by the aggregate. Neighboring but unattached keratinocytes then sense the apparent increase in substrate elasticity, and via a process of durotaxis, preferentially migrate towards the aggregate (Figure 7). With each neighboring keratinocyte that joins the aggregate, a positive mechanical feedback loop is created by which more and more keratinocytes are recruited to join the nascent epithelial sheet.

In closing, with regards to pathophysiological relevance, note that the stiffnesses of the PA gels used in this study are consistent with atomic force microscopy (AFM) measurements of the stiffness of the human papillary dermis, specifically, 0.82 kPa and 1.12 kPa (median elastic moduli) for specimens of papillary dermis extracted from breast and abdominal skin, respectively [102]. These measurements provide a clearer picture of the substrate stiffnesses that keratinocytes might perceive *in vivo*, and they are substantially lower than values of elastic modulus reported from macroscopic tissue-level mechanical tests [103]. Along similar lines, AFM measurements on wounded rat skin found that the elastic modulus of granulation tissue increased from 18.5 kPa at day 7 to 29.4 kPa at day 9 [104]. Because the process of re-epithelialization during wound healing takes place on a bed of granulation tissue that changes its stiffness and biochemical composition as a function of time, I believe that keratinocyte aggregate formation (and hence nascent epithelial sheet development) is mediated, at least in part, by durotactic responses occurring at the cellular level. Furthermore, the fibrous nature of granulation tissue and ECM likely extends the role of durotaxis and mechanosensing across much larger distances than is observed on non-fibrous materials of comparable stiffness, such as PA gels [62, 93]. If true, building from the results of my initial experiments, one can envision new wound care therapies targeting the keratinocyte durotactic response with the goal of speeding-up the rate of re-epithelialization of chronic wounds.

2.5 CONCLUSION

As observed in my experiments, keratinocytes cultured on pepsin digested type I collagen coated soft PA gels exhibit (i) smaller spread contact areas, (ii) increased migration velocities, and (iii) increased rates of aggregate formation with more cells per

aggregate than do keratinocytes cultured on stiff gels. Together with the differences observed in substrate displacements, distance rank (DR), and radius of cooperativity (RC), my findings are reflective of what I perceive as increasingly cooperative behavior of keratinocytes cultured on soft versus stiff gels during the process of aggregate formation, i.e., the observation that individual cells, couples, and aggregates cultured on soft gels under High Ca^{2+} conditions seem to better coordinate their efforts to achieve local nascent epithelial sheet formation compared to the increasingly stochastic cell-cell contact events that lead to nascent sheet formation from similar collections of cells, couples, and aggregates cultured on stiff substrates. Although more work is required to elucidate the specific mechnobiological mechanisms involved, I hypothesize that the differences in keratinocyte aggregate formation observed in my experiments are associated with an enhanced expression of β4 integrin along the periphery of aggregates evolving on soft substrates which ultimately leads to increased durotactic cell-cell signaling generated via local substrate deformations.

2.6 ACKNOWLEDGEMENTS

Support for this project was provided by the National Institutes of Health (R03-AR063967) and the Roy J. Carver Charitable Trust (#14-4384). I thank Sandeep Bodduluri, and Joseph Reinhardt for assistance in displacement tracking, and Sailahari Ponnaluri for assistance in cell hand tracking and cell aggregate counting. I also thank Kelly Messingham for assistance with immunolabeling, and Janet Fairley, George Giudice, and Thomas Magin for insightful discussions on this work.

Chapter III. SUBSTRATE STIFFNESS MODULATE PROTEIN EXPRESSION IN HUMAN KERATINOCYTES

3.1 INTRODUCTION

Recent studies have highlighted the importance of the mechanical properties of the environment, including substrate stiffness, in regulating keratinocytes proliferation, differentiation, force generation, migration, and aggregate formation [29, 32, 34, 72]. However, the underlying proteins and pathways controlling these processes remain unclear. The Rho family of small GTPases, specifically RhoA, Rac, and Cdc42 have been of particular interest in the context of mechanosensing. In general, Rho regulates stress fiber formation and cell contraction, whereas Rac and Cdc42 regulate the formation of lamellipodia and fillopodia, respectively, and promote protrusive activities [105, 106]. Rho-kinase (ROCK), originally identified as the effector of the small Rho GTPases, plays a major role in mediating rearrangement of the actomyosin cytoskeleton downstream of Rho [106]. RhoA together with ROCK (*i.e.*, the Rho/ROCK pathway) is mainly associated with the activation of actomyosin contractility. It activates the serine/threonine kinases ROCK1 and ROCK2, which in turn, phosphorylates myosin regulatory light chains (MLC2), myosin phosphatase target subunit 1 (MYPT1), and other substrates like the LIM Kinases (LIMK) [105].

Previous studies have shown that Rho/ROCK regulates keratinocyte homeostasis and the balance between proliferation and terminal differentiation [43]. Depletion of ROCK1 and ROCK2 via RNAi demonstrated that knockdown of ROCK1 and ROCK2 increased and inhibited keratinocyte terminal differentiation, respectively [42]. RhoA was also found to be crucial for contraction and directed migration of keratinocytes in a scratch wound healing assay [107].

In Chapter II, substrate stiffness was found to affect keratinocyte aggregate formation, spread area, and migration speed. However, the precise pathways and mechanisms responsible for this behavior are unclear. Here, I investigate the effect of inhibiting Rho kinase, with Y27632 [108] on keratinocyte aggregate formation. In addition, a comprehensive protein screen was performed via a broad-spectrum proteomics analysis in order to identify differences in protein expression. Selected proteomics results were validated using western blot. My results give new insights on the role of different proteins and pathways in mechanotransduction in this system.

3.2 MATERIALS AND METHODS

3.2.1 Cell Culture

Neonatal human epidermal keratinocytes (HEKn) (Fisher Scientific, Waltham, MA) were thawed and cultured in keratinocyte serum free medium (KSFM) (Invitrogen) supplemented with 1% penicillin-streptomycin and 0.1% amphotericin B, in a humidified incubator maintained at 37 °C and 5%/95% CO_2/air. Passage three cells were plated onto the surface of polyacrylamide (PA) gels at a density of approximately 4,000 cells/cm^2. Three hours after culturing the cells the calcium of the medium was elevated from 0.09 mM to 1.2 mM by adding the proper amount of $CaCl_2$. This moment was defined as t = 0 hr and the experiment continued until t = 24 hr.

3.2.2 Polyacrylamide Gels

Thin polyacrylamide (PA) gels approximately 100 μm in thickness were polymerized onto the surface of cleaned coverglass (d = 40 mm) as described previously. Briefly, the ratios of 2%/0.25% and 7.5%/0.3% acrylamide/bis-acrylamide were used to

fabricate soft and stiff PA gels, respectively. Pepsin-digested collagen was covalently attached to the surface of the gel using Sulfo-SANPAH. The samples were sterilized under UV light for 15 minutes and stored at 4 °C until needed.

3.2.3 Chemical Inhibition with Y27632

At the time of adding $CaCl_2$, Y27632 was also added to the medium of the cells in three soft and three stiff samples to a final concentration of 10 µM.

3.2.4 Time-Lapse Imaging

Time-lapse live cell images were acquired with a Nikon Eclipse Ti inverted microscope equipped with wide-field epifluorescent and DIC microscopy capabilities. Both DIC and fluorescent images were taken with a CFI plan Apo 10X DIC objective. Time –lapse images were taken every five minutes over the duration of the experiment.

3.2.5 Cell Classification and Aggregate Counting

In order to quantify the rate of keratinocytes aggregate formation in the acquired images, the number of single cells and the number of cells per aggregate were counted every hour over the 24 hour duration of the experiment (*c.f.*, chapter II and [32]).

3.2.6 Cell Number

In parallel sets of experiments, the effect of adding Y27632 on cell proliferation was determined by counting cells at t = 24 hr. Counting the number of cells was done by trypsinizing the cells on the gels surface. One ml of trypsin was added to the gel surface and left for 10 minutes. The cell suspension was pipetted up-down several times and the samples were checked under a microscope to make sure that all the cells were released from the gel. The number of cells then was counted with a hemocytometer.

3.2.7 Substrate Displacement

In order to explore the effect of Y27632 drug on keratinocyte force generation, substrate deformations generated by the cells were quantified as described previously [32]. Briefly, the changes in spatial distribution of the fluorescent beads embedded in the substrate were tracked using an image-based correlation algorithm. The quantified displacements were plotted over the corresponded DIC images of the cells.

3.2.8 Protein Extraction and Silver Staining

Protein content of the keratinocytes 24 hr after increasing the calcium of medium was extracted using a modified RIPA buffer, including 20 mM triethylammonium bicarbonate (TEAB) (Thermo Scientific, Rockford, IL, USA), 0.1% Rapigest (Waters Corp., Milford, MA), and 0.5% sodium deoxycholate (SDC)(Sigma Aldrich) with 1X HaltTM protease inhibitor cocktail (Thermo Scientific, Rockford, IL, USA). The protein extract was centrifuged for 15 minutes at 13,000 g. Cell lysate protein concentration was estimated using the Bradford (Bio-Rad Laboratories, Hercules, CA) method. 20 µg of protein lysate was mixed with beta mercaptoethanol and heated at 98 °C for 4 minutes. The mixture of protein with beta mercaptoethanol and blue buffer were resolved with a 10% sodium dodecyl sulfate-polyacrylamide gel electrophoresis (SDS-PAGE) gel at 40 mA constant current for 30 minutes.

The SDS PAGE gels were fixed for 20 minutes with fixation solution (Silver Satin Plus, Bio-Rad Laboratories, Hercules, CA) containing 50% reagent-grade methanol, 10% reagent-grade acetic acid, 10% fixative enhancer concentrate, and 30% deionized distilled water. Following the fixation, the gels were rinsed with distilled deionized water two time, each time for 10 minutes on a rocker.

The gels were stained with a solution of 5% silver complex solution, 5% reduction moderator solution, 5% image development reagent, 50% development accelerator solution and 35% deionized water. After about 30 minutes, the staining reaction was stopped using 5% acetic acid. Densitometry analysis was performed in Image Studio (LI-COR Biotechnology, Lincoln, NE).

3.2.9 SDS-PAGE and Direct Infusion of Differentially-Expressed Protein

Equal amounts of protein, as determined by the BCA assay (Bicinchoninic acid protein assay), were denatured and reduced, and separated via SDS-PAGE (10-20% gradient Criterion gel, Bio-Rad Laboratories, Hercules, CA). The gels were fixed using 30% isopropanol and 2% phosphoric acid, and stained using Sypro-Ruby. Gels were imaged using a ChemDoc imager (BioRad) to confirm protein concentration and sample integrity, and to identify those protein bands that were differentially regulated between treatment types. The gels were then counter-stained with colloidal Coomassie G250, and the selected differentially expressed gel bands were excised with a scalpel. Care was taken to minimize dust contamination during all steps and MS grade reagents were used in all processing steps. Low retention pipette tips and microfuge tubes were used as well to minimize non-specific adsorptive loss of proteins and peptides during handling.

The excised bands were chopped into small pieces ($<1mm^3$) using a scalpel then destained by addition of 400 µl of a 1:1 acetonitrile/water solution, followed by shaking at room temperature for fifteen minutes. The destaining solutions were changed and replenished until there was no visible dye left in the gel pieces (typically 2-3 rounds of destaining). Upon removal of the destaining solution, 250 µl of 100% acetonitrile was added to dehydrate the gel pieces. The samples were incubated at room temperature on a

shaker for ten minutes and the majority of acetonitrile was removed by pipetting. The remaining acetonitrile was removed by vacuum centrifugation min.

Ten µl of reduction/alkylation buffer (1mM TCEP(tris(2-carboxyethyl)phosphine), 2.5 mM C-AM (chloroacetamide), 0.5% SDC (sodium deoxycholate), 20 TEAB (triethyl ammonium bicarbonate) was added to each sample, and the sample incubated at 37 ˚C for 30 minutes. The samples were then washed once with 400 µl of 1:1 acetonitrile/water to remove excess reagent, followed by dehydration with acetonitrile as described above.

A modified digestion protocol adopted from Havlis *et al.* was used for in-gel digestion [109]. A small volume (2-4 µl) of concentrated trypsin (Promega, Madison, WI) was added to each sample on ice and the samples were incubated for one hour at 4 ˚C to allow trypsin to permeate the gel pieces prior to digestion while also rehydrating them. Following incubation, 30 µl of digestion buffer (20mM TEAB, 0.5% w/v SDC) was added to each sample and the samples were incubated at 55 ˚C for 30 minutes. This approach exploits the improved thermal stability of proteomics-grade trypsin over native trypsin, and allows for shorter reaction times while also minimizing autolytic digestion of the protease during incubation – a particularly advantageous aspect of the Havlis protocol, as autolytic trypsin peaks can predominate MS spectra in cases where the protein of interest is of either low abundance or is poorly digested by trypsin (or both). The reaction was quenched by addition of 200 µl of 50% acetonitrile and 0.1% formic acid (FA), followed by shaking for two hours at room temperature to extract the digested peptides. The samples were then centrifuged and the peptide-containing supernatant was transferred to a new tube and taken to dryness in a vacuum centrifuge.

The samples were re-suspended in 20 µl of 0.1% FA, and incubated in a bath sonicator for one minute to ensure solubilization of the dried peptides. The samples were then desalted using C18 ZipTips (Merck Millipore, Billerica, MA) to reduce the presence of interfering substances (salts, residual buffers, TCEP, C-AM) prior to MS analysis. Samples were applied to pre-wetted ZipTips by pipetting, followed by washing with 5% methanol in 0.1% FA. Samples were eluted from the ZipTips into clean tubes with 10 µl of 50% acetonitrile, 0.1% FA.

3.2.10 Identification of Proteins from Excised Gel Bands by Chip-based Nano-ESI MS

Peptides were directly infused into the MS (Q-Exactive Orbitrap, ThermoFisher Scientific) using a chip-based nano ESI source (NanomateTriversa, Advion, Ithaca, NY). This approach allowed for sensitive detection and fragmentation of the peptides while eliminating potential carryover issues inherent to standard nano-LC-MS/MS approaches, as the samples are electrosprayed through single-use nozzles on the ESI chip. Combined with the significantly enhanced electrospray efficiency of a chip-based nanospray, this approach is well-suited for MS-based identification of proteins excised from gel bands.

Spectra were acquired using data-dependent acquisition mode (DDA) under the control of Xcalibur software (ThermoFisher Scientific). The method was divided into four segments, each of which were thirty seconds in length, with the MS acquiring data in small, defined m/z range windows in each segment (typically 200-300 m/z wide). These settings allow the MS to acquire more data on lower-abundance peptides than would be obtained if the instrument were to acquire data from a typical full scan m/z range used in proteomic experiments (*e.g.*, 380-1,800 m/z). The ranges used for segments 1-4 were: (1) 300-500 m/z, (2) 500-750 m/z, (3) 750-1,000 m/z), and (4) 1,000 – 1,500 m/z.

Within each segment, a "Top 10" strategy was employed, wherein the top ten most abundant precursor ions (protonated peptides, in this case) within each full-scan MS were selected for fragmentation using higher energy C-trap dissociation (HCD), thus yielding both an intact mass for each peptide as well as a collection of sequence-informative ions in the MS/MS spectra. These are later searched against a database to identify the protein(s) of interest. Additional relevant MS settings were as follows: full scan resolution = 140,000 (at m/z = 200), MS^2 scan resolution = 17,500, isolation width = 2.0 m/z, dynamic exclusion = 30 sec, relative collision energy (rCE) = 32. Dynamic exclusion is a setting that prohibits the instrument from re-fragmenting peptides which have already been fragmented for a defined length of time, thereby avoiding repeated re-sampling the same ten most-abundant peptides. Instead, the MS will trap and fragment the next ten most abundant peptides that are observed in the full scan spectrum until the defined length of time is up.

3.2.11 In-solution Digestion and Tandem Mass Tagging of Keratinocyte Lysate for Quantitative LC-MS/MS Analysis

Tandem mass tagging (TMT) is an isotopic labeling approach that enables simultaneous identification and quantification of hundreds – and often thousands – of proteins from as many as ten samples in a single LC-MS/MS experiment. These labels contain a primary amine-reactive moiety, and derivatize peptides at their N-termini, and in the case of peptides cleaved at lysine resides, at lysine epsilon amino groups. Upon MS/MS fragmentation, the labels are released from their respective peptides (for quantification), while the peptide is also cleaved between amide bonds along the amino acid backbone to yield sequence-informative ions (for identification).

Equal amounts of protein from the keratinocyte lysate of each sample were concentrated by precipitation with the addition of concentrated trichloroacetic acid (TCA)

and acetone to final concentrations of 10% and 75%, respectively, followed by incubation at -20 ˚C for one hour. The precipitated material was pelleted by centrifugation at 20,000g RCF at 4 ˚C for 10 minutes, and the supernatant discarded. The resultant pellet was washed one time with 300 µl of chilled acetone, followed by a second round of centrifugation as performed above. The pellets were resolubilized in 5µl of 2.5X reduction/alkylation/denaturation buffer (20mM TEAB, pH 8.0, 2.5mM TCEP, 7.5mM C-AM, 1.5% w/v SDC,), and incubated at 37 ˚C for 15 minutes. This approach allows for simultaneous reduction and alkylation of Cys-Cys disulfide bonds, while also minimizing the off-target alkylation of non-sulfhydryl moieties often encountered when using higher concentrations of alkylating reagent (*e.g.*, 50 mM iodoacetamide). SDC was used in lieu of conventional lab detergents (*e.g.*, SDS, CHAPS, TWEEN, Triton X-100) as the primary denaturant, as it is compatible with tryptic digestion and can be quantitatively depleted from the reaction buffer following digestion (common lab detergents are difficult to remove from preparations of tryptic peptides and as a result, impede downstream LC-MS analysis).

The samples were then diluted three-fold with addition of 20 mM TEAB, and trypsin added to a final concentration of 1:100 enzyme-to-substrate. The samples we allowed to digest overnight at 37 ˚C. Five µg aliquots of each digest were then derivatized with their respective TMT label (Pierce, Rockville, IL) according to the manufacturer's protocol (adjusted for volume/peptide amount) for two hours at room temperature. The reaction was quenched by addition of triethyl amine, and the sample was pooled and taken to dryness in a vacuum centrifuge. The dried material was re-suspended in 1% FA and sonicated to yield a precipitate of SDC, which was removed by centrifugation. The TMT-labeled peptides were transferred to a new tube, and washed with 300 µl of ethyl acetate to

deplete residual SDC. The upper phase (SDC-containing ethyl acetate) was discarded and the lower phase taken to dryness [110].

3.2.12 2D LC-MS/MS Analysis of TMT-labeled Samples

Offline 2D LC-MS/MS was performed as detailed in Zakirova *et al.* [111]. This approach utilizes two-dimensional reversed phase chromatography as a means to decrease sample complexity prior to its introduction into the MS [112, 113]. In this protocol, the first-dimension separation is performed at high pH, and the analytical separation occurs at low pH. This technique was shown to demonstrate superior orthonogality of separation compared to other two-dimensional chromatographic combinations (*e.g.*, ion exchange/reversed phase, HILIC/reversed phase). Dried, TMT-labeled peptides were re-suspended in 20mM ammonium formate (pH = 10), and applied to C18 reversed phase spin columns that were wetted and equilibrated in the same buffer system. The samples were then eluted into five fractions with stepwise increases of acetonitrile (in increments of 10% acetonitrile, from 10-50%) in 20 mM ammonium formate, pH 10. The samples were then taken to dryness and re-constituted in 20 µl of 0.1% FA and transferred to autosampler vials.

Four µl of each fraction was analyzed by nano-LC-MS/MS using a UPLC1000 nano LC (plumbed in a vented trap/elute configuration) interfaced with a Q-Exactive Orbitrap MS. Samples were applied to a 0.075 x 20 mm C18 PepMap trapping column (3 µm particle size) for online concentration and de-salting, and separated using a 150 x 0.075 mm C18 PepMap column (1.8 µm particle size) over a 2.5 hour linear gradient of increasing concentrations of mobile phase B (99.9% acetonitrile, 0.1% FA) from 2-45% MPB at 300 nl/min. The column temperature was held at 40 ˚C using a Phoenix S and T Butterfly heater.

Major MS settings were as follows: full scan range m/z = 380-1,250, MS^2 scans with minimum m/z = 100, full scan resolution = 140,000 (at m/z =200), MS^2 resolution = 35,000 (at 200 m/z), rCE = 32, dynamic exclusion = 60 seconds, isolation width = 1.2 m/z. Two key features of this MS method are (1) the high resolution used in the MS^2 scans, and (2) the relatively narrow isolation window when trapping peptide for HCD MS/MS. The high, and consequently slower than normal, resolution setting is needed to ensure the baseline resolution of TMT reporter ion peaks from which the relative quantification of proteins across samples is derived. These peaks differ by 0.07 Da, and therefore the lower resolution settings typically used in shotgun proteomics would not allow for their separation. As for the narrow isolation window of 1.2 m/z, this is used to minimize the possibility that two parent ions (peptides) are co-isolated and fragmented. While it is a relatively simple task for most software platforms to identify both peptides from these chimeric MS/MS spectra, it is impossible to assign the relative amount of reporter signal to their respective parent ions, which results in quantitative inaccuracies that stem from reporter ion signal compression.

3.2.13 Identification of Stiffness Regulated Proteins via LC-MS/MS

Samples were analyzed using liquid chromatography–mass spectrometry (LC-MS/MS) (Q-Exactive). PMi Preview software was used to survey the data files and results were used to choose the precursor and fragment ion mass tolerances (4 ppm, 0.02 Da, respectively) as well as dynamic modifications. Uniprot Human database was used (downloaded in May 2015). The following settings were used to search the data using SEQUEST and MSAMANDA as the search algorithms: dynamic modification; oxidation / +15.995 Da (M), static modifications of TMT6plex / +229.163 Da (N-Terminus, K),

Carbamidomethyl +57.021 (C). Proteome Discoverer (PD) setting unique+razor was used to choose peptides for quantification. In quantitation, node normalization mode was set to total peptide amount, which sums the peptide group abundances for each sample and determines the maximum sum for all files. A normalization factor was then calculated from the sum of the sample and the maximum sum in all files. The co-isolation threshold was set to 50%. Both for SEQUEST and MSAMANDA the Percolator feature of PD was used to set a false discovery rate (FDR) of 0.01. Peptides passing this cutoff value were exported to JMP 8.0.2 (SAS, Cary, NC) for data cleaning and statistical analysis. Proteins identified in all biological replicates were used for quantitative analysis. PD was used to calculate abundance ratio per experimental category for each protein. After transformation of the raw ratios, t-tests were used to test differences sample means. Benjamini Hochberg method was used for multiple test correction (false discovery rate= 0.25).

3.2.14 Western blot

Western blots for specific proteins of interest were conducted to provide confirmation of the proteomics results. Separated protein was transferred electrophoretically to pure nitrocellulose membranes (thickness = 0.045 μm). Each blot was treated with primary antibodies, rabbit polyclonal anti-transferrin (Thermo Fisher) and mouse monoclonal cytokeratin 10, and then reacted with secondary antibodies, rabbit IgG (H&L) secondary antibody IRDye800CW® conjugated (Rockland Immunochemicals) and mouse IgG (H&L) antibody IRDye700DX® conjugated (Rockland Immunochemicals), respectively. The immunoreactive proteins were detected by scanning on an Odyssy Li-COR (Li-COR Biosciences) and the relative density of each band was determined using Image Studio software.

3.2.15 Statistical Analysis

Statistical significance ($p < 0.05$) was determined by performing either two way ANOVA or Student's t test with *post-hoc* Tukey analysis in Prism (GraphPad Software, Inc., La Jolla, CA).

3.3 RESULTS

3.3.1 Cell Number and Morphology

The addition of Y27632 to the medium rapidly changed cell morphology on both soft and stiff gels (Figure 14).

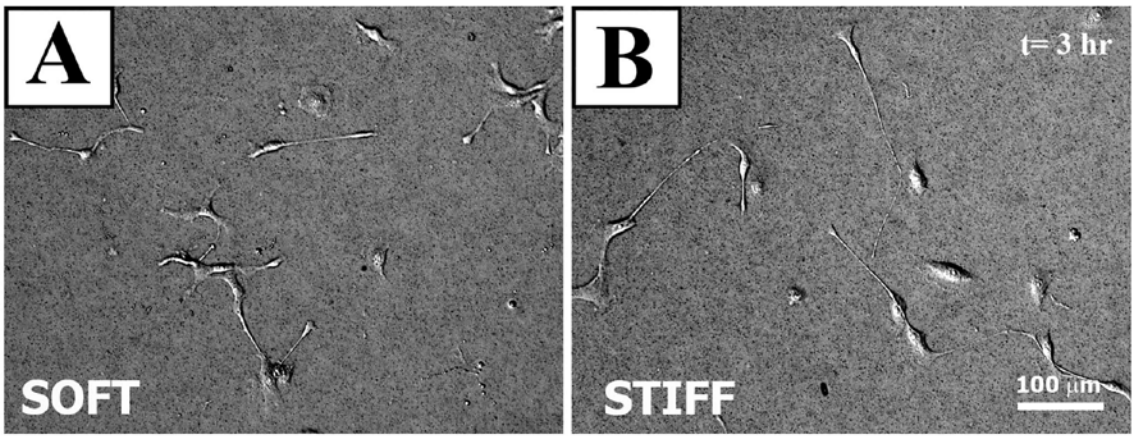

Figure 14. Keratinocytes morphological changes three hours after treatment with Y27632 on A) soft and B) stiff substrates. The cells developed thin, highly extended and flexible processes in response to Y27632.

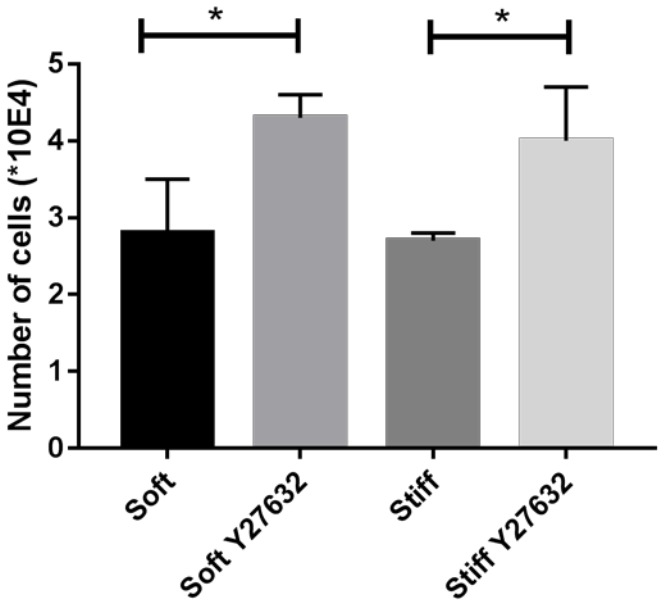

Figure 15. Average number of cells 24 hr after treating keratinocytes with 10 µM Y27632 drug in treated and non-treated samples.

Total cell number (Figure 15) was approximately 1.5 time higher after 24 hr for Y27632 treated soft and stiff gels compared to controls ($p < 0.001$). No significant difference was found between untreated soft and stiff samples ($p = 0.67$).

3.3.2 Aggregate Formation Analysis

The effects of Y27632 on keratinocyte aggregate formation on soft and stiff substrate were assessed by imaging and tracking the keratinocytes during aggregate formation.

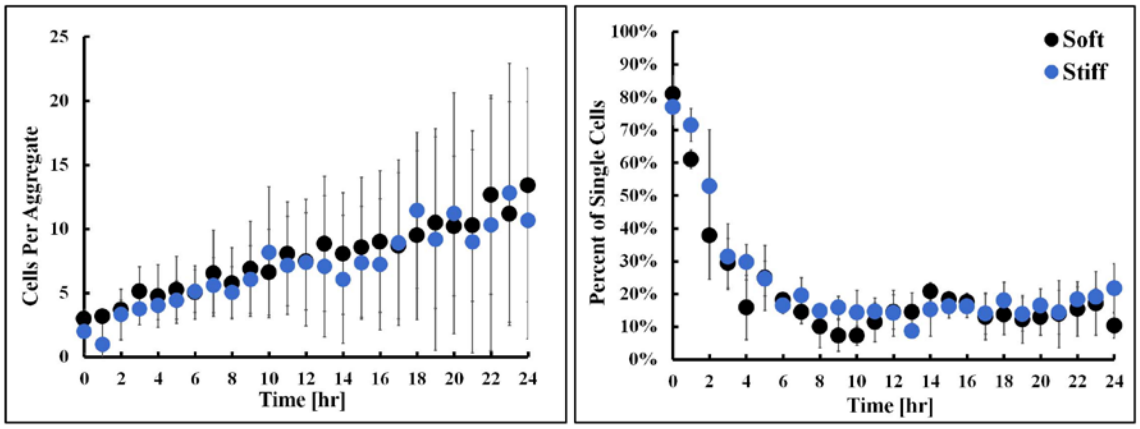

Figure 16. Number of cells per aggregate and percentage of single cells over time in soft and stiff, Y27632 treated and non-treated samples.

The simultaneous addition of $CaCl_2$ to the medium induced the keratinocytes to form aggregates (Figure 16). Neither the number of cells per aggregate ($p = 0.12$) or the number of single cells ($p = 0.38$) differed significantly between soft and stiff gels. These results indicate that Y27632 eliminates the differences in aggregate formation previously observed on soft and stiff gels [32].

3.3.3 Substrate Displacements During Aggregate Formation

Substrate deformations in the soft PA gel in the first three hours was comparable to what was reported previously [32]. The addition of Y27632 rapidly reduced soft substrate displacements compared to controls (Figure 17). In Y27632 treated samples, the average displacements ranged from a maximum of 8.79 ± 4.55 μm at t = 0 hr to a minimum of 3.44 ± 2.07 μm, 35 minutes after adding the Y27632. As aggregates formed, substrate displacements gradually increased to 6.75 ± 4.54 μm at t = 24 hr. Previously, untreated HEKn on soft gels produced average displacements ranging from 8.5 ± 5.0 μm at t = 0 hr to 28.2 ± 15.7 μm at t = 24 hr. In those samples the single largest displacements tracked was 73.8 μm, which occurred at t = 24 hr. Here, the single largest displacement was five times lower at 23.63 μm at t = 0 (Figure 17).

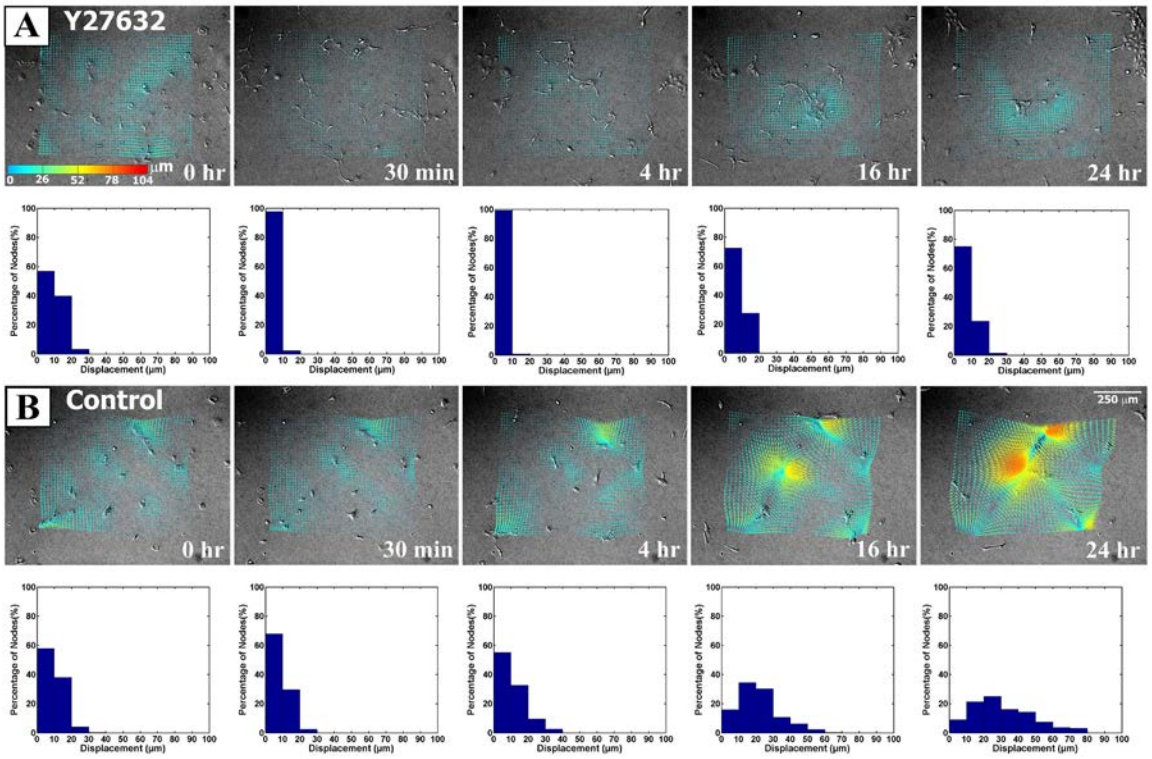

Figure 17. Substrate displacements made by the (A) Y27632 treated and (B) non-treated keratinocytes at the indicated time points. Color maps of the displacement fields, as well as histograms of substrate displacement magnitudes show that Y27632 substantially reduced cell traction forces.

3.3.4 Silver Stain

Because quantitative differences in HEKn behavior on soft and stiff gels exist, and disruption of the Rho/ROCK pathway with Y27632 eliminated these substrate-stiffness dependent differences, we hypothesized that differences in protein expression between the two conditions also likely exists. In order to quickly screen for such putative differences, HEKn protein lysate from soft stiff gels was obtained at t = 24 hr, separated by size via SDS-PAGE, and then silver stained in order to detect differential protein expression for low abundance proteins [114] (Figure 18).

The first three bands adjacent to the ladder show the profile of proteins extracted from three separate soft gel experiments. The next four bands show the profile for four separate stiff gel experiments. Several bands, as indicated by red dots between the ladder

and the samples of interest, appeared to show differential protein expression (Figure 18). Densitometry analysis on these bands indicted that protein in the 70-85 kDa had the greatest difference between conditions (Figure 19). Therefore, as a starting point, we performed a direct infusion proteomics analysis on this band from one soft gel in order to identify the protein in this band.

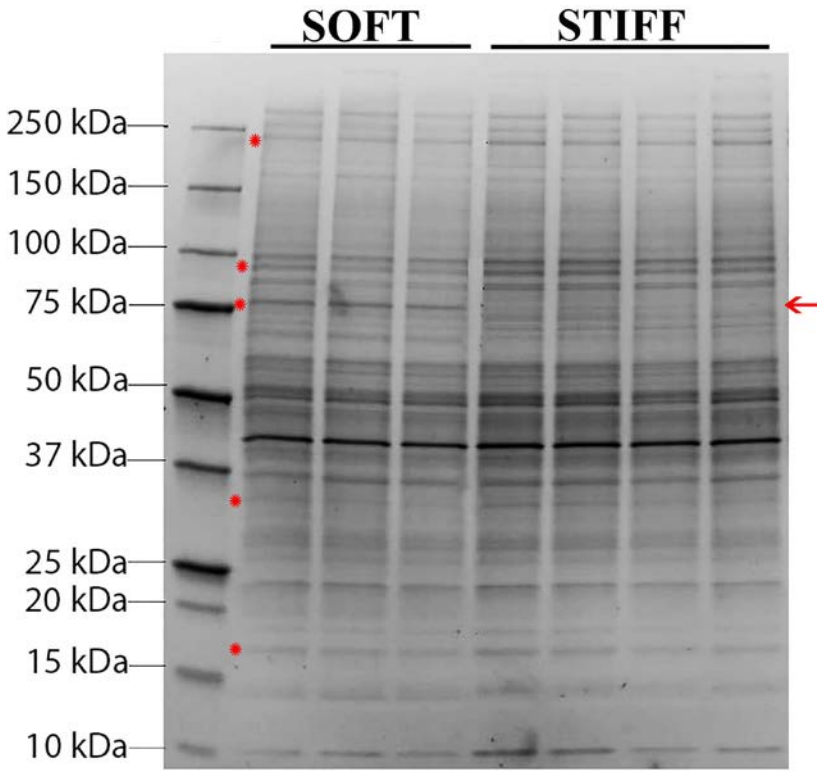

Figure 18. Silver Stain image of the SDS-page loaded with protein lysates from soft and stiff substrates. Red dots indicate bands that appear to indicate differential protein expression. The red arrow shows the prominent band around 77 kDa molecular weight.

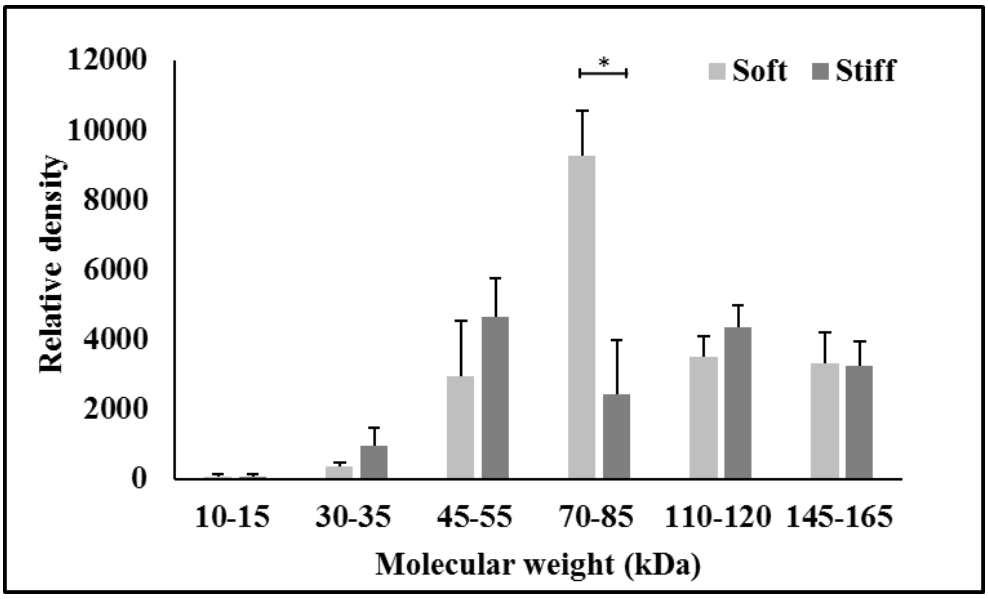

Figure 19. Densitometry on silver stained SDS-PAGE gel of Figure 18. A significant difference in protein expression was found for the band in the 70-85 kDa range.

3.3.5 Direct Infusion

The 70-85 kDa band for one of the soft gel samples was removed and the constituent protein identified via direct infusion. Several proteins were identified from their peptide fragments (**Error! Reference source not found.**). Serotransferrin was identified as the most likely candidate based on coverage and the number of unique peptides detected. Western blots confirmed that this protein was indeed present and differentially expressed (Figure 20). Densitometry analysis on these bands indicated that the abundance of serotransferrin on soft gels was twice that on stiff gels.

Table 4. Direct infusion results

	Checked	Mas	Accession	Description	Coverage	# Peptides	# PSMs	# Unique Peptides	# Protein Groups	# AAs	MW [kDa]	calc. pI
1	☐	✓	Q96GX8	Uncharacterized protein C16orf74 OS=Homo sapiens GN=(	59%	1	2	1	1	76	8.1	4.35
2	☐	✓	P42702	Leukemia inhibitory factor receptor OS=Homo sapiens GN=	2%	1	1	1	1	1097	123.7	5.72
3	☐	✓	P35908	Keratin, type II cytoskeletal 2 epidermal OS=Homo sapiens	12%	7	8	6	1	639	65.4	8.00
4	☐	✓	Q96T55	Potassium channel subfamily K member 16 OS=Homo sapi	8%	1	1	1	1	309	34.1	8.63
5	☐	✓	P11021	78 kDa glucose-regulated protein OS=Homo sapiens GN=H	8%	4	4	4	1	654	72.3	5.16
6	☐	✓	P02787	Serotransferrin OS=Homo sapiens GN=TF PE=1 SV=3	15%	8	9	8	1	698	77.0	7.12
7	☐	✓	P04264	Keratin, type II cytoskeletal 1 OS=Homo sapiens GN=KRT1	11%	6	6	5	1	644	66.0	8.12
8	☐	✓	Q6NT55	Cytochrome P450 4F22 OS=Homo sapiens GN=CYP4F22 I	5%	1	1	1	1	531	61.9	8.73
9	☐	✓	P13645	Keratin, type I cytoskeletal 10 OS=Homo sapiens GN=KRT1	15%	7	8	7	1	584	58.8	5.21
10	☐		P48668	Keratin, type II cytoskeletal 6C OS=Homo sapiens GN=KRT	2%	1	1	1	1	564	60.0	8.00
11	☐		P19012	Keratin, type I cytoskeletal 15 OS=Homo sapiens GN=KRT1	2%	1	2	1	1	456	49.2	4.77
12	☐		O95399	Urotensin-2 OS=Homo sapiens GN=UTS2 PE=1 SV=1	6%	1	1	1	1	124	14.3	7.80
13	☐		P13646	Keratin, type I cytoskeletal 13 OS=Homo sapiens GN=KRT1	4%	2	3	2	1	458	49.6	4.96
14	☐		Q04695	Keratin, type I cytoskeletal 17 OS=Homo sapiens GN=KRT1	2%	1	2	1	1	432	48.1	5.02
15	☐		P19013	Keratin, type II cytoskeletal 4 OS=Homo sapiens GN=KRT4	2%	1	1	1	1	534	57.2	6.61

.

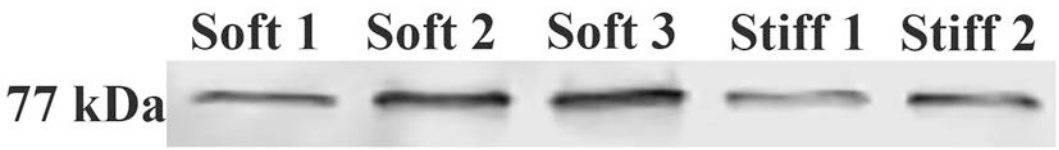

Figure 20. Western blot for serotransferrin. The band for serotransferrin presentes at 77 kDa molecular weight. The bands are darker on soft samples (n=3) compared to stiff ones (n=2).

3.3.6 2D LC-MS/MS Analysis of TMT-labeled Samples

A full analysis was performed on protein lysates from soft and stiff gels in order to obtain a more comprehensive view of other differences in protein expression. A total of 1,179 proteins, 846 protein groups, and 1641 peptide groups were identified in the cell lysates. Of these, 467 proteins were further excluded from the analysis because the peptides used to identify these proteins were not unique. The relative abundance of the remaining 712 proteins was calculated and sorted according to the t-test p-values. 56 proteins were identified with p-values less than 0.05 (Table 5). Forty of these proteins were more abundant on stiff gels with an abundance ratio (AR) less than 1 (AR < 1), and 16 were more abundant on soft gels (AR > 1).

Table 5. List of identified proteins differentially expressed and sorted from lowest to highest for p-values < 0.05 first for AR >, followed by AR < 1

Accession	Description	AR (soft/stiff)	P-value
P28331	NADH-ubiquinone oxidoreductase 75 kDa subunit, mitochondrial	1.31	0.005
P02787	Serotransferrin	1.57	0.009
H0YAA0	Uncharacterized protein (Fragment)	1.42	0.010
P07437	Tubulin beta chain	1.44	0.011
P62851	40S ribosomal protein S25	1.54	0.013
Q969M3	Protein YIPF5	1.22	0.016
P31943	Heterogeneous nuclear ribonucleoprotein H	1.57	0.028
Q13630	GDP-L-fucose synthase	1.52	0.028
Q14534	Squalene monooxygenase	1.58	0.029
P08758	Annexin A5	1.31	0.038
Q5VSL9	Striatin-interacting protein 1	1.54	0.039
Q9Y5F2	Protocadherin beta-11	2.04	0.041
P21333	Filamin-A	1.55	0.042
P12270	Nucleoprotein TPR	1.23	0.043
P00491	Purine nucleoside phosphorylase	1.63	0.048
Q09666	Neuroblast differentiation-associated protein AHNAK	1.28	0.049
P49368	T-complex protein 1 subunit gamma	0.54	0.000
Q15717	ELAV-like protein 1	0.79	0.000
Q15393	Splicing factor 3B subunit 3	0.82	0.000
P68363	Tubulin alpha-1B chain	0.79	0.002
Q01085	Nucleolysin TIAR	0.64	0.002
Q9Y320	Thioredoxin-related transmembrane protein 2	0.77	0.006
P17844	Probable ATP-dependent RNA helicase DDX5	0.54	0.011
O94906	Pre-mRNA-processing factor 6	0.51	0.011
P52209	6-phosphogluconate dehydrogenase, decarboxylating	0.77	0.012
A6NDG6	Phosphoglycolate phosphatase	0.75	0.014
Q16629	Serine-arginine-rich splicing factor 7	0.64	0.016
Q16222	UDP-N-acetylhexosamine pyrophosphorylase	0.65	0.016
P17980	26S protease regulatory subunit 6A	0.44	0.017
Q04637	Eukaryotic translation initiation factor 4 gamma 1	0.68	0.018
P60842	Eukaryotic initiation factor 4A-I	0.86	0.018
P61221	ATP-binding cassette sub-family E member 1	0.68	0.019
Q9Y3F4	Serine-threonine kinase receptor-associated protein	0.45	0.020
Q99426	Tubulin-folding cofactor B	0.70	0.020
P57088	Transmembrane protein 33	0.48	0.024
Q15370	Transcription elongation factor B polypeptide 2	0.77	0.025
P17987	T-complex protein 1 subunit alpha	0.61	0.026
P11216	Glycogen phosphorylase, brain form	0.79	0.026
Q9UQE7	Structural maintenance of chromosomes protein 3	0.89	0.028
P26599	Polypyrimidine tract-binding protein 1	0.68	0.029

Table 5-continued

O75083	WD repeat-containing protein 1	0.79	0.031
P09211	Glutathione S-transferase P	0.67	0.032
P04843	Dolichyl-diphosphooligosaccharide--protein glycosyltransferase subunit 1	0.89	0.033
Q99798	Aconitate hydratase, mitochondrial	0.73	0.038
Q9NTZ6	RNA-binding protein 12	0.64	0.038
Q5JXB2	Putative ubiquitin-conjugating enzyme E2 N-like	0.50	0.039
Q16851	UTP--glucose-1-phosphate uridylyltransferase	0.73	0.040
Q92747	Actin-related protein 2-3 complex subunit 1A	0.68	0.040
Q9HB71	Calcyclin-binding protein	0.48	0.043
Q15738	Sterol-4-alpha-carboxylate 3-dehydrogenase, decarboxylating	0.78	0.043
Q02750	Dual specificity mitogen-activated protein kinase kinase 1	0.74	0.044
P62820	Ras-related protein Rab-1A	0.67	0.047
O95782	AP-2 complex subunit alpha-1	0.74	0.048
O00487	26S proteasome non-ATPase regulatory subunit 14	0.68	0.048
Q96PK6	RNA-binding protein 14	0.54	0.049
O60506	Heterogeneous nuclear ribonucleoprotein Q	0.70	0.050

3.4 DISCUSSION

Several studies have indicated that keratinocytes proliferation, differentiation, and migration, the major cell processes involved in re-epithelialization, are affected by substrate stiffness [29, 32, 34, 72]. I hypothesize that changes in the stiffness/mechanical properties of the wound bed during the healing process also affect and regulate keratinocyte behavior. As a corollary, if the mechanical properties of the wound bed deviate from some normal physiological range of values, then an aberrant wound healing process with delayed re-epithelialization unfolds and manifests as a chronic wound. Some evidence for this idea can be found in the fact that a common feature of chronic wounds is a sclerotic, or stiffened, dermal extracellular matrix (ECM) at the margins of the wound bed [6, 7]. In order to better understand how mechanical cues regulate keratinocyte behavior, I analyzed how modulating cytoskeletal force generation via the administration of the rho-kinase inhibitor Y27632 removed the influence of substrate stiffness on keratinocyte behavior. Then, a

comprehensive proteomics analysis was done in order to identify which proteins were differentially expressed on the two substrates.

Previously, I observed significantly higher rates of aggregate formation on soft gels versus stiff ones [32]. I attributed this behavior to enhanced mechanical signaling between cells and aggregates via deformations in the PA gel. These deformations provided mechanical cues that directed the cells to join to together and form cell-cell junctions. I reasoned that if these mechanical cues were blocked then cell behavior, including the rate of aggregate formation, should be independent of substrate displacement. To test this idea, I used Y27632 and found that differences in the rate of aggregate formation vanished. In addition, the presence of Y27632 significantly reduced substrate deformations, and thus force generation by the keratinocytes. Y27632 is a non-specific rho-kinase inhibitor that blocks ROCK, which in turn prevents recruitment of actin filaments and reduces cell traction forces.

Previous studies have reported an increase in the directed migration of keratinocytes and their ability to more rapidly cover the gap in a scratch wound healing assay in the presence of Y27632 [107, 115]. RhoA-null keratinocytes showed impaired directional migration in the assay [107]. It is possible that Y27632 also increased the persistence time (*i.e.*, the characteristic time in which a cell undergoing a random walk will appear to be moving in a directed manner) of keratinocytes on both soft and stiff gels in this study, which could have overridden any putative mechanical cues that drove aggregate formation on the soft gels. In contrast, Sarkar *et al*. indicated the absence of any significant effect of Y27632 on keratinocyte migration [116]. They also observed that Y27632 induced

morphological changes, such as large membrane ruffles and elongated tails, that were consistent with my observations [116].

In addition to changes in migration, Y27632 can also alter keratinocyte proliferation and differentiation [42, 43, 115, 117-119]. McMullan *et al*. reported that Y27632 increased keratinocyte proliferation [43], a result consistent with this study. McMullan *et al.* also reported that keratinocyte differentiation is regulated by Rho/ROCK signaling. Keratinocyte terminal differentiation, assessed by the presence of involucrin, a protein present in the cornified envelope, decreased in response to the irreversible inactivation of Rho via the addition of the chemical C3 [43].

Others have reported that keratinocytes terminal differentiation can be triggered by culture on a soft substrate [29, 34, 120]. In my previous work I also saw indicators of terminal differentiation on soft PA gels compared to stiff [32]. Lock *et al*. [42] found that the ROCK isoforms ROCK 1 and ROCK 2 play different roles in keratinocyte behavior. Knockdown of ROCK 1 eliminated expression of keratin 5, which is expressed in basal keratinocytes, in 2 days post-confluence cultures, whereas knockdown of ROCK 2 eliminated expression of keratin 10, which is expressed in terminally differentiated keratinocytes. ROCK 1 knockdowns also had significantly elevated involucrin, another maker for terminal differentiation, compared to controls and ROCK 2 knockdowns had significantly less. Adhesion to fibronectin was dependent on ROCK isoform expression, but adhesion to collagen IV and laminin 332 was not.

Although these results are supportive of my overall hypothesis, formation rate could be an evidence of the role of Rho kinases in mechanosensing pathway of keratinocytes and its potential role in their proliferation and differentiation.

In order to achieve all-inclusive protein identification I performed broad-spectrum proteomics to investigate the proteins expressed differently on substrate with different stiffnesses. Protein lysates from three soft and three stiff samples were analyzed by LC-MS/MS (Q-Exactive). A total number of 56 proteins were expressed significantly different in soft and stiff substrate samples. 40 proteins expressed higher in stiff and 16 proteins expressed higher in soft, which may indicate that in general proteins are expressed higher in stiff versus the soft substrate. There are several hints in the presented proteomics results as the protein candidates that would be a part of keratinocytes mechanosensing pathways or could be altered in response to substrate stiffness: proteins in metabolic processes, mitochondrial or ribosomal proteins, and also nucleus and RNA transcriptional proteins. Finding the potential contribution of these proteins requires further studies.

One of the most prominent protein candidates which both silver stain and proteomics results indicated to be expressed higher in soft versus stiff substrates was serotransferrin. My preliminary results performing western blot for serotransferrin also confirmed the presence of serrotransferrin, probably higher in soft samples, in cell lysates.

Serotransferrin, also known shortly as transferrin, is an iron binding protein that transport iron from the sites of absorption (duodenum) and red blood cell recycling macrophages to the regions of iron metabolism [121, 122] particularly tissue involved in erythropoiesis and the tissues with actively dividing cells [122]. Transferrin binds ferric ions in the bloodstream and transports this bound iron to cells where it is released by a process of receptor-mediated endocytosis [123]. The main source of transferrin is the liver [124, 125]. Other organs have been reported to produce transferrin including testis [126] and brain [127-129]. *In vitro*, transferrin has been a component of cell media to support

cell proliferation and differentiation and as an antioxidant [122, 130, 131]. The keratinocyte serum free medium used in my studies also contains about 10 μM of transferrin according to the provider company. I believe that the transferrin presented in protein lysate of the cells is probably the outcome of transferrin endocytosis since to the best of my knowledge there is no evidence of transferrin produced by keratinocyte cells.

Remarkably, previous studies reported the effect of actin organization in the amount of transferrin uptake by the cells [132-135]. Endocytosis relies on rearrangement of the cortical actin filament that lies directly underneath the plasma membrane. Studies with actin-depolymerizing agents have shown that minor de-polymerization of the actin cytoskeleton can stimulate endocytosis. However, greater depolarization of actin was found to prevent endocytosis. These results indicated the effect of local actin remodeling on endocytosis, which could be a combination of polymerization and de-polymerization [135]. Enhanced actin polymerization as well as the highly organized actin filaments formed in the cells cultured on the stiff substrate versus the soft ones could make the process of transferrin endocytosis easier in these cells. Hence, the higher levels of transferrin detected in the cells on the soft substrate could be due to the elevated transferrin uptake in these cells.

In addition, previous studies reported the elevation of transferrin-mediated iron uptake in proliferating and differentiating cells [122, 131, 136-138]. Transferrin could provide the iron needed for the cell proliferation and also works as an antioxidant in metabolically active cells [139]. One would speculate the increased levels of serotransferrin in the cells cultured on soft substrate could be due to higher rates of cell proliferation. However my cells-counting results did not show any significance difference in the number

of cells in soft and stiff substrates. Others and my previous studies have shown the presence of differentiation markers in the keratinocytes on the soft substrate. Yet to the best of my knowledge no one reported the elevated levels of transferrin uptake in differentiating keratinocytes.

There are also evidences of impairment of transferrin uptake by human malignant keratinocytes under oxidative stress [140]. Activated forms of Rac and Rho have been shown to inhibit transferrin-receptor-mediated endocytosis of transferrin [141-144]. Further analysis should be provided to seek these possibilities as well.

3.5 CONCLUSION

In this work, I sought if substrate stiffness modulate protein expression in keratinocytes. I used Y27632 to inhibit Rho kinase proteins in soft and stiff substrates. Treating cells with Y27632 impaired keratinocytes ability to generate deformation in the underlying substrates. The significant difference in the rate of aggregate formation observed in the absence of Y27632 was vanished after the treatment with Y27632. These results hint the role of Rho kinases in keratinocyte mechanostransduction and force generation.

Proteomics analysis was performed to achieve all-inclusive protein identification of the protein lysate from keratinocytes on soft and stiff substrates. The results indicate 56 protein candidates being expressed differently in soft and stiff samples. Serotransferrin is the most prominent protein candidate present higher in soft versus stiff lysates. I believe that this observation is probability a result of different endocytosis levels of transferrin presented in the cells medium on soft and stiff substrates. Further analysis needs to be performed to verify the presence of higher levels of serotransferrin in soft samples and the

reasoning behind that. In addition, further investigations needs to be performed on the rest of the protein candidates probably being expressed differently in soft and stiff samples.

Together my results indicated the importance of Rho kinases in keratinocyte mechanotransduction and force generation. I also provided a list of protein candidates probably being expressed differently in soft and stiff substrates.

3.6 ACKNOWLEDGEMENTS

Support for this work was provided by the National Science Foundation (National Science Foundation CAREER CMMI 1452728) and the Carver Charitable Trust (#14-4384). I would like to thank James Evans, Jon Mike Reed, and Gogce Crynen for performing proteomics. I also thank Sathivel Chinnathambi for performing Western Blot and help in proteomics sample preparation.

Chapter IV. MOUSE KERATINOCYTES WITH MUTED KERATIN INTERMEDIATE FILAMENTS DEMONSTRATE SUBSTRATE STIFFNESS DEPENDENT AGGREGATE FORMING CAPACITY

4.1 INTRODUCTION

Cells interact dynamically with the extracellular matrix (ECM) in a manner dependent on the mechanical properties of the microenvironment. These mechanical interactions play an important role in cell morphology [31, 32, 145-147], migration [31, 32, 34, 148], proliferation [34], differentiation [29, 33, 34], apoptosis [148], force generation [38], and ECM remodeling [32, 38].

Cells primarily interact mechanically with the ECM through integrin-rich anchoring junctions, including hemidesmosomes and focal adhesions [40]. Integrins are transmembrane receptors that connect the ECM to the cytoskeleton. It is well-established that actin-bound integrins play an essential role in cell mechanosensing and force generation [149]; however, whether intermediate filament (IF)-bound integrins, such as the keratins prominent in keratinocytes, play similar roles remains unclear.

Keratin IFs are known to provide mechanical support to the plasma membrane and cell body [150], and they maintain the integrity of the epidermis and dermal-epidermal junction through desmosomal and hemi-desmosomal adhesions, respectively [9]. Two major integrins found in focal adhesions are $\alpha_3\beta_1$ and $\alpha_2\beta_1$ whose ligands are laminin-332 and collagen type I, respectively. The only known integrin that connects ECM to keratin filaments is $\alpha_6\beta_4$. This integrin along with CD151, plectin, the bullouse pemphigoid proteins BP180 and BP230, and laminin 332, forms a hemidesmosome [151]. Recent evidence suggests that deep interactions between focal adhesions and hemidesmosomes, specifically with respect to dynamic cell processes, such as cell migration and re-epithelialization [44, 45], exist and may be mediated by plectin [44, 45, 49]. Seltman *et al.* used keratin muted mouse keratinocytes to investigate how the absence of keratin IF

affected hemidesmosomal complex formation and keratinocyte migration [152]. They reported that the knock out (KO) cells lost their ability to form stable hemidesmosome due to altered localization of the hemidesmosomal proteins plectin and $\alpha_6\beta_4$. In another study, it was shown that muting keratin 8/18 in hepatic epithelial cells altered the response of the cells to substrate stiffness and actin filament organization [10].

Previously, I investigated the effects of substrate stiffness on human keratinocyte morphology, migration, and aggregate formation [32]. I found that keratinocytes behaved differently on soft (~1.2 kPa) polyacrylamide (PA) gels compared to stiff (~24 kPa) gels, particularly with respect to the process of forming aggregates, which appeared more directed, possibly due to mechanical communication through the substrate. In this work, using the same methodology, I investigated the role of keratin IFs in keratinocyte force generation and aggregate formation by comparing the performance of keratin muted (KO) and wild type (WT) mouse keratinocytes. My results demonstrate a significant change in the ability of KO cells to spread out, form actin filaments, deform the substrate, and join into multi-cellular aggregates.

4.2 MATERIAL AND METHODS

4.2.1 Cell Culture

WT and KO mouse keratinocytes with muted expression for all type I keratin chains were obtained as a kind gift from Prof. Thomas Magin (University of Leipzig). The isolation of primary mouse keratinocytes of KO and WT cells and their characterization is described elsewhere [153]. Keratinocytes were cultured on type I rat tail collagen (Invitrogen, Carlsbad, CA) coated cell culture dishes and maintained in an incubator with

95%/5% air/CO_2 at 37 °C. Cells were cultured in DMEM/Ham's F12 (F 9092-0.46: Biochrom Ltd., Cambourne, United Kingdom), supplemented with chelex-treated (Chelex 100 Resin, Bio-Rad, Hercules, CA) 10% fetal bovine serum (Gibco/ThermoFisher Scientific, Waltham, MA) [154], 0.18 mM adenine (Sigma Aldrich), 0.5 mg/ml hydrocortisone (Sigma Aldrich), 2.5 µg/ml insulin (Sigma Aldrich), 100 pM cholera toxin (Sigma Aldrich), 10 ng/ml EGF (Gibco/ThermoFisher), 2 mM glutamax (Gibco/ThermoFisher), and 1 mM sodium pyruvate (Gibco/ThermoFisher).

4.2.2 Polyacrylamide Gels

Polyacrylamide (PA) gels measuring approximately 100 µm in thickness were polymerized onto the surfaces of No. 1 glass cover slips as described previously [31, 32]. Briefly, ratios of 2% acrylamide/0.25% bis-acrylamide and 7.5% acrylamide/0.3% bis-acrylamide were used to fabricate soft and stiff PA gels with nominal stiffnesses of 1.2 kPa and 24 kPa, respectively. 0.5 µm diameter FluoSpheres® carboxylate-modified microspheres (#F8812, Life Technologies/ThermoFisher Scientific) were embedded in the gels. Pepsin digested type I collagen (Advanced Biomatrix, Carlsbad, CA) was crosslinked to the surface of the gels using Sulfo-SANPAH. The gels were then sterilized under UV light for 15 minutes and stored at 4 °C for later use.

4.2.3 Time-Lapse Live Cell Imaging: Aggregate Formation & Substrate Displacement Tracking

Cells were trypsinized and resuspended in the culture medium described above except that the calcium concentration was increased to 1.2 mM (*i.e.*, high Ca^{2+} medium) in order to induce keratinocyte aggregate formation *via* the calcium switch [81]. The cells were then plated onto the gels at the density of 16,000 cells/cm^2. Time-lapse live cell imaging was carried out using a Nikon Eclipse Ti inverted microscope equipped with a

Perfect Focus System (PFS). Gels were positioned inside of a micro-environmental gas chamber (H201 Gas Chamber, Okolab, Pozzuoli, Italy) positioned within a cage incubator that fits over the microscope stage. This system maintains a temperature of 37 °C and humidified air with 5% CO_2. Differential interference contrast (DIC) images were acquired for each gel every 5 minutes for 24 hours. Accompanying fluorescent images were also taken in order to measure substrate displacements.

The ability of keratinocytes to join into aggregates was determined by counting the number of single cells remaining in the field over time. The number of single cells present in the microscope field was counted manually every hour over the 24 hour period of the experiment. Four conditions spanning either soft or stiff PA gels and either KO or WT mouse keratinocytes were each examined in triplicate. The effect of substrate stiffness on KO and WT keratinocytes cell morphology was also assessed by measuring the surface area of single cells via ImageJ (National Institutes of Health, Bethesda, MD). Substrate displacement fields on soft PA gels were calculated by tracking microsphere displacements with a custom template matching digital image correlation algorithm [32, 65]. All displacement tracking and visualization was done in MATLAB. Note that substrate displacements on stiff gels were too small to track.

4.2.4 Immunofluorescence

In order to visualize actin formation, in a parallel sets of experiments, WT and KO cells were fixed with 0.4% paraformaldehyde for 1 hr at room temperature at the 3 hr, 6 hr, and 24 hr time points. The cells were then permeabilized using 0.1% Triton-X for 10 minutes. A 1:40 ratio of the phalloidin (Alexa Fluor® 594 dye, Life Technologies/ThermoFisher Scientific) was applied to the cells for 90 minutes at 37 °C.

The samples were then washed with PBS for 20 minutes and mounted onto microscope slides with Prolong® Gold Antifade Mountant with DAPI (Life Technologies) in order to visualize keratinocyte nuclei. Immunofluorescence images were acquired using a Nikon Ti-Eclipse inverted C2 laser scanning confocal microscope.

4.2.5 Statistical Analysis

Statistical analysis was conducted in Prism (GraphPad Software, Inc., La Jolla, CA) using two-way ANOVA with cell type (KO/WT), stiffness (soft/stiff), and time as co-factors.

4.3 RESULTS

4.3.1 Substrate Stiffness Affects Cell Morphology and Cytoskeletal Structure

Both WT and KO keratinocytes attached to the PA gels within an hour of plating and began migrating, making contact with the neighboring cells, and forming aggregates. This process unfolded in a manner that was dependent on cell phenotype and substrate stiffness (Figure 21). On soft gels, KO keratinocytes were more rounded, less spread out, and possessed smaller lamellipodium compared to WT keratinocytes (Figure 21). On stiff gels, the single cell area of both KO and WT keratinocytes ranged between 1.4 and 2.4 times greater than the area on soft gels. On both soft and stiff gels, single cell area was significantly smaller ($p < 0.001$) for KO compared to WT (Table 6).

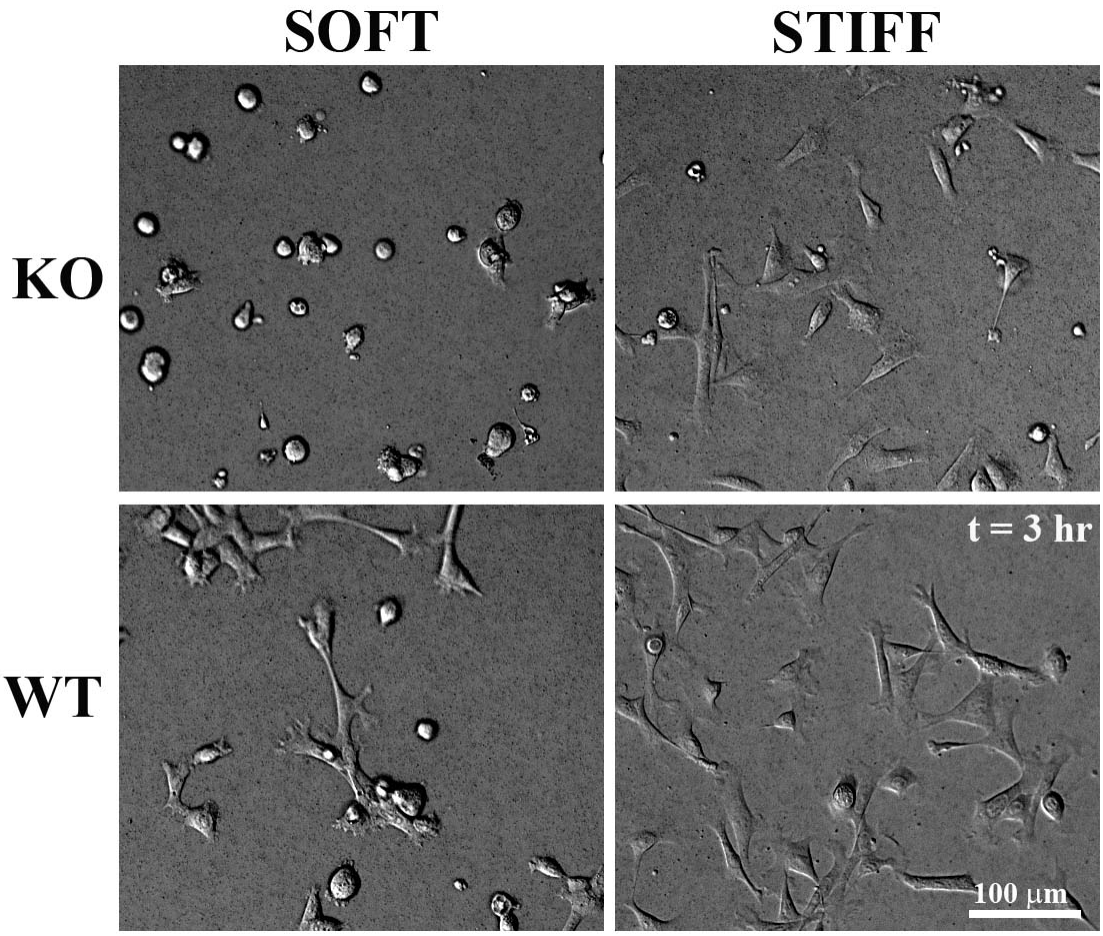

Figure 21. KO and WT cell morphology on soft and stiff substrate three hours after plating the cells onto the PA gels. KO cells on soft PA gels are more rounded with fewer protrusions compared to WT and stiff gels.

Table 6. Single cell area over time for each condition

	Cell Area ($x10^3$ μm^2)				
Condition	1 hr	2 hr	4 hr	8 hr	12 hr
Soft WT	6.3 ± 3.27	7.01 ± 6.47	6.46 ± 3.09	9.05 ± 4.86	12.33 ± 6.07
Soft KO	4.13 ± 2.31	4.62 ± 2.19	4.72 ± 2.18	4.20 ± 2.13	5.12 ± 2.53
Stiff WT	11.29 ± 5.59	11.67 ± 6.22	11.97 ± 5.06	13.46 ± 7.02	13.38 ± 5.15
Stiff KO	6.97 ± 4.22	6.83 ± 3.75	7.07 ± 3.33	7.99 ± 5.56	7.51 ± 5.02

Differences in actin cytoskeleton organization were also observed on soft and stiff PA gels (Figure 22). WT on stiff gels had fully formed actin filaments, both as single cells and as part of an aggregate. WT on soft gels also possessed well-formed actin filaments.

The filaments, however, were not as prominent as WT on stiff gels. Actin filaments for KO on soft gels were the least prominent and were dispersed cortically into patches. Actin filament organization for KO on stiff resembled that of WT on soft.

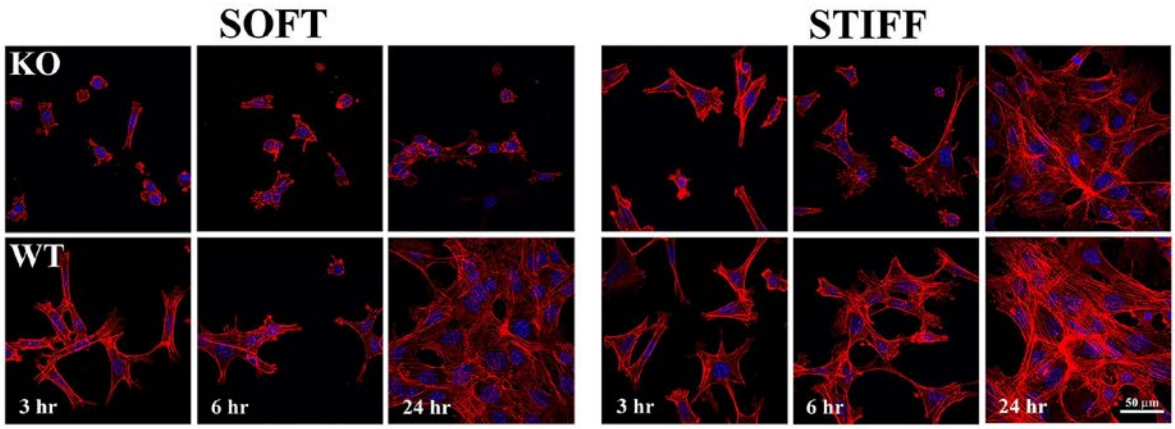

Figure 22. Immunofluorescent images of F-actin (red) and cell nuclei (blue). More F-actin was with greater organization was visible in WT compared to KO and on stiff compared to soft PA gels.

4.3.2 Substrate Stiffness Affects Aggregate Formation in WT and KO Cells

The number of single cells remaining in the field each hour over 24 hours was used as a measure of the potential for aggregate formation (Figure 23). The number of single cells remaining in the field decreased approximately three-fold faster for WT on soft gels compared to KO on soft and KO on stiff gels (Figure 24). The number of single cells for WT on soft gel also decreased one and half-fold faster compared to WT on stiff gels. These data indicate that aggregates formed faster for WT on soft gels compared to KO on soft, KO on stiff, and WT on stiff gels. These observations are consistent with my previous finding that the rate of human keratinocytes aggregate formation on soft samples was significantly higher than on stiff ones [32].

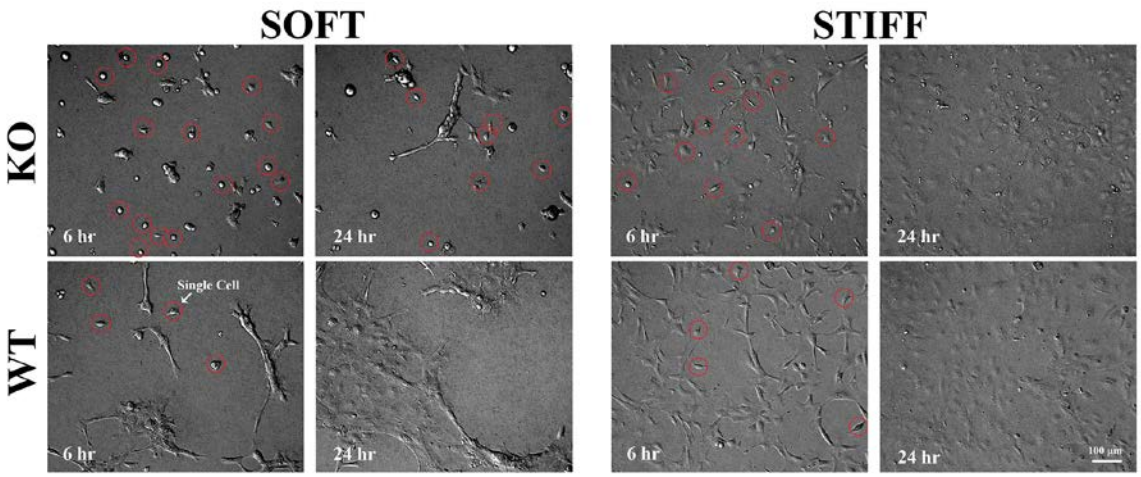

Figure 23. Aggregate formation of KO and WT samples on soft and stiff PA gel. The red circles correspond to single cells. The number of single cells were counted at different time points for WT and KO cells on soft and stiff samples. Single cells were still present on KO soft gels after 24 hrs, but not for the other three conditions.

Another metric used to assess differences in the rate of aggregate formation was the time it took for 80% of the cells to join into an aggregate (Table 7). On soft gels it took 1.7 hr ± 0.6 hr until 80% of the WT cells were joined into an aggregate. By comparison, it took significantly longer (6.3 hr ± 3.5 hr, $p < 0.03$) for the KO cells to have 80% of the cells associated with an aggregate. The number of single cells continued to decrease over time in WT until no single cells remained. In contrast, even after 24 hr, 6.6% ± 1.9% of the KO cells were still single. Interestingly, approximately 85% of KO cells that joined into an aggregate later detached from it.

On stiff gels, it took longer (2.7 hr ± 0.6 hr) for 80% of WT cells to join into aggregates compared to soft gels. The rate at which the percentage of single cells in the image decreased followed that of WT cells on soft gels at later time points (Figure 24).

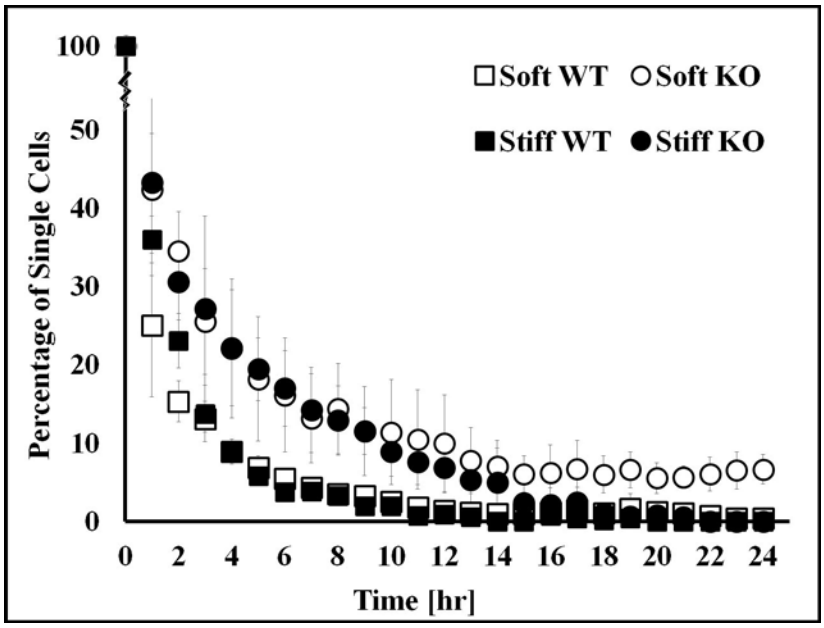

Figure 24. Number of single cells remaining in a field. The decrease was faster for WT compared to KO. Single KO cells still remained on soft gels after 24 hours.

Table 7. Aggregate formation measurements based on the percentage of single cells remaining in the field

Condition	Time (hr): Less than 20% of cells are single	Time (hr): Less than 2% of cells are single
Soft KO	6.3 ± 3.5	-
Soft WT	1.7 ± 0.6	11.0 ± 1.7
Stiff KO	5.3 ± 2.1	15.7 ± 2.1
Stiff WT	2.7 ± 0.6	9.7 ± 1.2

For KO cells the time that it took until 80% of the cells were in an aggregate (5.3 hr ± 2.1 hr) on stiff gels matched the time observed on soft gels. Unlike on soft gels, no single KO cells remained on the stiff gel after 24 hours.

4.3.3 Substrate Displacements on Soft PA Gels are Much Lower for KO than WT

Both KO and WT keratinocytes exerted traction forces on the soft PA gels and produced displacement fields that increased in magnitude during the course of the experiment as aggregates formed (Figure 25). Histograms of the displacement fields, such as the representative fields presented in Figure 25, show that substrate displacements increased substantially over time for both KO and WT on soft PA gels, and that these

displacements were greater for WT compared to KO. These differences were also significant for the other fields examined.

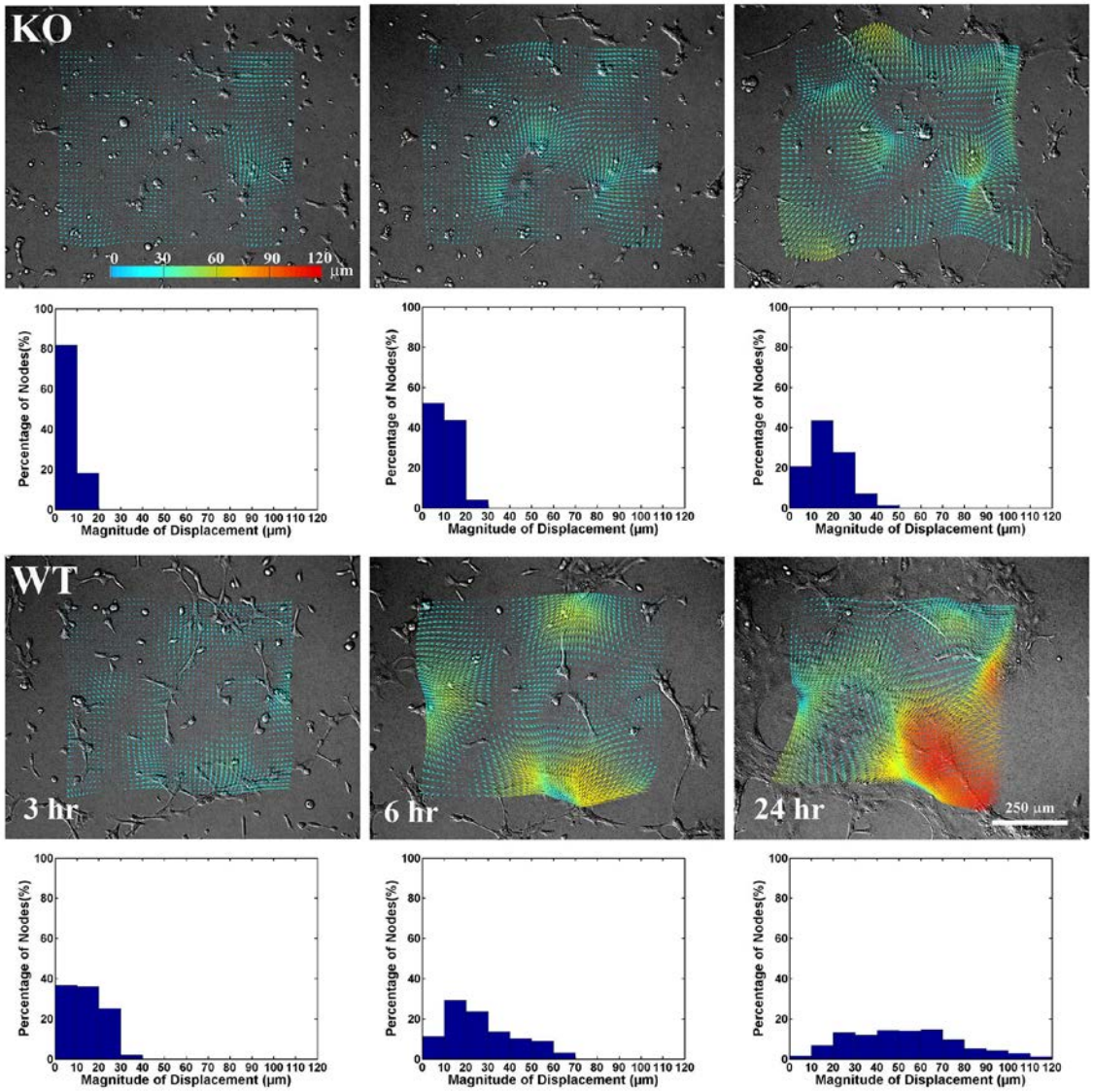

Figure 25. Displacement tracking of WT and KO cells over time on soft PA gels for one set of experiments at 3 hr, 6 hr, and 24 hr. The tracked displacements are overlaid on DIC images. Arrows show the direction and magnitude of substrate displacement. Below each image is its corresponding histogram showing the percentage of tracked substrate locations (*i.e.*, nodes) with a given amount of displacement. The magnitude of the displacements increased with time and was higher for WT than for KO.

The maximum displacements in WT quickly increased and then plateaued to an average value of 101.8 ± 4.9 at 14 hr (Figure 26). These values were significantly larger ($p < 0.001$) compared to KO, which increased at a slower rate to an average value of 64.8 ±

3.0 at 17 hrs. The average of the top 10% of the displacements also indicated significant differences between KO and WT (Table 8). For KO, the top 10% of displacements increased from 15.4 μm ± 1.9 μm at three hours to 48.0 μm ± 12.3 μm at 24 hours ($p < 0.001$). For WT, the displacements were much higher at 21.2 μm ± 6.0 μm at three hours and 91.8 μm ± 9.5 at 24 hours ($p < 0.001$).

The area of the field experiencing large displacements was also greater for WT compared to KO (Table 9). The average percentage of tracked locations (*i.e.*, nodes) exceeding 30 μm of displacement was significantly higher ($p < 0.03$) for WT (30.4 μm ± 14.5 μm compared to KO (2.1 μm ± 2.4 μm).

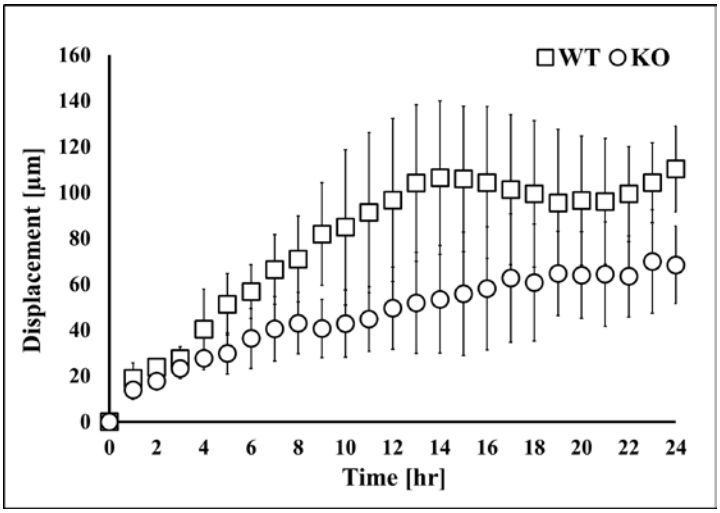

Figure 26. Maximum displacement in KO and WT on soft PA gels over time. Data are presented as the average and standard deviation of three samples for each cell type. A two-way ANOVA indicates that maximum displacements were significantly higher ($p < 0.001$) in WT compared to KO.

Table 8. Average and standard deviation of the top 10% of displacements in the field at 3, 6, and 24 hours

	Displacement (μm)		
	3 hr	**6 hr**	**24 hr**
KO	15.4 ± 1.9	23.6 ± 4.5	48.0 ± 12.3
WT	21.2 ± 6.0	46.8 ± 12.5	91.8 ± 9.5

Table 9. Percentage of nodes in the displacement field exceeding 30 μm at 3, 6, and 24 hours

	Percentage of Nodes		
	3 hr	**6 hr**	**24 hr**
KO	0.0 ± 0.0	2.1 ± 2.4	36.2 ± 21.5
WT	1.8 ± 3.2	30.4 ± 14.5	69.6 ± 10.8

4.4 DISCUSSION

Previously, I found that human neonatal keratinocytes were affected by PA gel substrate stiffness [32]. These cells had decreased surface area, more cellular protrusions, more directed migration, and higher rates of aggregate formation on soft compared to stiff Pa gels. These behaviors suggest that mechanical communication through a deformable substrate increases cooperative behavior amongst keratinocytes as they join to form nascent epithelium. Consistent with this study, both WT and KO mouse keratinocytes, in the same PA gel system, showed reduced surface area and an increased rate of aggregate formation on soft versus stiff PA gels. Muting keratin intermediate filament, however, dramatically amplified these behaviors, clearly illustrating that the keratin cytoskeleton also plays an important role in keratinocyte mechanobiology.

KO keratinocytes on soft PA gels (~1.2 kPa) had impaired actin organization, similar to what was observed in keratin 8/18 KO hepatic epithelial cells, as reported by Bordeleau *et al*. [10]. These cells had altered actin fiber organization on soft (1.8 kPa and 3 kPa), fibronectin (FN)-coated PA gels compared to stiff FN-coated glass. Whereas the actin filaments in WT hepatic epithelial cells were long and interconnected, k8/18 KO actin filaments were short and not interconnected. K8/18 local cell stiffness was also found to be lower than for WT. The changes in cytoskeletal organization and cell stiffness were attributed to Rho/ROCK signaling, a pathway well known to be modulated by mechanical

interactions involving the cytoskeleton and the surrounding extracellular matrix [106]. These findings are consistent with and complementary to my results showing reduced actin organization and substrate displacements for KO compared to WT.

In addition, I found that the rate of KO aggregate formation was reduced significantly on soft PA gels. Interestingly, KO keratinocyte on stiff PA gels (~24 kPa) behaved similarly to WT. This finding highlights the complexity of mechanical interactions in driving cell behavior. Such interactions could have important implications for re-epithelialization, where temporal and spatial changes in wound bed composition and mechanical properties, along with various cellular factors, such as cytoskeletal organization, anchoring junction formation, and pathway signaling, combine to drive the healing process. In this context, the soft substrate may represent an optimal condition where keratins augment the force generating/sensing capacity of the cell such that mechanical cues from substrate deformations enhance the formation and stabilization of cell-cell junctions. On stiff gels, the mechanics is different, and it drives cell behavior in a manner that is less dependent on this putative augmentation by keratins.

The role of keratins/intermediate filaments in force generation is unclear. Recently, desmosomal proteins, which anchor to intermediate filaments, have been investigated for their role in regulating keratinocyte force generation [155]. Broussard *et al.* demonstrated that strengthening or disrupting desmoplakin-intermediate filament interactions in A431 cells, an immortalized human keratinocyte cell line derived from epidermoid carcinoma, served to increase or diminish, respectively, cell-substrate and cell-cell forces in both cell pairs and cell sheets [155]. Changes in cell force generation were strongly correlated to actin filament organization, which in turn was modulated by desmosome-keratin linkages.

The reduction in KO keratinocyte force generation in our study could be due to similar mechanism, where the absence of desmosome-keratin interactions also modulates force generation of the actin cytoskeleton.

The KO mouse keratinocytes studied here have been extensively characterized on tissue culture plastic [152, 156-159]. Seltmann *et al*. reported that KO were more deformable and thus more invasive than WT [157], and Ramms *et al*. found that KO were less stiff and smaller than WT [159]. More recently, Homberg *et al*. showed muting k5 or k14 downregulates desmosomal proteins, weakens epithelial sheet integrity, and produces the blistering disease epidermolysis bullosa simplex [158]. The absence of demosome-keratin interactions in the KO keratinocytes also diminished the stability of cell-cell adhesions on soft PA gels, as evidenced by the fact that more than 85% of these cells were forming an aggregate but left it during the 24 hour of the experiment. Although this behavior was less apparent, it also occurred on stiff PA gels, and could partially account for the slower rate of aggregate formation compared to WT.

In addition, keratin filaments were found to be necessary for localizing hemidesmosomal proteins [152, 156]. Furthermore, without keratin, plectin-β4 interactions are lost, as keratin stabilizes plectin- β4 integrin interactions by limiting β4 phosphorylation [158]. Although we did not examine hemidesmomal proteins in this study, it is reasonable to hypothesize that a loss of plectin-β4 interactions was also responsible for the alterations in actin organization, the reduction in force generation, and the rate of aggregate formation observed in this study. Since plectin is the only junction protein known to be shared by both hemidesmosomes and focal adhesions, plectin is a strong candidate for where the mechanical linkage between the actin-myosin and keratin intermediate filament

components of the cytoskeleton may be, potentially via interactions between hemidesmosome and focal adhesions [44-46]. In a study on the dynamic relationship between hemidesmosome protein complexes and focal contacts, Ozawa *et al*. showed that hemidesmosomes disassembly in HaCat cells could be induced by using antibodies to block against the α6 or β4 integrin subunits [44]. Doing so induced cell rounding and concentrated actin into cortical patches similar to those observed here for KO on soft PA gels.

4.5 CONCLUSION

Live-cell imaging and deformation tracking microscopy (DTM) was performed on WT and KO keratinocytes on collagen coated polyacrylamide gels with two different stiffnesses, soft (nominal 1.2 kPa) and stiff (nominal 24 kPa) in order to better understand the role of keratin IFs in keratinocyte mechanosesning and force generation.

I found that KO cells were less spread out, had impaired actin filament formation, could not generate force on the substrate and finally hardly could aggregate on soft substrates.

These results suggest that keratin IFs play a role in cytoskeletal force generation, as evaluated by alterations in behaviors such as aggregate formation and substrate deformations.

4.6 ACKNOWLEDGEMENTS

Support of this work was provided by the National Science Foundation (National Science Foundation CAREER CMMI 1452728), National Intstitutes of Health (NIH NIAM

R03 AR063967) and the Carver Charitable Trust #14-4384. I also thank Sathivel Chinnathambi for assistance with cell culture and Thomas Magin for providing mouse keratinocytes and providing additional insight.

Chapter V. SUBSTRATE DISPLACEMENTS INDUCE DIRECTED KERATINOCYTE MIGRATION

5.1 INTRODUCTION

Cell migration is an essential part of many physiological and pathological processes in the body, including tissue morphogenesis [160], inflammation [161], and wound healing [69]. Re-epithelialization during the wound healing is a result of migration, proliferation, and differentiation of the peripheral keratinocytes along the edge of the wound [2, 6, 162]. Aberrant or delayed re-epithelialization increases the risk of infection and the severity of scar tissue formation, and it contributes to the development and persistence of chronic wounds [2, 3, 20]. Until recently, the regulation of re-epithelialization and keratinocytes migration were largely understood in terms of biochemical signals, but recent interest in the mechanobiology of tissues suggests that physical forces and mechanical cues from the wound bed may also play an important role in the healing process.

In a previous study, I explored how substrate stiffness affects human keratinocyte behavior and found that mechanical cues did influence the process of re-epithelialization [32]. Specifically, I found that the formation of nascent human keratinocyte aggregates was significantly different on soft versus stiff polyacrylamide gels, with smaller spread contact area, increased migration velocities, increased rates of aggregate formation with more cells per aggregate in keratinocytes cultured on soft gels versus stiff ones [32]. In addition, the keratinocytes on soft PA gels appeared to migrate in a directed manner towards the forming cell aggregates in response to mechanical communication through the deformable substrate. Such directed migration was not apparent on the stiff PA gels. However, I were unable to clearly demonstrate that the keratinocytes were responding to these putative mechanical signals, possibly because multiple cells produced a spatially and temporally heterogeneous milieu of deformations in the substrate.

Lo *et al.* demonstrated that mechanical deformations in a flexible substrate induced with a blunted microneedle could direction cell migration [163]. Reinhart-King *et al.* [96] found that endothelial cells on soft PA gels were able to interact with each other by sensing mechanical forces exerted between them through the substrate. The dispersion, or tendency of these cell pairs to migrate away from their initial location, was significantly reduced compared to that of single cells. Because each cell modulates the tractions it exerts on the substrate in response to those of the adjacent cell, the mechanical environment is dynamic and not controlled in a manner that clearly illustrates the relationship between mechanical signals from the substrate and cell behavior.

In order to better clarify such relationships, I replaced one of the cells with a controlled local displacement in the gel substrate via the use of a needle and servo-controlled micromanipulator. I imaged and analyzed the response of single human keratinocytes to controlled local substrate deformations induced by the micromanipulation of a needle inserted into the gel. I also examined the effect of adding either Y27632, a Rho kinase inhibitor, or blebbistatin, a myosin II inhibitor, on keratinocyte behavior. The results of this study gives new insights on the mechanism by which the cells sense and response to mechanical signals from their environment.

5.2 MATERIAL AND METHODS

5.2.1 Polyacrylamide Gel Preparation

Thin polyacrylamide (PA) gels approximately 100 μm in thickness were polymerized on the surfaces of glass bottom petri dishes as described previously [31, 32]. Briefly, the ratios of 2.0%/0.25% and 7.5%/0.3% acrylamide/bis-acrylamide were used to

fabricate soft (1.2 kPa) and stiff (24 kPa) PA gels, respectively. FluoSpheres® Carboxylate-Modified Microspheres (#F8812, Life Technologies, Carlsbad, CA) measuring 0.5 μm in diameter were embedded inside the gels to facilitate deformation tracking in the gels. Pepsin-digested collagen was attached covalently to the surface of the gel with Sulfo-SANPAH. The samples were sterilized under UV light for 15 minutes and stored at 4 °C for later use.

5.2.2 Cell Culture

Neonatal human epidermal keratinocytes (HEKn) (Fisher Scientific, Waltham, MA) were cultured in keratinocyte serum free medium (KSFM) (Invitrogen) supplemented with 1% penicillin-streptomycin and 0.1% amphotericin B in a humidified incubator maintained at 37 °C and 5%/95% CO_2/air. Passage three cells were plated at a low density of approximately 200 cells/cm^2 onto the surface of polyacrylamide (PA) gels that were attached to glass bottom petri dishes (MatTec Corp., Ashland, MA). The calcium of the medium was elevated from a baseline concentration of 0.09 mM to 1.2 mM by adding $CaCl_2$ to the medium in order to trigger epithelial sheet formation via the calcium switch [32, 81, 82]. HEKn were allowed to attach and equilibrate for three hours in the incubator before imaging with the microscope.

5.2.3 Time-Lapse Live Imaging

Once the samples had equilibrated, they were transferred to a temperature-controlled microscope enclosure (CO_2 Microscope Cage Incubation System, Okolab, Pozzuoli, Italy) with recirculating air that integrates with a micro-environmental gas chamber (H201-K-Frame, Okolab, Pozzuoli, Italy) (Figure 27). This setup provides 37 °C, humidified air with 5% CO_2 via a manual gas mixer and pump to the samples so that

extended time-lapse imaging is possible. Time-lapse images were acquired with a Nikon Eclipse Ti inverted microscope equipped with wide-field epifluorescent and differential interference contrast (DIC) microscopy capabilities and a DS-Qi1 Nikon camera. DIC and fluorescent images pairs were acquired with a CFI plan Apo 10X DIC objective combined with a 1.5X magnifier.

5.2.4 Needle-Induced PA Gel Deformations

Controlled local mechanical deformations in the PA gel substrate were produced by inserting a sterile 0.25 mm x 75mm acupuncture needle (Tai-Chi Brand, Suzhou Shenlong Medical Apparatus Co., Ltd., Suzhou, China) into the gel. The needle was secured to a high-resolution linear actuator (M-230.25, PI (Physik Instrumente) LP, Auburn, MA), controlled with MTESTQuattro software (ADMET, Norwood, MA), and mounted to a high-precision, manual linear stage (462 XYZ-M ULTRAlign, Newport Corp., Irvine, CA).

Single keratinocytes that were at least 350 μm away from any neighboring cells were located and imaged. Circles measuring either 100 μm or 200 μm in radius and centered on the cell nucleus were drawn on the live image. The needle tip was then inserted approximately 40 μm into the gel at a location on the circle (Figure 27). The actual needle tip to cell nuclei distance was consistent amongst the three 100 μm conditions at 84.0 μm ± 5.7 μm, 85.9 μm ± 4.4 μm, and 86.4 μm ± 6.0 μm, for Soft-100, Soft-Y27632, and Soft-Bleb, respectively and defined below. The actual distance for Soft-200 was 182.3 μm ± 5.4 μm. The needle was then displaced at a constant rate of 1 μm/min, a rate on par with both the average instantaneous velocity of single keratinocytes and the keratinocyte-induced substrate deformations reported on soft PA gel previously [32].

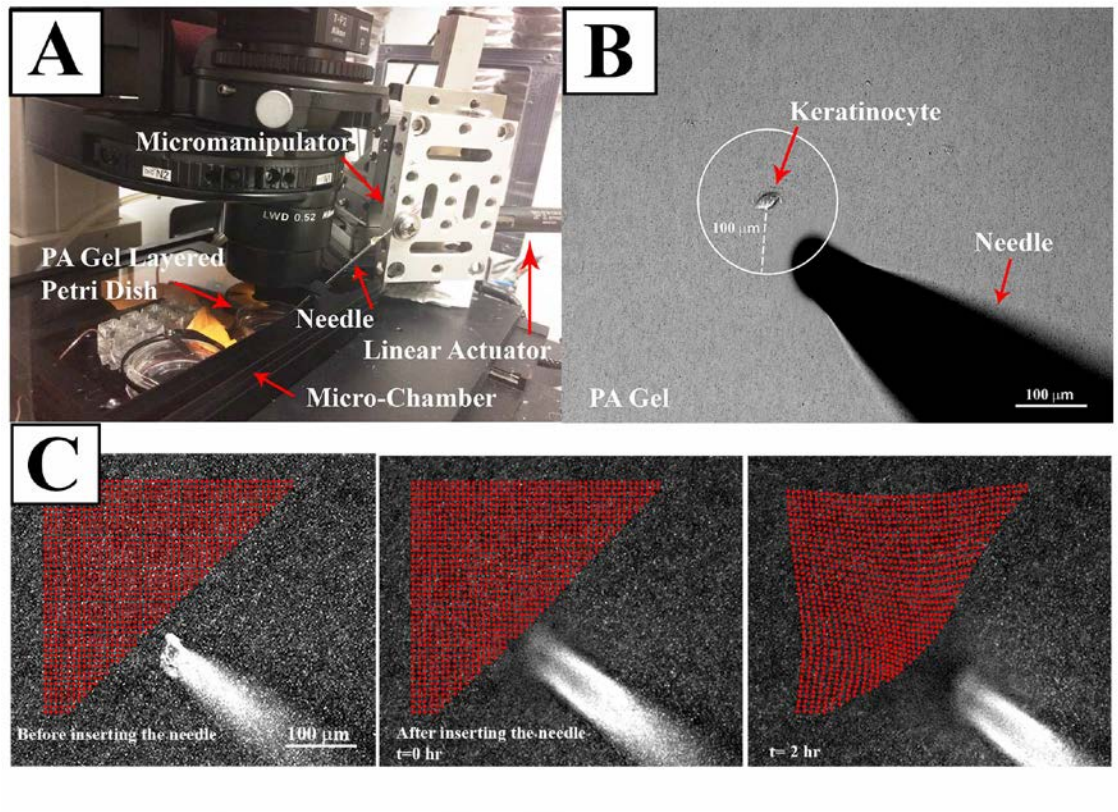

Figure 27. Experimental setup to apply controlled mechanical deformations to the PA gel. A) The PA gel is placed within a microscope-mounted micro-chamber contained with an environmentally controlled enclosure. A servo-controlled liner actuator drives needle movement via a high-precision micromanipulator (B) A single keratinocyte is identified and the needle is inserted a prescribed distance away from the centroid of the cell.

After the needle was inserted into the substrate, time-lapse images were taken at a five-minute interval for two hours, which corresponded to the amount of time available before the needle began to exit the image. Analysis of control experiments indicated that this two-hour period was substantially larger than the average persistence time of these cells. As many as three sequential experiments were conducted on each gel, such that all experiments were conducted within 10 hours of the start of the experiment. Parallel control experiments, where the needle was absent, were acquired every five minutes over 24 hr. Persistence time was calculated from these experiments by fitting the mean squared displacements to the persistent random walk model of cell motility (described in 5.2.9).

5.2.5 Chemical Inhibitors

The Rho kinase inhibitor, Y27632 (ALX-270-333-M001, Enzo Life Sciences, Inc., Farmingdale, NY) [43, 115, 117-119], and a myosin II inhibitor, blebbistatin (ab120425, Abcam, Cambridge, MA) [116, 164], were added to the culture medium of some experiments in order to assess how inhibiting components of the mechanosensing and force generating machinery of the cytoskeleton affected keratinocyte behavior in response to the needle. One hour after the cells were added to the PA gels (*i.e.*, 2 hours before imaging began) either Y27632 or blebbistatin was added to the culture medium to produce a final concentration of 50 µM of inhibitor.

5.2.6 Experimental Conditions

Four different experimental conditions involving substrate displacement with the needle were investigated, where the initial distance of the needle away from the cell (Soft-100, Soft-200) and the effects of chemical inhibition (Soft-Y27632, Soft-Bleb) on cell migration were investigated (Table 10). An additional control condition, where the needle was absent, was also examined (Table 10). Ten cells were analyzed for each condition.

Table 10. Experimental conditions

Condition	Gel	Needle Location	Chemical Inhibitor	n
Soft-100	1.2 kPa	100 µm	-	10
Soft-200	1.2 kPa	200 µm	-	10
Soft-Y27632	1.2 kPa	100 µm	Y27632 50 µM	10
Soft-Bleb	1.2 kPa	100 µm	Blebbistatin 50 µM	10
Control-Soft	1.2 kPa	-	-	10

5.2.7 Displacement Tracking of the Substrate

PA gel substrate displacements were measured by using a custom MATLAB algorithm based on spatial cross-correlation between subsequent image pairs of the

embedded fluorescent microspheres [65], as was done previously [32]. Specifically, a triangular array of evening spaced grid points was placed on a subset of the image that contained the cell and extended to the location of needle insertion. Subwindows around each grid point were then correlated between image pairs to obtain the corresponding displacements in the substrate. The grid point positions were updated and used to generate the subwindows for correlation between the next image pair. In this manner, the grid point positions track with the microspheres in the deforming substrate. Thus, it was straightforward to describe the 2D position vector of the substrate, $\bar{r}_s(t)$, and the incremental substrate displacement between frames, $\bar{u}_s(t) = \bar{r}_s(t) - \bar{r}_s(t-1)$, at time, *t*. The accumulated substrate displacements were then used to calculate the Lagrangian strain.

5.2.8 Cell Motility

The 2D position of the cell, $\bar{r}_c(t)$, was determined by hand tracking the location of the nucleus in each image using the Manual Tracking plugin in ImageJ (National Institutes of Health, Bethesda, MD). In the experiments involving the needle, it was necessary to distinguish between cell movement from cell motility versus cell movement from needle-induced deformations in the substrate. Thus, the total incremental displacement of the cell, $\bar{u}_c(t)$, between image pairs is given by:

$$\bar{u}_c(t) = \bar{u}_m(t) + \bar{u}_s(t) \qquad (1)$$

where $\bar{u}_m$ is the incremental displacement of the cell due to cell motility (*i.e.*, $\bar{u}_m(t) = \bar{r}_m(t) - \bar{r}_m(t-1)$),and $\bar{u}_s$ is the incremental displacement of the underlying substrate. Here, $\bar{u}_s$ was made coincident with the position of the cell via linear interpolation from the displacements measured in the surrounding set of tracked grid points. For the limiting case of no substrate displacement (*i.e.*, when there is no needle and $\bar{u}_s(t) =$

0), cell movement is from cell motility alone. The position vector of the cell due to cell migration alone, $\bar{r}_m$ was then calculated from eq. (1) as

$$\bar{r}_m(t) = \bar{r}_m(t-1) + \bar{u}_c(t) - \bar{u}_s(t) \qquad (2)$$

Both and $\bar{r}_m$ and $\bar{u}_m$, which I refer to as the adjusted position vector and adjusted cell displacements, respectively, were used in the data analysis described below.

5.2.9 Persistency

Mean-squared displacement (MSD) was calculated for the soft control experiments via the persistence random walk model [165-167], given by:

$$< d^2 >= 2S^2P[t - P(1 - e^{-\left(\frac{t}{P}\right)}] \qquad (3)$$

where *S* is cell speed, *P*, is the persistence time, and t is the time between images [96, 168, 169].

5.2.10 Directional Migration Analysis, Circular Statistics

The directional migration of the cells was also analyzed by plotting the polar the angle of the adjusted cell displacement vector, $\theta_{\bar{r}_m}$, of 10 cells acquired in two hours of experiments. Theta was calculated by taking the inverse tangent of r_y/r_x for each cell position vector. Statistical analyzes of the directional migration of the cells was performed using matlab's Circular Statistics Toolbox, CircStat [170]. Rayleigh test was performed on theta values of the cells in each four different experimental condition to inspect the directional or uniform distribution of theta. Rayleigh test was also performed on 10 cells in soft control samples. In order to have a comparable results, the test was performed on the angles of cell position vector of the first two hours in control experiments as well.

In addition, V test were performed to assess whether the mean values of theta in Soft-100, Soft-200, Soft-Y27632, and Soft-Bleb samples were in the same direction as the needle movement.

5.2.11 Displacement Analysis

To seek the relation between the direction of adjusted cell displacement vector, $\bar{u}_m$, and the direction of displacement in underlying substrate, $\bar{u}_s$, polar histograms of the angle of adjusted cell position vector, $\theta_{\bar{r}_m}$, and the angle of displacement vector of the underlying substrate, $\theta_{\bar{u}_s}$, was plotted.

In addition, the alignment angle phi (ϕ) between , $\bar{r}_m$ and $\bar{u}_s$ was measured [171]. If $\phi = 0$, it means that there is a perfect alignment between the direction of displacements occurring underneath of the cell and the cells migration direction. The cumulative probability distribution function $\bar{\mathrm{P}}(\phi)$ was also constructed. Here, if ϕ is uniformly distributed, meaning that there is no preferential alignment toward the direction of underlying substrate, the probability function would be a straight line from probability 0 at 0° to probability 1 at 90°.

5.3 RESULTS

5.3.1 Substrate Displacements

PA gel substrate displacements were measured and plotted by using a custom MATLAB algorithm (Figure 28).

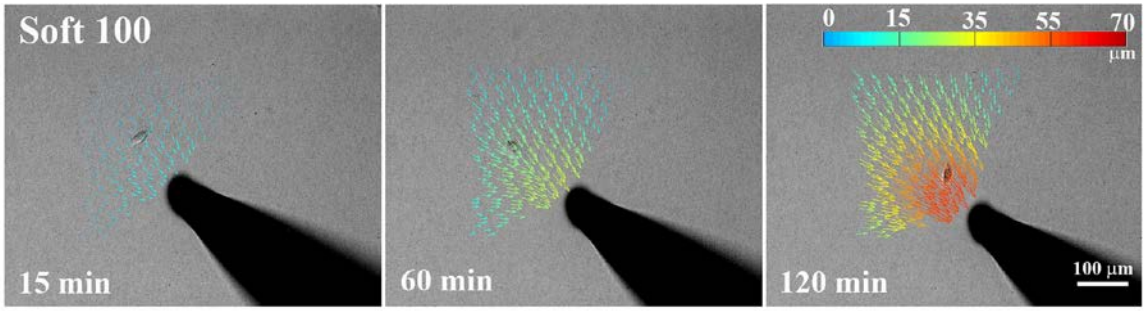

Figure 28. Displacement field of the substrate measured by a custom MATLAB algorithm.

5.3.2 Cell Motility: Control Experiment

In control soft PA gel, keratinocytes appeared to have a spread out lamelopodia at the leading edge of migrating cells. However, time-lapse live cell imaging indicated that the cells inclined to change their migration direction vibrantly. Plotting the migration path of the Control-Soft cells also indicated that the cells path is highly convoluted (Figure 29).

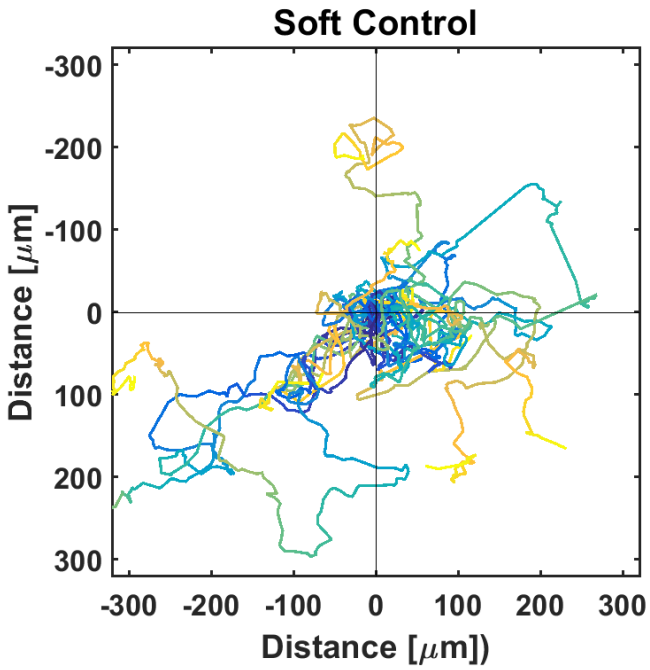

Figure 29. Keratinocyte migration path on soft control experiments.

Cell's persistency was calculated from equation (3) for the control experiment to quantify keratinocyte random migration behavior on soft PA gel. The calculated persistence time was 14.4 ± 17 minutes. Therefore the duration of needle-inserted

experiments was chosen to be two hours to ascertain that the migration path of the cells in these experiments is not just the result of the cell's random walk.

5.3.3 Cell Motility: Needle Experiments

In Soft-100 and Soft-200 samples, keratinocyte appeared to have the same morphology as the Control-Soft experiments with a spread out lamelopodia at the leading edge (Figure 30).

To assess the influence of local mechanical deformations on the cell migration, the adjusted migration path of 10 cells from 4 different needle-inserted experiments were plotted (Figure 31). As this figure shows the cells path were rigorously affected by the needle. Remarkably, in Soft-100 and Soft-200 samples the cells pivoted their migration direction toward the needle and ultimately traced the needle.

To assess the effect of blocking different part of mechanosensing pathways on cells behavior, Y27632 and blebbistatin were used to inhibit Rho-kinase and myosin II respectively. Treating the cells with Y27632 and blebbistatin dramatically changed the keratinocyte morphology (Figure 30). Both drugs induced the formation of highly extended cell bodies.

Interestingly, Y27632 and blebistatin also affected the cells response to the needle-induced local mechanical deformations. The Y27632 treated cells did not alter their migration direction toward the needle. Plotting the adjusted Y27632-treated cells path showed that the cells appeared to have a random migration direction, without any preference toward the needle (Figure 31).

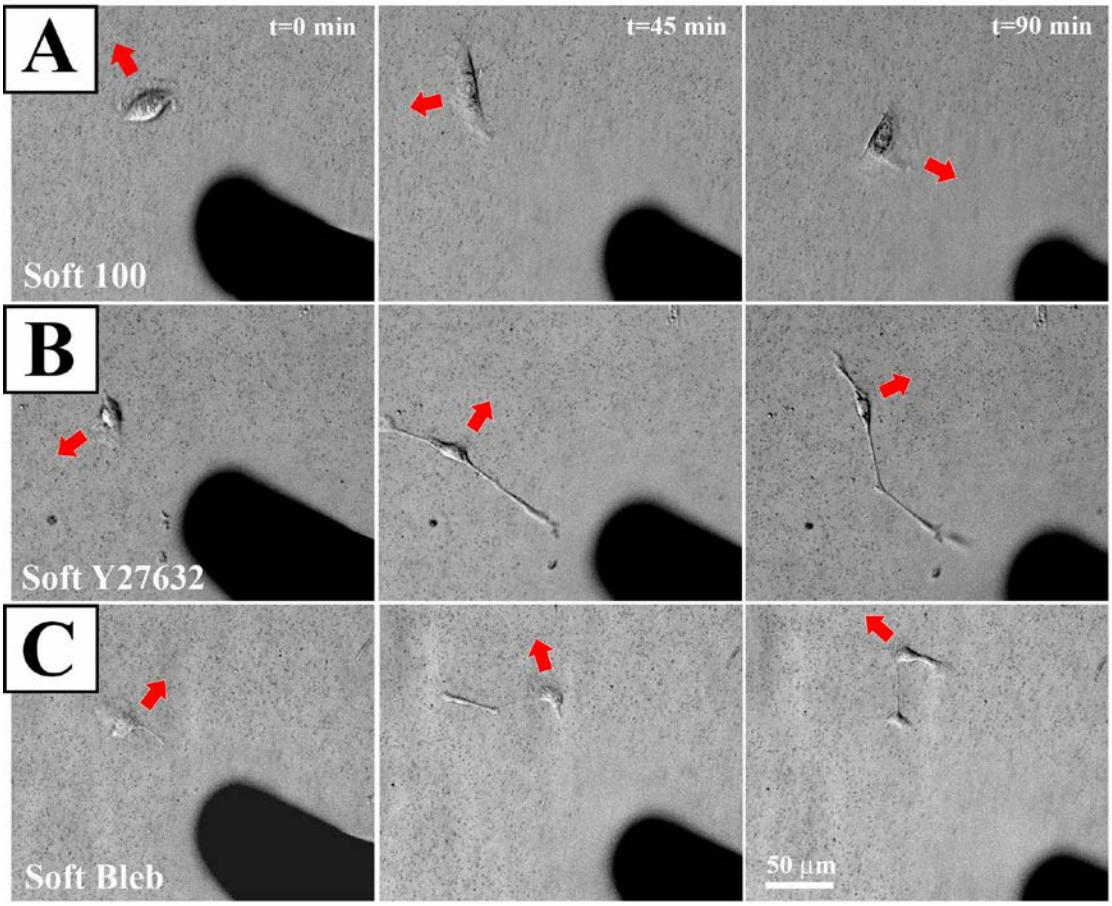

Figure 30. Keratinocytes morphology and migration direction on (A) Soft-100, (B) Soft-Y27632, and (C) Soft-Bleb gels at t = 0 min, t = 45 min, and t = 90 min while applying the local mechanical deformations with the needle. Red arrows show the migration direction of the cell.

The cell path in blabbistatin treated cell was not like Y276732 treated cell, nor like not-treated cells. The cell paths were neither elongated toward the needle nor going away from it. Instead, the same as blebbistatin control sample, the blebbistatin-treated cells did not migrate much away from their starting points (Figure 31).

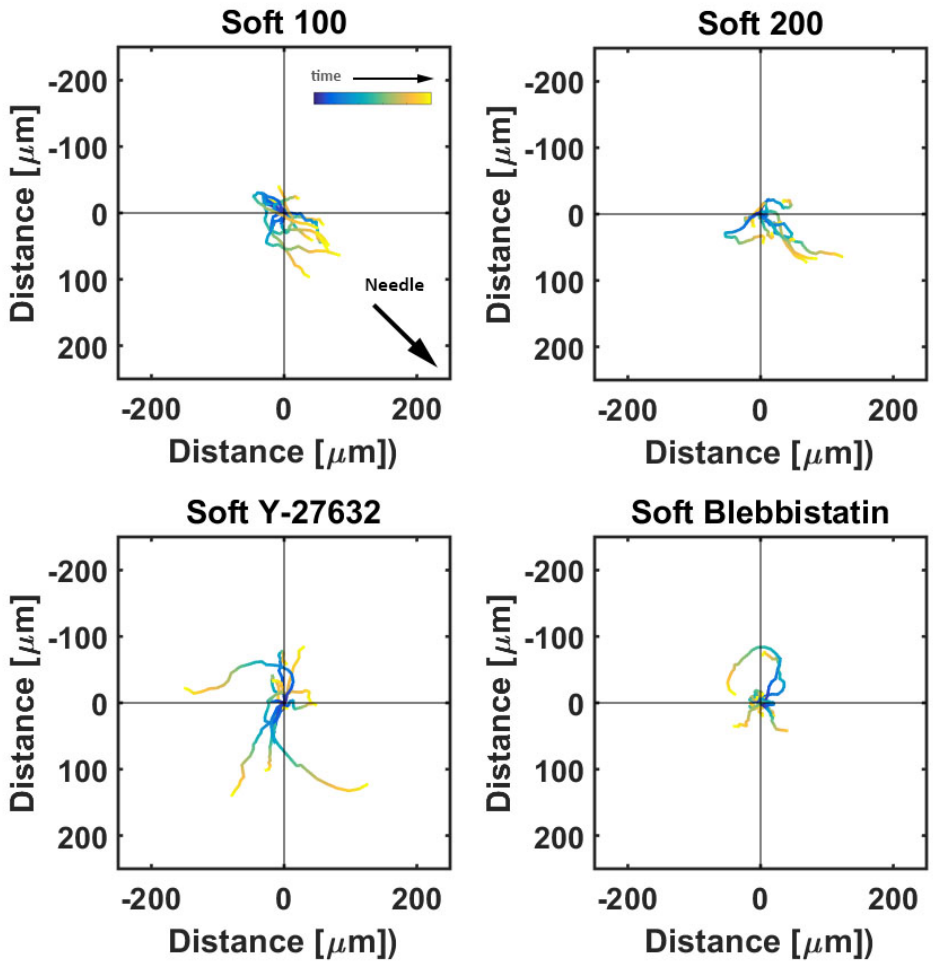

Figure 31. Adjusted Cell Motility on Soft PA gels. Each line shows the adjusted position of the cell centroid where the underlying substrate displacement induced by the needle has been subtracted out. Each cell path is color coded to show the relative time along the path from its beginning at the origin (dark blue) to the final tracked adjusted position (yellow). The majority of cells moved toward the displacing needle for needles initially position at either 100 µm or 200 µm from the cell centroid. Exposure to Rho kinase inhibitor Y27632 or the actin-myosin inhibitor blebbistatin interrupted this directed movement.

5.3.4 Directional Migration Analysis Results

The polar histogram of theta ($\theta_{\bar{r}_m}$), the angle of cell adjusted displacement vector in all the 10 cells for four different experimental condition is shown in Figure 32 (red bars). Ryleigh test results was performed on theta and showed a significant directional migration in Soft-100 and Soft-200 samples (P <<0.001) and not a directional migration (uniform distribution of theta) in Soft-Y27632 and Soft-Bleb samples. Moreover, performing V test

on theta values confirmed that in Soft-100 and Soft-200 cases the directional migrations of the cells were is the direction of needle movement ($p << 0.001$).

Rayleigh test on Control-Soft cells showed no directional migration in control samples.

5.3.5 Displacement Analysis

Polar-plots showing the direction of cell adjusted displacement vector and displacements underneath of the cells confirmed that the displacements generated mainly by the needle were in the same direction in all four conditions, and also the cells position vector in Soft-100 and Soft-200 samples were in the same direction as of the substrate displacements; in oppose to Soft-Y27632 and Soft-Bleb samples that there was not any directionality in their cells position vector (Figure 32).

The cumulative probability distribution function of the angle between the cell migration adjusted displacement vector and substrate displacements, also verified the preferential migration of cells on Soft-100 and Soft-200 samples in the direction of substrate displacements. As Figure 33 shows, ϕ distribution is narrower in Soft-100 and Soft-200 samples versus Soft-Y27632 and Soft-Bleb ones. The approximately uniform distribution of ϕ for Soft-Y7632 and Soft-Bleb confirms the non-preferential migration of drug treated cells.

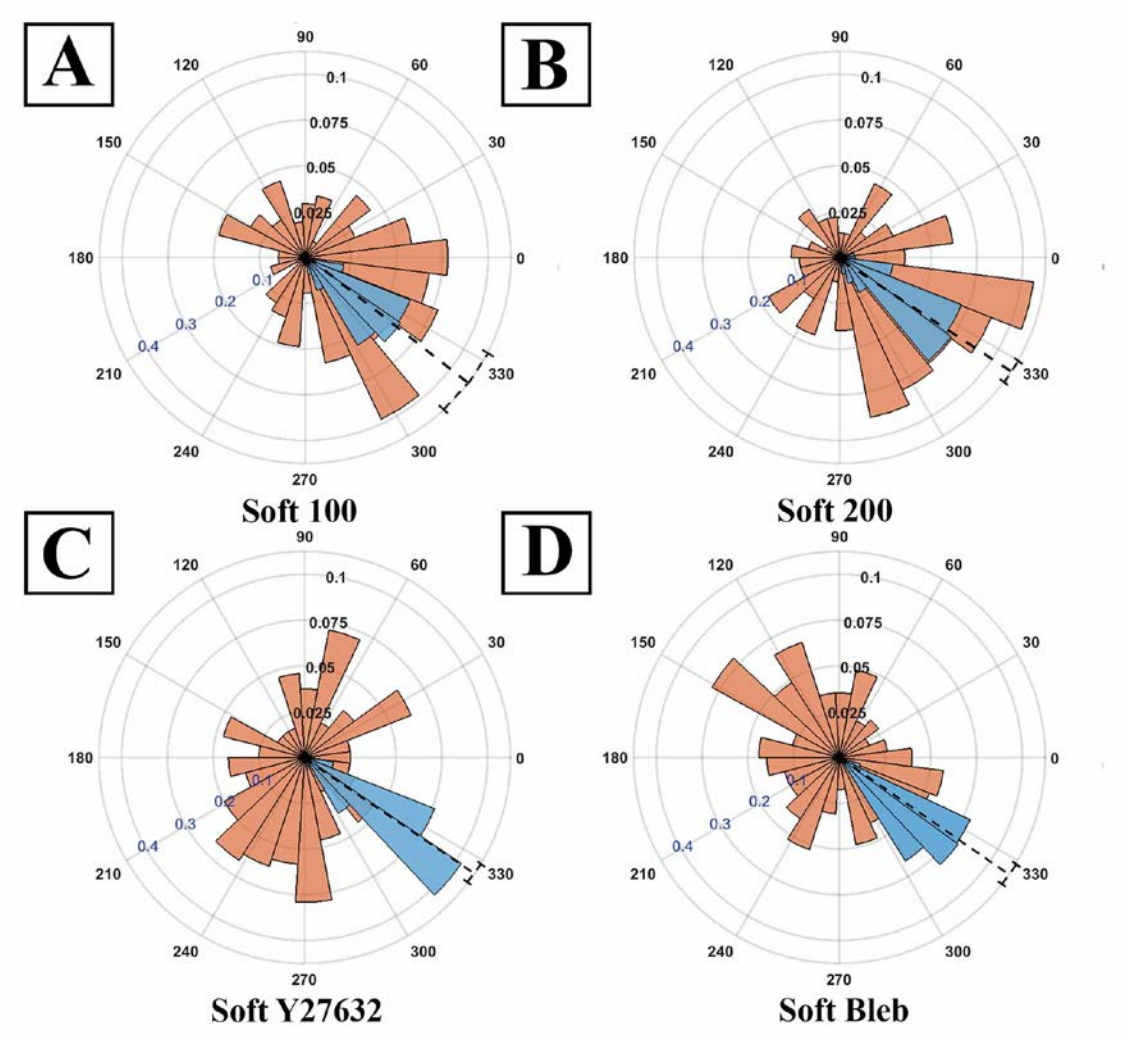

Figure 32. Polar histograms $\boldsymbol{\theta}_{\bar{r}_m}$(red) and $\boldsymbol{\theta}_{\bar{r}_s}$ (blue) in A) Soft-100, B) Soft-200, C) Soft-Y27632, and D) Soft-Bleb samples. The dashed line shows the mean and standard deviation the angle at which the needle displaced. For all conditions, the displacements of the substrate aligned with the direction of needle movement. Rayleigh test indicate that cell movement ($\boldsymbol{\theta}_{\bar{r}_m}$) is directed towards the needle for Soft 100 and Soft 200 samples, but not for soft-Y27632 or Soft-Bleb ($p << 0.001$). V-test shows a significant directional migration toward the needle (dashed line) in Soft-100 and soft-200 samples ($p << 0.001$). [Polar histogram plots are normalized by dividing the number of observations in bin/total number of observations (probability).]

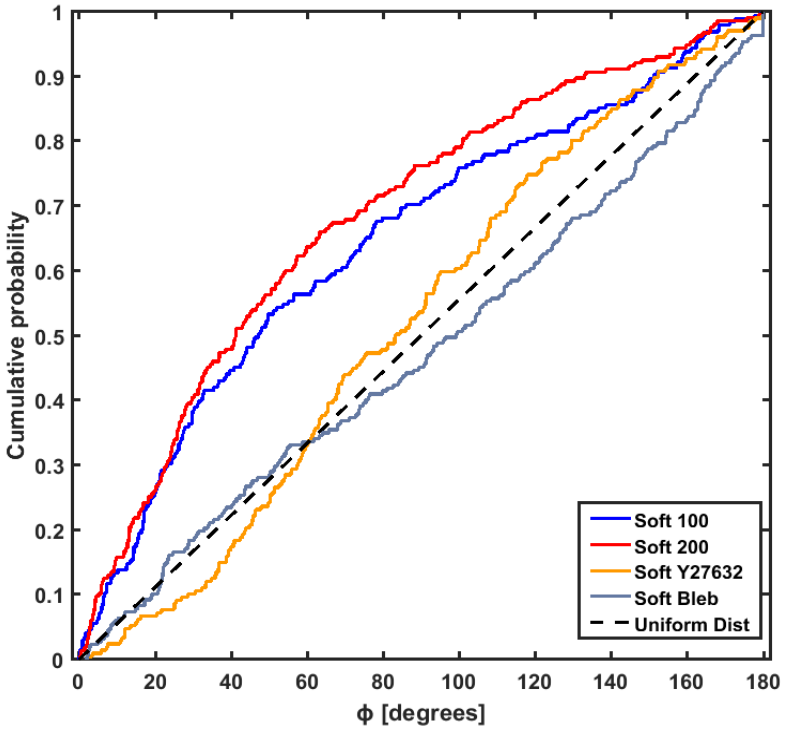

Figure 33. The cumulative probability distribution of $\boldsymbol{\phi}$, the angle between the cell position vector and the displacement underneath the cell.

5.4 DISCUSSION

This study explores the cells responses to the local mechanical signals and the effect of inhibiting two different elements of cells mechanosensing pathway on cells migration behavior. The results of these experiments indicate that the cells sense the mechanical deformations in their underling substrate. These results are in agreement with the previous study by Lo *et al*. that showed the 3T3 fibroblast cells made lamelopodium toward a poking glass needle and migrate toward the needle in case of being pulled or migrate away from it in case of being pushed by the needle [163]. Reinhart-King *et al.* also investigated the cell-cell communications through compliant substrates in endothelial cells. Their results indicated the potential mechanical influence of neighboring cells through cues generated by cellular traction stresses extending through the substrate [96]. In a previous study our

group showed that keratinocyte aggregate formation was expedited in soft PA gel substrate compared to stiff ones possibly as a result of elevated mechanical signaling through deformations generated in the soft substrate [32]. The current study eliminated the complications of my previous study for having too many cells in the field, which made excluding one pure mechanical signal impossible. Here I investigated single cells behavior, which were at least 100 µm away from the neighboring cells to eliminate any chemical or mechanical signal from the adjacent cells and analyzed the effect of substrate deformations made by a mechanical object on the cell migration behavior.

My results indicated that the cells follow the needle in case of being continuously pulled by the needle. Poking and pulling the substrate with the needle would make local tension in front of the needle and probably induces strain-stiffening due to the high strains applied to PA gel [172]. If the cells sense local mechanical deformations or the local stiffness of the substrate is unclear.

This study also explores the effect of inhibiting two sets of proteins, Rho-associated protein Kinase and myosin II by Y27632 and blebbistatin drug on cells respond to mechanical signals. Interestingly inhibiting Rho Kinase proteins impaired the cells respond to the mechanical signaling and impeded their needle-following behavior. Y27632 is a well-known Rho-kinase inhibitor [108]. Previous studies on the effect of Y27632 drug on keratinocytes showed that this drug inhibited keratinocyte differentiation and increase its proliferation [42, 43, 115, 117-119]. Y27632 has also been reported to increase directional migration of keratinocyte in scratch wound healing assay which is in consistence with my results of increased confinement ratio in control non-poking Y27632 treated samples versus

control non-poking soft samples (Appendix B) [107, 115]. Although RhoA-null keratinocytes showed impaired directional migration in scratch wound healing assay [107].

Sarkar *et al*. investigated the effect of inhibiting myosin II by blabbistatin on keratinocyte migration by developing confluent cell islands and quantified migration as fold increase in island area over time [116]. They reported that using blabbistatin increased the migration of keratinocytes significantly. They also tried using Y27632 drug in their set up and reported no significant change in cells migration. They described the same morphological changes as what I saw in keratinocyte treated by blebbistatin and Y27632, inducing formation of large membrane ruffles and elongated tails. It is noteworthy that blabbistatin inhibits both myosin IIA and myosin IIB. There are evidences showing that these two types of myosin II have reveres effect on enhancing or reducing migration of fibroblast and lung carcinoma [161, 164]. Inhibiting myosin II at different levels by blebbistatin could be the reason that I did not see increased keratinocyte migration in my experiments. To the best of my knowledge no study has been performed on the effect of Y27632 or blebbistatin on keratinocyte force generation behavior.

Rho/Rho kinase pathway is regulated by integrin-dependant mechanosensing pathways [173]. Integrins are the main transmembrane receptors for ECM proteins. They physically connect the ECM to the cell's cytoskeleton, specifically via the actin microfilaments, therefore they are the best candidates for being the mechanosensors of the substrate [40]. An increase in substrate stiffness recruits more integrin proteins to the site of adhesion, which in turn activates more focal adhesion kinase (FAK). The increase in FAK activity also stimulates the Rho/ROCK (Rho kinase) pathway. Rho is a family of small GTPases that activate Rho kinase (ROCK), which in turn regulates myosin light

chain (MLC) phosphorylation. Phosphorylated MLC is necessary for engagement of actomyosin generated intracellular tension [41]. Rho kinase also seems to induce and maintain stress fibers by increasing contractility via MLC phosphorylation and by stabilizing actin filaments through LIMK activation, which results in cofilin phosphorylation.

In order to have a directed migration, Rho, Rac and cdc42 should act in concert in the cell body and lamellipoidum. Rho/ROCK pathway and actomyosin activity are postulated to turn off lamellipodia in other regions of the cell and aid directional cell migration [174]. Indeed, it is reported that reducing RhoA, RhoC or ROCK activity can lead to multiple and/or larger lamellopodia [175]. These reports are in consistent with elongated tails and multiple lamellipodia seen in Y27632 treated cells in my experiments.

Studies on fibroblasts showed that ROCK also inhibited Rac [176]. Interestingly, increasing mechanical tension by applying external strain to cells also inhibited Rac and blocked lamellipodia, indicating that mechanical tension may mediate the effect of Rho, ROCK and myosin on Rac [177]. In my poking experiments, tension is highest along the needle, which may cause suppression of Rac along the sides and leads to a directed migration toward the needle [178].

Inhibition of Rho kinase with Y27632 impairs the actomyosin interactions in the cells, which blights this mechanosensing pathway. Impeded migration of keratinocytes treated with Y27632 toward the mechanical deformations could be due to interrupted Rho/Rho kinase signaling pathway. Rho kinase inhibition disrupts Rac regulation, which results in formation of multiple lamellipodium and impaired cell directional migration [175].

Inhibiting myosin II by blabbistatin is also damaging the Rho/Rho kinase pathway. However, probably since myosin II is a downstream protein compared to Rho kinase in this pathway, inhibiting myosin II does not have as rigorous impact on the cell respond to the mechanical signal as inhibiting Rho kinase.

5.5 CONCLUSION

In this work, I investigated the keratinocytes response to local mechanical deformations. Acupuncture needle was used to make local mechanical deformations 100 µm and 200 µm away from isolated single cells. The cells on the soft substrate mostly changed their direction toward the needle and followed that. In addition, Y27632 and blebbistatin drugs were used to investigate the effect of inhibiting Rho kinase and myosin phosphorylation, respectively, on the keratinocyte response. The results indicated that treating the cells with Y27632 and blebbistatin impaired keratinocytes response to local mechanical deformations generated by the needle. Together my results reveals new insights in keratinocytes mechanotransduction and the importance of Rho kinases and myosin phosphorylation in keratinocytes response to local mechanical signals.

5.6 ACKNOWLEDGEMENTS

Support for this work was provided by the National Science Foundation (CAREER 1452728) to E.A.S. In addition, J.C.S. acknowledges the Dermatology Foundation for their support of this work through a career development award.

Chapter VI. CONCLUSION AND FUTURE WORK

6.1 CONCLUSION AND FUTURE WORK

In this thesis, I investigated the potential role of mechanical properties of the wound bed on keratinocyte behavior during wound healing. Polyacrylamide (PA) gels with tunable stiffness were used to study the effect of substrate stiffness on human keratinocyte migration and aggregate formation. The results of this study indicated that the cells on soft gels had significantly lower surface area, increased migration velocity, and increased rates of aggregate formation with higher number of cells per aggregate. These results together suggest that mechanical interactions can strongly influence keratinocyte behavior, particularly in terms of aggregate formation. Specifically, large substrate deformations in the soft gel might signal and guide keratinocytes to join into aggregates. Y27632, a chemical inhibitor for Rho kinases, was used to block the Rho/ROCK mechanotransduction pathway in keratinocytes. The deformations mad by the cells were impaired in the presence of Y27632, and the previously observed differences in aggregate formation on soft and stiff gels vanished. These results further support the idea that mechanical signals play an important role in keratinocyte activity.

Broad-spectrum proteomics was performed in order to deduce which proteins and pathways might by differentially expressed on the soft and stiff substrates. From this analysis, 56 proteins were found to differ in the soft versus stiff substrates. One of the most prominent of these proteins was serotransferrin. A secondary analysis of pathways is ongoing.

The role of keratin intermediate filaments in keratinocyte mechanosensing was investigated using the PA gel system. Type I keratin-muted mouse keratinocytes and their wild type pairs were analyzed on soft and stiff substrate. Knock-out keratinocyte were less

spread out, had impaired actin formation, generated less force on the substrate, and did not form aggregates as readily as wild type cells. The substantial reduction in force generation by knock out cells as unexpected because intermediate filaments are not generally known to affect actin-myosin cytoskeletal force generation. These results revealed the importance of keratin filament in keratinocyte mechanosensing and force generation. I hypothesis that the crosstalk between keratin filaments and actin filaments through pectin is an important regulator of keratinocytes mechanotransduction, though this proposition remains to be tested. Further analysis should be performed to investigate these potential interactions, as well as other components of the focal adhesion.

Keratinocytes response to local mechanical deformations was studied using a microneedle mounted onto a micromanipulator that was connected to servo-controlled linear actuator. Keratinocytes responded to needle-induced substrate deformations by changing their direction and migrating toward the needle. Inhibiting Rho/ROCK or actin-myosin II interactions with Y27632 and blebbistatin, respectively, impaired directed migration of keratinocyte toward the needle. This experiment clearly showed that keratinocytes in high calcium due respond to mechanical signals from the environment. The same set up could be used to study different cell types' response to mechanical deformation in variant conditions. This set up also provide a unique possibility to study proteins specifically involved in mechanostransduction of cells. For example by performing live-cell imaging on fluorescence tagged proteins, one should be able to track expression and spatial distribution of the tagged proteins in response to mechanical signal.

I believe the future step for this study is to replace polyacrylamide gel with an extracellular matrix more representative of granulation tissue in wound healing. For

instance collagen could be used as keratinocyte substrate and collagen stiffness could be regulated by using different crosslinks or collagen concentration. The other aspect of wound healing missed in this study is investigating keratinocyte sheet behavior. Using engineered skin to study wound healing should more closely mimic the *in vivo* situation.

Together, I introduced new platforms to study cells mechanotransduction and their response to mechanical signals. Here, I used these platforms to study the potential role of wound bed mechanical properties on keratinocytes behavior in re-epithelialization. My results reveal new insights on keratinocytes mechanobiology, which could help in the development of novel healing strategies.

LIST OF REFERENCES

1. VisionGain, *Advanced wound care: world market propspects 2011-2021*. 2011.
2. Evans, N.D., et al., *Epithelial mechanobiology, skin wound healing, and the stem cell niche.* journal of the mechanical behavior of biomedical materials, 2013. **28**: p. 397-409.
3. van der Veer, W.M., et al., *Potential cellular and molecular causes of hypertrophic scar formation.* Burns, 2009. **35**(1): p. 15-29.
4. Ogawa, R. and D.P. Orgill, *Mechanobiology of cutaneous wound healing and scarring*, in *Bioengineering Research of Chronic Wounds*. 2009, Springer. p. 31-42.
5. Witte, M.B. and A. Barbul, *General principles of wound healing.* Surg Clin North Am, 1997. **77**(3): p. 509-28.
6. Pastar, I., et al., *Epithelialization in Wound Healing: A Comprehensive Review.* Adv Wound Care (New Rochelle), 2014. **3**(7): p. 445-464.
7. Chao, C.Y.L., Y.P. Zheng, and G.L.Y. Cheing, *A novel noncontact method to assess the biomechanical properties of wound tissue.* Wound Repair and Regeneration, 2011. **19**(3): p. 324-329.
8. Marks, J.G., et al., *Lookingbill and Marks' principles of dermatology*. 4th ed. 2006, Philadelphia, PA: Saunders Elsevier. 331 p.
9. Selby, J.C., *Mechanobiology of Epidermal Keratinocytes: Desmosomes, Hemidesmosomes, Keratin Intermediate Filaments, and Blistering Skin Diseases.* Mechanobiology of Cell-Cell and Cell-Matrix Interactions, 2011: p. 169-210.
10. Bordeleau, F., et al., *Keratin 8/18 regulation of cell stiffness-extracellular matrix interplay through modulation of Rho-mediated actin cytoskeleton dynamics.* PLoS One, 2012. **7**(6): p. e38780.
11. Mescher, A.L., *Junqueira's basic histology: text and atlas*. 2013: Mcgraw-hill.
12. Bolognia, J.L., et al., *Dermatology*. Elsevier Health Sciences.
13. Darby, I., O. Skalli, and G. Gabbiani, *a-Smooth muscle actin is transiently expressed by myofibroblasts during experimental wound healing.* Lab Invest, 1990. **63**(1): p. 21-29.
14. Skalli, O., et al., *A monoclonal antibody against alpha-smooth muscle actin: a new probe for smooth muscle differentiation.* The Journal of cell biology, 1986. **103**(6): p. 2787-2796.
15. Tomasek, J.J., et al., *Myofibroblasts and mechano-regulation of connective tissue remodelling.* Nat Rev Mol Cell Biol, 2002. **3**(5): p. 349-63.
16. Gabbiani, G., C. Chaponnier, and I. Huttner, *Cytoplasmic filaments and gap junctions in epithelial cells and myofibroblasts during wound healing.* J Cell Biol, 1978. **76**(3): p. 561-8.
17. Spanakis, S.G., S. Petridou, and S.K. Masur, *Functional gap junctions in corneal fibroblasts and myofibroblasts.* Investigative ophthalmology & visual science, 1998. **39**(8): p. 1320-1328.
18. Li, B. and J.H. Wang, *Fibroblasts and myofibroblasts in wound healing: force generation and measurement.* J Tissue Viability, 2011. **20**(4): p. 108-20.
19. Xue, M. and C.J. Jackson, *Extracellular matrix reorganization during wound healing and its impact on abnormal scarring.* Advances in wound care, 2015. **4**(3): p. 119-136.

20. Wang, J., et al., *An updated review of mechanotransduction in skin disorders: transcriptional regulators, ion channels, and microRNAs.* Cellular and Molecular Life Sciences, 2015. **72**(11): p. 2091-2106.
21. Kurkinen, M., et al., *Sequential appearance of fibronectin and collagen in experimental granulation tissue.* Lab Invest, 1980. **43**(1): p. 47-51.
22. Reed, M.J., et al., *Differential expression of SPARC and thrombospondin 1 in wound repair: immunolocalization and in situ hybridization.* J Histochem Cytochem, 1993. **41**(10): p. 1467-77.
23. Bailey, A.J., et al., *Collagen polymorphism in experimental granulation tissue.* Biochem Biophys Res Commun, 1975. **66**(4): p. 1160-5.
24. Ehrlich, H.P. and T.M. Krummel, *Regulation of wound healing from a connective tissue perspective.* Wound Repair Regen, 1996. **4**(2): p. 203-10.
25. Miller, E.J., *Biochemical characteristics and biological significance of the genetically-distinct collagens.* Mol Cell Biochem, 1976. **13**(3): p. 165-92.
26. Doillon, C.J., et al., *Collagen fiber formation in repair tissue: development of strength and toughness.* Coll Relat Res, 1985. **5**(6): p. 481-92.
27. Levenson, S.M., et al., *The Healing of Rat Skin Wounds.* Ann Surg, 1965. **161**: p. 293-308.
28. Goffin, J.M., et al., *Focal adhesion size controls tension-dependent recruitment of alpha-smooth muscle actin to stress fibers.* Journal of Cell Biology, 2006. **172**(2): p. 259-268.
29. Trappmann, B., et al., *Extracellular-matrix tethering regulates stem-cell fate.* Nat Mater, 2012. **11**(7): p. 642-9.
30. Connelly, J.T., et al., *Actin and serum response factor transduce physical cues from the microenvironment to regulate epidermal stem cell fate decisions.* Nature Cell Biology, 2010. **12**(7): p. 711-U177.
31. Pelham, R.J., Jr. and Y. Wang, *Cell locomotion and focal adhesions are regulated by substrate flexibility.* Proc Natl Acad Sci U S A, 1997. **94**(25): p. 13661-5.
32. Zarkoob, H., et al., *Substrate Stiffness Affects Human Keratinocyte Colony Formation.* Cell Mol Bioeng, 2015. **8**(1): p. 32-50.
33. Engler, A.J., et al., *Matrix elasticity directs stem cell lineage specification.* Cell, 2006. **126**(4): p. 677-89.
34. Wang, Y., et al., *Substrate stiffness regulates the proliferation, migration, and differentiation of epidermal cells.* Burns, 2012. **38**(3): p. 414-20.
35. Lo, C.-M., et al., *Cell movement is guided by the rigidity of the substrate.* Biophysical journal, 2000. **79**(1): p. 144-152.
36. Califano, J.P. and C.A. Reinhart-King, *Substrate stiffness and cell area predict cellular traction stresses in single cells and cells in contact.* Cellular and molecular bioengineering, 2010. **3**(1): p. 68-75.
37. Zemel, A. and S. Safran, *Active self-polarization of contractile cells in asymmetrically shaped domains.* Physical Review E, 2007. **76**(2): p. 021905.
38. Discher, D.E., P. Janmey, and Y.L. Wang, *Tissue cells feel and respond to the stiffness of their substrate.* Science, 2005. **310**(5751): p. 1139-43.
39. Janostiak, R., et al., *Mechanosensors in integrin signaling: the emerging role of p130Cas.* Eur J Cell Biol, 2014. **93**(10-12): p. 445-54.

40. Schwartz, M.A., *Integrins and extracellular matrix in mechanotransduction.* Cold Spring Harb Perspect Biol, 2010. **2**(12): p. a005066.
41. Huang, S. and D.E. Ingber, *Cell tension, matrix mechanics, and cancer development.* Cancer Cell, 2005. **8**(3): p. 175-6.
42. Lock, F.E. and N.A. Hotchin, *Distinct roles for ROCK1 and ROCK2 in the regulation of keratinocyte differentiation.* PLoS One, 2009. **4**(12): p. e8190.
43. McMullan, R., et al., *Keratinocyte differentiation is regulated by the Rho and ROCK signaling pathway.* Curr Biol, 2003. **13**(24): p. 2185-9.
44. Ozawa, T., et al., *Dynamic relationship of focal contacts and hemidesmosome protein complexes in live cells.* J Invest Dermatol, 2010. **130**(6): p. 1624-35.
45. Tsuruta, D., et al., *Hemidesmosomes and focal contact proteins: Functions and cross-talk in keratinocytes, bullous diseases and wound healing.* Journal of Dermatological Science, 2011. **62**(1): p. 1-7.
46. Hopkinson, S.B., et al., *Focal Contact and Hemidesmosomal Proteins in Keratinocyte Migration and Wound Repair.* Adv Wound Care (New Rochelle), 2014. **3**(3): p. 247-263.
47. Chaudhuri, O., et al., *Extracellular matrix stiffness and composition jointly regulate the induction of malignant phenotypes in mammary epithelium.* Nat Mater, 2014. **13**(10): p. 970-8.
48. Rabinovitz, I., I.K. Gipson, and A.M. Mercurio, *Traction forces mediated by alpha6beta4 integrin: implications for basement membrane organization and tumor invasion.* Mol Biol Cell, 2001. **12**(12): p. 4030-43.
49. Mercurio, A.M. and I. Rabinovitz, *Towards a mechanistic understanding of tumor invasion--lessons from the alpha6beta 4 integrin.* Semin Cancer Biol, 2001. **11**(2): p. 129-41.
50. Rabinovitz, I. and A.M. Mercurio, *The integrin alpha6beta4 functions in carcinoma cell migration on laminin-1 by mediating the formation and stabilization of actin-containing motility structures.* J Cell Biol, 1997. **139**(7): p. 1873-84.
51. Rabinovitz, I., A. Toker, and A.M. Mercurio, *Protein kinase C-dependent mobilization of the alpha6beta4 integrin from hemidesmosomes and its association with actin-rich cell protrusions drive the chemotactic migration of carcinoma cells.* J Cell Biol, 1999. **146**(5): p. 1147-60.
52. O'Connor, K.L., L.M. Shaw, and A.M. Mercurio, *Release of cAMP gating by the alpha6beta4 integrin stimulates lamellae formation and the chemotactic migration of invasive carcinoma cells.* J Cell Biol, 1998. **143**(6): p. 1749-60.
53. Dupont, S., et al., *Role of YAP/TAZ in mechanotransduction.* Nature, 2011. **474**(7350): p. 179-83.
54. Sawada, Y., et al., *Force sensing by mechanical extension of the Src family kinase substrate p130Cas.* Cell, 2006. **127**(5): p. 1015-26.
55. Reichelt, J., *Mechanotransduction of keratinocytes in culture and in the epidermis.* Eur J Cell Biol, 2007. **86**(11-12): p. 807-16.
56. Harris, A.K., D. Stopak, and P. Wild, *Fibroblast traction as a mechanism for collagen morphogenesis.* Nature, 1981. **290**(5803): p. 249-251.
57. Harris, A.K., P. Wild, and D. Stopak, *Silicone rubber substrata: a new wrinkle in the study of cell locomotion.* Science, 1980. **208**(4440): p. 177-179.

58. Tan, J.L., et al., *Cells lying on a bed of microneedles: an approach to isolate mechanical force.* Proceedings of the National Academy of Sciences, 2003. **100**(4): p. 1484-1489.
59. Dembo, M. and Y.L. Wang, *Stresses at the cell-to-substrate interface during locomotion of fibroblasts.* Biophysical Journal, 1999. **76**(4): p. 2307-2316.
60. Wang, J.H.C. and J.S. Lin, *Cell traction force and measurement methods.* Biomechanics and Modeling in Mechanobiology, 2007. **6**(6): p. 361-371.
61. Marganski, W.A., M. Dembo, and Y.L. Wang, *Measurements of cell-generated deformations on flexible substrata using correlation-based optical flow.* Methods Enzymol, 2003. **361**: p. 197-211.
62. Rudnicki, M.S., et al., *Nonlinear strain stiffening is not sufficient to explain how far cells can feel on fibrous protein gels.* Biophys J, 2013. **105**(1): p. 11-20.
63. Maskarinec, S.A., et al., *Quantifying cellular traction forces in three dimensions.* Proc Natl Acad Sci U S A, 2009. **106**(52): p. 22108-13.
64. Wang, Y.L. and R.J. Pelham, Jr., *Preparation of a flexible, porous polyacrylamide substrate for mechanical studies of cultured cells.* Methods Enzymol, 1998. **298**: p. 489-96.
65. Raghupathy, R., et al., *Identification of regional mechanical anisotropy in soft tissue analogs.* J Biomech Eng, 2011. **133**(9): p. 091011.
66. Butler, J.P., et al., *Traction fields, moments, and strain energy that cells exert on their surroundings.* Am J Physiol Cell Physiol, 2002. **282**(3): p. C595-605.
67. Yang, Z.C., et al., *Determining substrate displacement and cell traction fields - a new approach.* Journal of Theoretical Biology, 2006. **242**(3): p. 607-616.
68. Selby, J.C., *Mechanobiology of Epidermal Keratinocytes: Desmosomes, Hemidesmosomes, Keratin Intermediate Filaments, and Blistering Skin Diseases*, in *Mechanobiology of Cell-Cell and Cell-Matrix Interactions*. 2011, Springer. p. 169-210.
69. Martin, P., *Wound healing--aiming for perfect skin regeneration.* Science, 1997. **276**(5309): p. 75-81.
70. Eming, S.A., *Biology of Wound Healing*, in *Dermatology*, J.L. Bolognia, Jorizzo, J.L., Schaffer, J.V., Editor. 2012, Elsevier Saunders: Philadephia.
71. Evans, N.D., et al., *Epithelial mechanobiology, skin wound healing, and the stem cell niche.* J Mech Behav Biomed Mater, 2013. **28**: p. 397-409.
72. Mertz, A.F., et al., *Cadherin-based intercellular adhesions organize epithelial cell-matrix traction forces.* Proc Natl Acad Sci U S A, 2013. **110**(3): p. 842-7.
73. Wang, Y., et al., *Substrate stiffness regulates the proliferation, migration, and differentiation of epidermal cells.* Burns, 2012. **38**(3): p. 414-420.
74. Doyle, A.D., et al., *One-dimensional topography underlies three-dimensional fibrillar cell migration.* The Journal of cell biology, 2009. **184**(4): p. 481-490.
75. Watt, F.M., P.W. Jordan, and C.H. O'Neill, *Cell shape controls terminal differentiation of human epidermal keratinocytes.* Proc Natl Acad Sci U S A, 1988. **85**(15): p. 5576-80.
76. Anon, E., et al., *Cell crawling mediates collective cell migration to close undamaged epithelial gaps.* Proc Natl Acad Sci U S A, 2012. **109**(27): p. 10891-6.

77. Kim, J.H., et al., *Propulsion and navigation within the advancing monolayer sheet.* Nat Mater, 2013. **12**(9): p. 856-63.
78. Trepat, X., et al., *Physical forces during collective cell migration.* Nature Physics, 2009. **5**(6): p. 426-430.
79. Kirsner, R.S., et al., *Spray-applied cell therapy with human allogeneic fibroblasts and keratinocytes for the treatment of chronic venous leg ulcers: a phase 2, multicentre, double-blind, randomised, placebo-controlled trial.* Lancet, 2012. **380**(9846): p. 977-85.
80. Hunyadi, J., et al., *Keratinocyte grafting: a new means of transplantation for full-thickness wounds.* J Dermatol Surg Oncol, 1988. **14**(1): p. 75-8.
81. Zamansky, G.B., U. Nguyen, and I.N. Chou, *An immunofluorescence study of the calcium-induced coordinated reorganization of microfilaments, keratin intermediate filaments, and microtubules in cultured human epidermal keratinocytes.* J Invest Dermatol, 1991. **97**(6): p. 985-94.
82. Watt, F.M., *Influence of cell shape and adhesiveness on stratification and terminal differentiation of human keratinocytes in culture.* J Cell Sci Suppl, 1987. **8**: p. 313-26.
83. Leigh, I.M. and F.M. Watt, *The culture of human epidermal keratinocytes*, in *The Keratinocyte Handbook*. 1994, Cambridge University Press: Cambridge England ; New York, NY, USA. p. 43-51.
84. Cras, J., et al., *Comparison of chemical cleaning methods of glass in preparation for silanization.* Biosensors and Bioelectronics, 1999. **14**(8): p. 683-688.
85. Aratyn-Schaus, Y., et al., *Preparation of complaint matrices for quantifying cellular contraction.* J Vis Exp, 2010(46).
86. Chan, S.H., D.T. Võ, and T.Q. Nguyen. *Subpixel motion estimation without interpolation*. in *Acoustics Speech and Signal Processing (ICASSP), 2010 IEEE International Conference on*. 2010. IEEE.
87. Tang, X., et al., *A novel cell traction force microscopy to study multi-cellular system.* PLoS Comput Biol, 2014. **10**(6): p. e1003631.
88. Selby, J.C. and M.A. Shannon, *Mechanical response of a living human epidermal keratinocyte sheet as measured in a composite diaphragm inflation experiment.* Biorheology, 2007. **44**(5-6): p. 319-48.
89. Toyjanova, J., et al., *High Resolution, Large Deformation 3D Traction Force Microscopy.* Plos One, 2014. **9**(4).
90. Tsuruta, D., et al., *Hemidesmosomes and focal contact proteins: functions and cross-talk in keratinocytes, bullous diseases and wound healing.* J Dermatol Sci, 2011. **62**(1): p. 1-7.
91. Hartwig, B., et al., *Laminin-5-deficient human keratinocytes: defective adhesion results in a saltatory and inefficient mode of migration.* Exp Cell Res, 2007. **313**(8): p. 1575-87.
92. Peyton, S.R. and A.J. Putnam, *Extracellular matrix rigidity governs smooth muscle cell motility in a biphasic fashion.* J Cell Physiol, 2005. **204**(1): p. 198-209.
93. Winer, J.P., S. Oake, and P.A. Janmey, *Non-linear elasticity of extracellular matrices enables contractile cells to communicate local position and orientation.* PLoS One, 2009. **4**(7): p. e6382.

94. Wen, J.H., et al., *Interplay of matrix stiffness and protein tethering in stem cell differentiation.* Nat Mater, 2014. **13**(10): p. 979-87.
95. Guo, W.H., et al., *Substrate rigidity regulates the formation and maintenance of tissues.* Biophys J, 2006. **90**(6): p. 2213-20.
96. Reinhart-King, C.A., M. Dembo, and D.A. Hammer, *Cell-cell mechanical communication through compliant substrates.* Biophys J, 2008. **95**(12): p. 6044-51.
97. Hamill, K.J., et al., *BPAG1e maintains keratinocyte polarity through beta4 integrin-mediated modulation of Rac1 and cofilin activities.* Mol Biol Cell, 2009. **20**(12): p. 2954-62.
98. Sehgal, B.U., et al., *Integrin beta4 regulates migratory behavior of keratinocytes by determining laminin-332 organization.* J Biol Chem, 2006. **281**(46): p. 35487-98.
99. Lange, T.S., et al., *Divalent cations (Mg2+, Ca2+) differentially influence the beta 1 integrin-mediated migration of human fibroblasts and keratinocytes to different extracellular matrix proteins.* Exp Dermatol, 1995. **4**(3): p. 130-7.
100. Lange, T.S., et al., *Mg2+ and Ca2+ differentially regulate beta 1 integrin-mediated adhesion of dermal fibroblasts and keratinocytes to various extracellular matrix proteins.* Exp Cell Res, 1994. **214**(1): p. 381-8.
101. Grzesiak, J.J. and M.D. Pierschbacher, *Changes in the concentrations of extracellular Mg++ and Ca++ down-regulate E-cadherin and up-regulate alpha 2 beta 1 integrin function, activating keratinocyte migration on type I collagen.* J Invest Dermatol, 1995. **104**(5): p. 768-74.
102. Achterberg, V.F., et al., *The nano-scale mechanical properties of the extracellular matrix regulate dermal fibroblast function.* J Invest Dermatol, 2014. **134**(7): p. 1862-72.
103. Ni Annaidh, A., et al., *Characterization of the anisotropic mechanical properties of excised human skin.* J Mech Behav Biomed Mater, 2012. **5**(1): p. 139-48.
104. Goffin, J.M., et al., *Focal adhesion size controls tension-dependent recruitment of alpha-smooth muscle actin to stress fibers.* J Cell Biol, 2006. **172**(2): p. 259-68.
105. Hall, A., *Rho GTPases and the control of cell behaviour.* Biochem Soc Trans, 2005. **33**(Pt 5): p. 891-5.
106. Amano, M., M. Nakayama, and K. Kaibuchi, *Rho-kinase/ROCK: A key regulator of the cytoskeleton and cell polarity.* Cytoskeleton (Hoboken), 2010. **67**(9): p. 545-54.
107. Jackson, B., et al., *RhoA is dispensable for skin development, but crucial for contraction and directed migration of keratinocytes.* Mol Biol Cell, 2011. **22**(5): p. 593-605.
108. Ishizaki, T., et al., *Pharmacological properties of Y-27632, a specific inhibitor of rho-associated kinases.* Mol Pharmacol, 2000. **57**(5): p. 976-83.
109. Havliš, J., et al., *Fast-response proteomics by accelerated in-gel digestion of proteins.* Analytical chemistry, 2003. **75**(6): p. 1300-1306.
110. Masuda, T., M. Tomita, and Y. Ishihama, *Phase transfer surfactant-aided trypsin digestion for membrane proteome analysis.* Journal of proteome research, 2008. **7**(2): p. 731-740.

111. Zakirova, Z., et al., *Complementary proteomic approaches reveal mitochondrial dysfunction, immune and inflammatory dysregulation in a mouse model of Gulf War Illness.* PROTEOMICS-Clinical Applications, 2017.
112. Gilar, M., et al., *Comparison of 1-D and 2-D LC MS/MS methods for proteomic analysis of human serum.* Electrophoresis, 2009. **30**(7): p. 1157-1167.
113. Gilar, M., et al., *Two-dimensional separation of peptides using RP-RP-HPLC system with different pH in first and second separation dimensions.* Journal of separation science, 2005. **28**(14): p. 1694-1703.
114. Chevallet, M., S. Luche, and T. Rabilloud, *Silver staining of proteins in polyacrylamide gels.* Nature protocols, 2006. **1**(4): p. 1852-1858.
115. Gandham, V.D., et al., *Effects of Y27632 on keratinocyte procurement and wound healing.* Clin Exp Dermatol, 2013. **38**(7): p. 782-6.
116. Sarkar, S., T. Egelhoff, and H. Baskaran, *Insights into the Roles of Non-Muscle Myosin Iia in Human Keratinocyte Migration.* Cell Mol Bioeng, 2009. **2**(4): p. 486-494.
117. Chapman, S., et al., *Human keratinocytes are efficiently immortalized by a Rho kinase inhibitor.* J Clin Invest, 2010. **120**(7): p. 2619-26.
118. Strudwick, X.L., et al., *Combination of low calcium with Y-27632 rock inhibitor increases the proliferative capacity, expansion potential and lifespan of primary human keratinocytes while retaining their capacity to differentiate into stratified epidermis in a 3D skin model.* PLoS One, 2015. **10**(4): p. e0123651.
119. Terunuma, A., et al., *Efficient procurement of epithelial stem cells from human tissue specimens using a Rho-associated protein kinase inhibitor Y-27632.* Tissue Eng Part A, 2010. **16**(4): p. 1363-8.
120. Gupta, P., et al., *Substrate stiffness does affect the fate of human keratinocytes.* RSC Advances, 2016. **6**(5): p. 3539-3551.
121. MacGillivray, R.T., et al., *Two high-resolution crystal structures of the recombinant N-lobe of human transferrin reveal a structural change implicated in iron release.* Biochemistry, 1998. **37**(22): p. 7919-28.
122. Macedo, M.F. and M. de Sousa, *Transferrin and the transferrin receptor: of magic bullets and other concerns.* Inflamm Allergy Drug Targets, 2008. **7**(1): p. 41-52.
123. Jeffrey, P.D., et al., *Ligand-induced conformational change in transferrins: crystal structure of the open form of the N-terminal half-molecule of human transferrin.* Biochemistry, 1998. **37**(40): p. 13978-86.
124. Arosio, P., G. Cairo, and S. Levi, *The molecular biology of iron-binding proteins*, in *Iron in immunity, cancer and inflammation*. 1989, Wiley New York. p. 55-79.
125. Morgan, E., *Transferrin and transferrin iron.* Iron in biochemistry and medicine, 1974: p. 29-71.
126. Skinner, M.K. and M.D. Griswold, *Sertoli cells synthesize and secrete transferrin-like protein.* Journal of Biological Chemistry, 1980. **255**(20): p. 9523-9525.
127. Bloch, B., et al., *Transferrin gene expression visualized in oligodendrocytes of the rat brain by using in situ hybridization and immunohistochemistry.* Proceedings of the National Academy of Sciences, 1985. **82**(19): p. 6706-6710.

128. Aldred, A.R., et al., *Distribution of transferrin synthesis in brain and other tissues in the rat.* Journal of Biological Chemistry, 1987. **262**(11): p. 5293-5297.
129. Tsutsumi, M., M. Skinner, and E. Sanders-Bush, *Transferrin gene expression and synthesis by cultured choroid plexus epithelial cells. Regulation by serotonin and cyclic adenosine 3', 5'-monophosphate.* Journal of Biological Chemistry, 1989. **264**(16): p. 9626-9631.
130. Stocks, J., et al., *The inhibition of lipid autoxidation by human serum and its relation to serum proteins and α-tocopherol.* Clinical Science, 1974. **47**(3): p. 223-233.
131. CRICHTON, R.R. and M. CHARLOTEAUX-WAUTERS, *Iron transport and storage.* European Journal of Biochemistry, 1987. **164**(3): p. 485-506.
132. Hirschhorn, T. and M. Ehrlich, *Intimate and Facultative? Regulation of Clathrin-Mediated Endocytosis by the Actin Cytoskeleton*, in *Vesicle Trafficking in Cancer*. 2013, Springer. p. 33-56.
133. Gottlieb, T.A., et al., *Actin microfilaments play a critical role in endocytosis at the apical but not the basolateral surface of polarized epithelial cells.* The Journal of cell biology, 1993. **120**(3): p. 695-710.
134. Chandrasekar, I., et al., *Nonmuscle Myosin II Is a Critical Regulator of Clathrin-Mediated Endocytosis.* Traffic, 2014. **15**(4): p. 418-432.
135. Lamaze, C., et al., *The actin cytoskeleton is required for receptor-mediated endocytosis in mammalian cells.* J Biol Chem, 1997. **272**(33): p. 20332-5.
136. Karin, M. and B. Mintz, *Receptor-mediated endocytosis of transferrin in developmentally totipotent mouse teratocarcinoma stem cells.* Journal of Biological Chemistry, 1981. **256**(7): p. 3245-3252.
137. Kan, M. and I. Yamane, *Effects of ferrous iron and transferrin on cell proliferation of human diploid fibroblasts in serum-free culture.* In vitro, 1984. **20**(2): p. 89.
138. Vostrejs, M., P.L. Moran, and P.A. Seligman, *Transferrin synthesis by small cell lung cancer cells acts as an autocrine regulator of cellular proliferation.* Journal of Clinical Investigation, 1988. **82**(1): p. 331.
139. Halliwell, B., *Oxidative stress in cell culture: an under-appreciated problem?* FEBS letters, 2003. **540**(1-3): p. 3-6.
140. Cheng, J. and A. Vieira, *Oxidative stress disrupts internalization and endocytic trafficking of transferrin in a human malignant keratinocyte line.* Cell biochemistry and biophysics, 2006. **45**(2): p. 177-184.
141. Lamaze, C., et al., *Regulation of receptor-mediated endocytosis by Rho and Rac.* Nature, 1996. **382**(6587): p. 177.
142. Schmalzing, G., et al., *Involvement of the GTP binding protein Rho in constitutive endocytosis in Xenopus laevis oocytes.* The Journal of Cell Biology, 1995. **130**(6): p. 1319-1332.
143. Rodman, J.S. and A. Wandinger-Ness, *Rab GTPases coordinate endocytosis.* J Cell Sci, 2000. **113**(2): p. 183-192.
144. Ellis, S. and H. Mellor, *Regulation of endocytic traffic by rho family GTPases.* Trends in cell biology, 2000. **10**(3): p. 85-88.
145. Yeung, T., et al., *Effects of substrate stiffness on cell morphology, cytoskeletal structure, and adhesion.* Cell Motil Cytoskeleton, 2005. **60**(1): p. 24-34.

146. Levental, I., P.C. Georges, and P.A. Janmey, *Soft biological materials and their impact on cell function.* Soft Matter, 2007. **3**(3): p. 299-306.
147. Georges, P.C. and P.A. Janmey, *Cell type-specific response to growth on soft materials.* Journal of Applied Physiology, 2005. **98**(4): p. 1547-1553.
148. Wang, H.B., M. Dembo, and Y.L. Wang, *Substrate flexibility regulates growth and apoptosis of normal but not transformed cells.* American Journal of Physiology-Cell Physiology, 2000. **279**(5): p. C1345-C1350.
149. Mitchison, T.J. and L.P. Cramer, *Actin-based cell motility and cell locomotion.* Cell, 1996. **84**(3): p. 371-379.
150. Goldman, R.D., et al., *The function of intermediate filaments in cell shape and cytoskeletal integrity.* Journal of Cell Biology, 1996. **134**(4): p. 971-983.
151. Jones, J.C.R., S.B. Hopkinson, and L.E. Goldfinger, *Structure and assembly of hemidesmosomes.* Bioessays, 1998. **20**(6): p. 488-494.
152. Seltmann, K., et al., *Keratins mediate localization of hemidesmosomes and repress cell motility.* J Invest Dermatol, 2013. **133**(1): p. 181-90.
153. Gadiou, R., et al., *Temperature-programmed desorption as a tool for quantification of protein adsorption capacity in micro- and nanoporous materials.* Colloids Surf B Biointerfaces, 2009. **73**(2): p. 168-74.
154. Brennan, J.K., et al., *Improved methods for reducing calcium and magnesium concentrations in tissue culture medium: application to studies of lymphoblast proliferation in vitro.* In Vitro, 1975. **11**(6): p. 354-60.
155. Broussard, J.A., et al., *The desmoplakin/intermediate filament linkage regulates cell mechanics.* Mol Biol Cell, 2017.
156. Seltmann, K., et al., *Keratins Stabilize Hemidesmosomes through Regulation of beta4-Integrin Turnover.* J Invest Dermatol, 2015. **135**(6): p. 1609-20.
157. Seltmann, K., et al., *Keratins significantly contribute to cell stiffness and impact invasive behavior.* Proc Natl Acad Sci U S A, 2013. **110**(46): p. 18507-12.
158. Homberg, M., et al., *Distinct Impact of Two Keratin Mutations Causing Epidermolysis Bullosa Simplex on Keratinocyte Adhesion and Stiffness.* J Invest Dermatol, 2015. **135**(10): p. 2437-45.
159. Ramms, L., et al., *Keratins as the main component for the mechanical integrity of keratinocytes.* Proc Natl Acad Sci U S A, 2013. **110**(46): p. 18513-8.
160. Juliano, R.L. and S. Haskill, *Signal transduction from the extracellular matrix.* J Cell Biol, 1993. **120**(3): p. 577-85.
161. Sandquist, J.C., et al., *Rho kinase differentially regulates phosphorylation of nonmuscle myosin II isoforms A and B during cell rounding and migration.* J Biol Chem, 2006. **281**(47): p. 35873-83.
162. Wong, V.W., et al., *Pushing back: wound mechanotransduction in repair and regeneration.* J Invest Dermatol, 2011. **131**(11): p. 2186-96.
163. Lo, C.M., et al., *Cell movement is guided by the rigidity of the substrate.* Biophysical Journal, 2000. **79**(1): p. 144-152.
164. Even-Ram, S., et al., *Myosin IIA regulates cell motility and actomyosin-microtubule crosstalk.* Nat Cell Biol, 2007. **9**(3): p. 299-309.
165. Dunn, G.A., *Characterising a kinesis response: time averaged measures of cell speed and directional persistence.* Agents Actions Suppl, 1983. **12**: p. 14-33.

166. Othmer, H.G., S.R. Dunbar, and W. Alt, *Models of dispersal in biological systems.* J Math Biol, 1988. **26**(3): p. 263-98.
167. Wu, P.H., A. Giri, and D. Wirtz, *Statistical analysis of cell migration in 3D using the anisotropic persistent random walk model.* Nat Protoc, 2015. **10**(3): p. 517-27.
168. Stokes, C.L., D.A. Lauffenburger, and S.K. Williams, *Migration of individual microvessel endothelial cells: stochastic model and parameter measurement.* J Cell Sci, 1991. **99 (Pt 2)**: p. 419-30.
169. Lin, B., J. Yu, and S.A. Rice, *Direct measurements of constrained brownian motion of an isolated sphere between two walls.* Phys Rev E Stat Phys Plasmas Fluids Relat Interdiscip Topics, 2000. **62**(3 Pt B): p. 3909-19.
170. Berens, P., *CircStat: a MATLAB toolbox for circular statistics.* J Stat Softw, 2009. **31**(10): p. 1-21.
171. Tambe, D.T., et al., *Collective cell guidance by cooperative intercellular forces.* Nat Mater, 2011. **10**(6): p. 469-75.
172. Boudou, T., et al., *Nonlinear elastic properties of polyacrylamide gels: implications for quantification of cellular forces.* Biorheology, 2009. **46**(3): p. 191-205.
173. Huveneers, S. and E.H. Danen, *Adhesion signaling - crosstalk between integrins, Src and Rho.* J Cell Sci, 2009. **122**(Pt 8): p. 1059-69.
174. Ridley, A.J., *Rho GTPase signalling in cell migration.* Curr Opin Cell Biol, 2015. **36**: p. 103-12.
175. Vega, F.M., et al., *RhoA and RhoC have distinct roles in migration and invasion by acting through different targets.* J Cell Biol, 2011. **193**(4): p. 655-65.
176. Tsuji, T., et al., *ROCK and mDia1 antagonize in Rho-dependent Rac activation in Swiss 3T3 fibroblasts.* J Cell Biol, 2002. **157**(5): p. 819-30.
177. Katsumi, A., et al., *Effects of cell tension on the small GTPase Rac.* J Cell Biol, 2002. **158**(1): p. 153-64.
178. Munevar, S., Y. Wang, and M. Dembo, *Traction force microscopy of migrating normal and H-ras transformed 3T3 fibroblasts.* Biophys J, 2001. **80**(4): p. 1744-57.
179. Ng, M.R., et al., *Substrate stiffness regulates cadherin-dependent collective migration through myosin-II contractility.* J Cell Biol, 2012. **199**(3): p. 545-63.
180. Ray, A., et al., *Enhanced Directional Migration of Cancer Stem Cells in 3D Aligned Collagen Matrices.* Biophys J, 2017. **112**(5): p. 1023-1036.

Appendix A: Pre-formed Aggregate in Mouse Keratinocyte

To assess the role of keratin intermediate filaments in aggregate contraction, pre-formed aggregates were formed with WT and KO mouse keratinocytes. In order to prepare pre-formed aggregates 0.5 mm holes were punched through a 55 µm thick silicon sheet (McMASTER-CARR). These holes served as a mask that allowed me to form aggregate of a defined size. The masks were placed on top of the gels and 10 µl of high-density cell suspension were added to each hole. The gels with the cells and the mask on were left in incubator for 1.5 hours of incubation to let the cells attach, the mask was removed and the gels were washed twice with PBS. High Ca^{2+} medium were added to the gels and they were placed in the environmentally controlled microscope chamber. DIC and fluorescent images were taken every five minutes during 22 hr after culturing the cells.

In order to quantify the ability of pre-formed aggregates to contract and deform the substrate, the percentage of contraction of each pre-formed aggregate was calculated as $100 \times (A_o - A_i)/A_o$, where A_o is the initial area of the pre-formed aggregate and A_i is the area of pre-formed aggregate at $t = i$. The surface areas were measured using ImageJ.

Rate of Pre-formed Aggregate Contraction is Different in WT and KO Cells

Both WT and KO cells quickly formed cell-cell junctions with their neighbors and contracted in area (Figure A.1). No differences in the extent of contraction were observed between WT and KO pre-formed aggregates (73.8% ± 6.2% and 71.7% ± 5.3% respectively). However, significant difference in the rate was observed with WT and KO, reaching maximum area contraction at 5.5 hr ± 0.58 hr, 7.5 hr ± 1 hr, respectivly ($p < 0.02$). Once the area had contracted, both WT and KO pre-formed aggregates grew in size to form epithelial sheet. The time for outgrowth was delayed for WT compared to KO (Figure A.2).

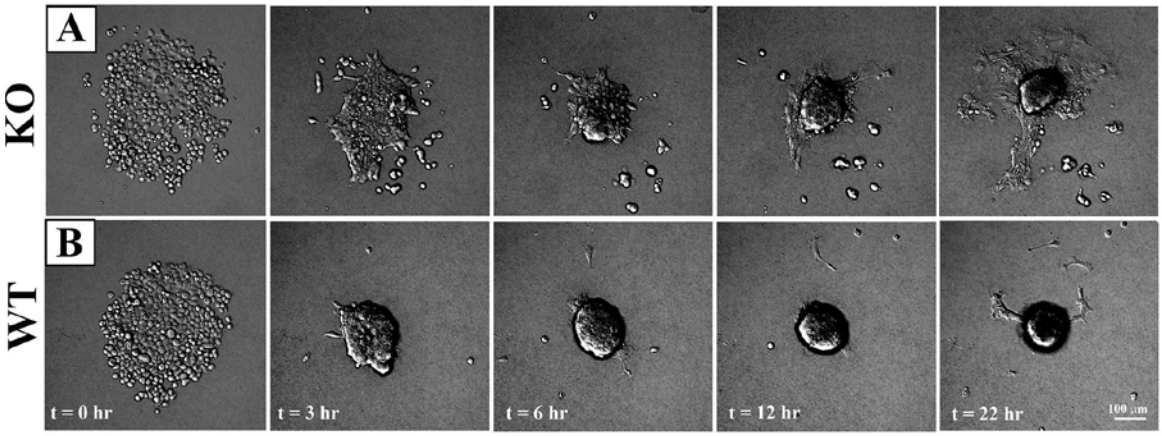

Figure A.1. Time-Lapse imaging showing area contraction for A) KO and B) WT cells on soft PA gel. WT pre-formed aggregates contracted faster and were more coherent compared KO samples. KO aggregates appeared to have more outgrowth.

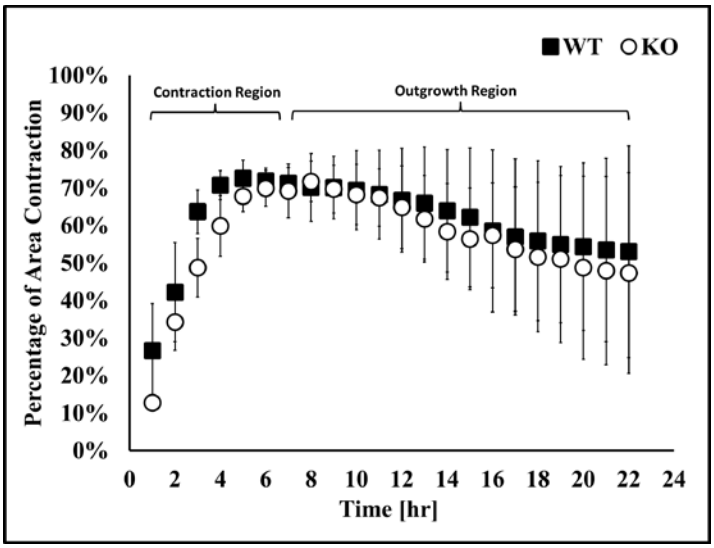

Figure A.2. Percentage of area contraction in WT and KO pre-formed aggregates

Appendix B: Control Experiments for Y27632 and Blebbistatin Treated Cells

Standard metrics for characterizing cell migration were assessed, including the confinement ratio (CR), defined as the net HEKn distance traveled over the total distance traveled, and the directionality ratio (DR), defined as the ratio of the sum of the projected cell velocity in the direction of needle movement to the sum of the cell velocities over the duration of the experiment [179, 180]. CR values range from 0 to 1 for random and completely directed movement, respectively. For the experiments involving the needle, the adjusted cell position was used to determine the DR, which ranges between -1 for a cell that moves in exactly the opposite direction of needle movement to 1 for a cell that moves in the direction of needle movement. All the indices were calculated for 10 cells, over two hours experiment.

$$CR = \frac{|\bar{r}_{t=0} - \bar{r}_{end}|}{\sum_{t=0}^{end} |\overline{\Delta r_t}|} \qquad (4)$$

$$DR = \frac{\sum_{t=0}^{end} \left(\frac{\overline{\Delta r_t} \cdot \bar{r}_{needle}}{|\overline{\Delta r_t}||\bar{r}_{needle}|}\right) |\bar{r}_t|}{\sum_{t=0}^{end} |\overline{\Delta r_t}|} \qquad (5)$$

Where $\bar{r}_{t=0}$ is the position vector of the cell at $t = 0$ when the needle is inserted, $\bar{r}_{end}$ is the position vector of the cell at the last time frame, $\bar{r}_{needle}$ is the direction vector of the needle, which is calculated as the mean direction of the needle in 10 experiments, and $\overline{\Delta r_t} = \bar{r}_t - \bar{r}_{t-1}$.

Cell Motility: Control Experiments

To investigate the influence of Y27632 and blebbistatin drug and substrate stiffness on the HEKn migration in the absence of the needle, the migration trajectory of 10 cells from four control conditions, soft-control, soft-Y27632-control, soft-blebbistatin-control, stiff control were plotted (Figure B.1). As Figure B.1 shows the cells path on soft PA gels were convoluted. The cells inclined to change their migration direction vibrantly and did

not show persistency in their migration path. In contrast, the cells paths on stiff PA gel samples appeared to be much straighter and not have the wavy pattern on the soft substrates. In order to quantify these observations, the Confinement Ratio (CR) was calculated for 10 cell paths in each condition. As presented in Table B.1, the CR value for the stiff control cells was (CR stiff control) which was 1.8 times higher than the CR value for the soft ones (CR soft control). These results are in consistence with the more restrained cell migration I observed on soft PA gels versus stiff samples.

Interestingly, the migration paths of the cells treated with Y27632 were not as convoluted as the path of the cells on the soft substrate and were approximating the cells path on the stiff substrate. Blebbistatin did not alter the wavy pattern of the cells migration path. However, the blebbistatin-treated cells were not able to migrate further away from their starting point. In consistence with my observations, treating the cells with Y27632 on the soft gel increased the CR value of the cells to 0.57 ± 0.22, meaning that Y27632-treated cell became less confined in their migration. Bebbistatin did not alter the CR value of the cell on soft substrate (0.34 ± 0.19).

Table B.1. The CR and DR for different experimental conditions

Sample Name	CR	DR
Soft 100	0.52 ± 0.23	0.46 ± 0.28
Soft 200	0.51 ± 0.27	0.43 ± 0.40
Soft Y27632	0.31 ± 0.22	0.05 ± 0.40
Soft Blebbistatin	0.55 ± 0.28	- 0.09 ± 0.31
Soft Control	0.34 ± 0.26	_
Soft+Y27632 Control	0.57 ± 0.22	_
Soft+Blebbistatin Control	0.34 ± 0.19	_
Stiff Control	0.61 ± 0.33	_

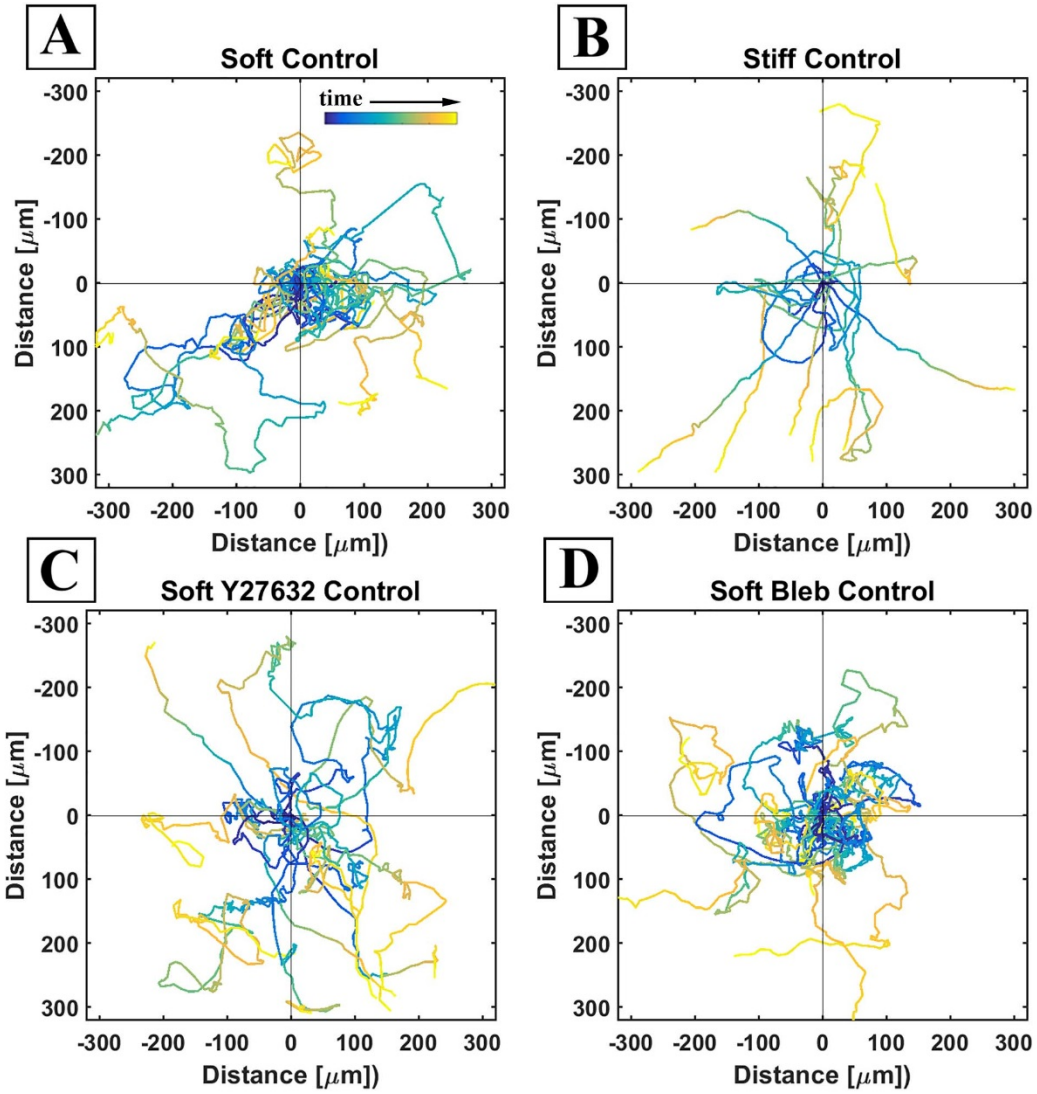

Figure B.1. Cell migration path in control experiments in the absence of needle over 24 hrs. A) Soft Control, B) Stiff Control, C) Soft Y27632 Control, and D) Soft Blebbistatin Control. The cells have a more persistence path in stiff control samples compared to soft control samples. Soft Y27632 control cells also show a more persistence path compared to soft control.

Cell Motility: Needle Experiments

To assess the influence of local mechanical deformations on the cell migration, the adjusted migration path of 10 cells from 4 different needle-inserted experiments were plotted (Figure 31). As this figure shows the cells paths were rigorously affected by the needle. Remarkably, in soft-100 samples the cells pivoted their migration direction toward the needle and ultimately traced the needle. In accordance with redirecting the migration

direction, the CR value of the cells also increased to (0.52 ± 0.23). In soft-200 samples, the cells showed identical trend as the soft-100 samples for most of the cells and the CR value of the cells increased to (0.51 ± 0.27) compared to control soft cells.

To assess the effect of blocking different part of mechanosensing pathways on cells behavior, Y27632 and blebbistatin treated cells were also examined in this set up. Interestingly, the Y27632 treated cells did not alter their migration direction toward the needle. Plotting the Y27632-treated cells path showed that the cells appeared to have a random migration direction, without any preference toward the needle. The CR value of theY27632 treated cells also did not altered in the presence of the needle. To quantify the proportion of the cells migration in the direction of needle movement, the Directionality Ratio (DR) of the cells were calculated. DR value was defined as the ratio of the sum of the projected cell velocity in the direction of needle movement to the sum of the cell velocities over the duration of the experiment. The DR value of soft-100 μm was 0.46 ± 0.28 and soft 200 μm was 0.43 ± 0.40 which was higher than soft Y27632 treated which was 0.05 ± 0.40, verifying the non-preferential migration of Y27632 –treated cells in the presence of the needle.

The cell path in blabbistatin treated cell was not like Y276732 treated cell, nor like untreated cells. The cell paths were neither elongated toward the needle nor going away from it. Instead, the same as blebbistatin control sample, the blebbistatin-treated cells did not migrate much away from their starting points. The CR value of the blebbistatin-treated samples also did not alter in the presence of needle. However, the DR value of blebbistatin-treated samples was reduced to -.09 ± 0.31, much lower than DR values in soft-100 and soft-200 samples.

Appendix C: Protocols

Making polyacrylamide gel substrate:

Materials:

Table C.1. Materials needed for making polyacrylamide gel

Name	Company	Catalog Number
40% Acrylamide	Biorad	#161-0140
2% Bis-Acrylamide	Fisher Scientific	#BP 1404
Ammonium persulfate (APS)	Fisher Scientific	#BP 150-20
N,N,N',N'-Tetramethylethylenediamine (TEMED)	Fisher Scientific	#BP 179
Sulfo-SANPAH	Thermo Scientific	#22589
FluoSpheres® Carboxylate-Modified Microspheres, 0.5 µm, Red Fluorescent	Life Technologies	#F8812
3-aminopropyltrimethyoxysilane (3-APTMS)	Sigma-Aldrich	#28, 177-8
Glutaraldehyde	Fisher Scientific	#G151-1
Keratinocyte-SFM	Gibco	#10724011
PBS	invitrogen	#00-3000
HEPES	Sigma	#H0887
Ethanol	Pharmco-AAper	
Methanol	Fisher Scientific	#A456-500
NaOH	Fisher Scientific	#SS255-1
37% HCL	sigma-Aldrich	
cover glass, 40mm CIR. #1.5	Warner Instruments	#64-1696
Pepsin Extracted Type 1 Collagen	Advanced Biomatrix	#5005-B
Human Epidermal Keratinocytes, neonatal	Life Technologies	#C-001-5C
Low Profile Parallel Plate Flow Chamber (RC-31)	Warner Instruments	

Steps:

1. Preparation of Polyacrylamide gel (PA gel) with different stiffness'

    1.1.Washing the coverslips
    1.2.Activating the coverslips (crosslinking of PA gel and coverslips)
    1.3.Making the PA gel

2. Crosslinking pepsin extracted type I collagen with PA gel using Sulfo-SANPAH

Protocols:

1.1. Washing the coverslips:

Materials: Alconox- Ethanol- Methanol- HCL 1M- deionized water –

1. Place coverslips into a 100 ml glass beaker filled halfway with 1% Alconox and sonicate 30 min in a water bath sonicator at 60^{o}C.
2. Rinse coverslips 10 times by swirling with deionized water. Sonicate with distilled water 30 min in sonicator at 60^{o}C.
3. Rinse the coverslips with 100% Ethanol and sonicate 30 min in sonicator.
4. Rinse the coverslips with 50% HCl (1 M)- 50% Methanol for 1 min.
5. Rinse coverslips 10 times by swirling with distilled water and let them to be dried at room temperature in a clean place, away from dust.

1.2. Activating the coverslips:

Materials: NaOH 0.1 M- 3-APTMS - Glutaraldehyde 0.5% (please scale up everything based on the size of the cover glass that you use)

6. Place a layer of parafilm on the bottom of a 100 ml petri dish.
7. Place up to 6, 12mm coverslips on top of the parafilm and cover them with 0.5 ml 0.1 M NaOH. Incubate for 3 min and then aspirate with pipet.
8. Working in a chemical hood, place 0.25 ml 3-APTMS on each coverslip. Incubate for 3 min and then aspirate the APTMS.
9. Rinse the coverslips once with deionized water in the same dish, remove the coverslips from the dish using the curved forceps and transfer them, with their treated-side facing up to a new dish. Wash the coverslips with deionized water 3 times on a rocker for 10 min each.
10. Using curved forceps, transfer the coverslips to a clean dish layered with parafilm and aspirates any remaining liquid with pipet or Kimwipe to blot the remaining water.
11. Cover each coverslip with 0.25 ml of 0.5% Glutaraldehyde in deionized water; incubate for 30 min in a chemical hood. Aspirate the Glutaraldehyde.
12. Rinse and wash the coverslips with deionized water 3 times on a rocker for 10 min each.
13. Dry the coverslips completely.

1.3. **Making the PA gel with different stiffnesses: soft (k≈1.2 kP), stiff (k≈24 kP):**

Materials: 40% Acrylamide- 2% Bis-acrylamide- 10% APS - TEMED- PBS- Fluorescent beads-deionized water

14. Sterilize 40% Acrylamide, 2% Bis-acrylamide, 10% APS and deionized water with 0.2 µm filter.
15. Using a clean Kimwipe, coat the microscope slides with Rain-X. Allow the circular coverslips to dry for at least 10 min. Buff off excess Rain-X with a Kimwipe. Remove dust and debris using optical tissue to obtain a clean surface.
16. Put a sheet of parafilm under the Biological hood and put that activated coverslips, with the treated surface up and the microscope slides on it. Sterilize them with UV light under the hood for one hour.
17. Prepare 10% ammonium persulfate (APS; 100 µg/ml water) shortly before use and sterile filter. Stocks can be frozen at -20 to be used at later dates. Replace the APS solution monthly.
18. Add 100 ul of beads solution to the water and sonicate it for 15 min.
19. Prepare the 40% acrylamide, 2% bis-acrylamide, water and TEMED to reach the desired acrylamide percentage (Table C.2).

Table C.2. Recipe for preparing polyacrylamide gel with various stiffness

(µL)	**SOFT (≈1.2 kPa)**	**STIFF (≈24 kP)**
%40 Acrylamide	250	940
%2 Bis-Acrylamide	625	750
ddH_2O	3992.5	3180
Bead	100	100
%10 APS	25	25
TEMED	7.5	7.5
Total	5000	5000
Final Acrylamide %	2	7.5
Final Bis-Acrylamide %	0.25	0.3

20. Mix the solution thoroughly and place the solution in vacuum chamber for 15 min.
21. Then add 10% APS to the acrylamide solution, mix briefly and IMMEDIATELY pour 10 µl per microscope slide in the biological safety hood.
22. Quickly place the activated coverslips on top of each gel before it begins to polymerize. Incubate this "sandwich" at room temperature until the acrylamide polymerizes. (Check the residual acrylamide solution in the 15 ml c-tube tube to determine when polymerization has occurred.
23. Slide off the coverslips and Place them into 6-well plates with 2 ml PBS/well.

24. Wash the hydrogels with PBS three times, on a rocker, 5 min per wash.
25. Wash the hydrogels with sterile water overnight on a rocker.

2- Crosslinking Pepsin Extracted Type 1 Collagen to the surface of PA gel.

Materials: HEPES (pH to 8.5), Pepsin extracted type I collagen, Sulfo-SANPAH (SS), DMSO, UV light

For total 4ml of the solution needed:

1. Warm SS to room temperature by holding it in your hand (normally kept in -20 freezer)
2. Weigh 2 mg of SS for each gel
3. Add in 8uL of DMSO
4. Vortex until SS completely dissolved. Note: there should be no clumps of SS, additionally, solution with be bright red color
5. Add 4mL of HEPES (PH 8.5).
6. Pipet 200 uL of solution onto PA gel
7. Place PA gel under UV light for 6 minutes
    a. Solution will turn brown
8. Rinse thoroughly with HEPES. PA gel should not have any solution remaining on it
9. Apply 200 uL more of solution onto PA gel
10. Place PA gel under UV light for 6 minutes
11. Rinse with HEPES thoroughly
12. Prepare collagen solution (100 ug/mL dissolved in 1X PBS)
13. Apply 200 uL of collagen solution to PA gel (100 ug/ml of collagen dissolved in 1X PBS), let the collagen sit on the gel for 2 hrs at room temperature or 24-48 in the refrigerator
14. Remove excess collagen before seeding cells.
15. Rinse with 1X PBS to remove excess collagen
16. Sterilize with UV light for 15 minutes before seeding cells.

Culturing primary human neonatal keratinocyte (HEKn) cells:

Materials:

Table C.3. Materials needed for culturing HEKn cell

Name	Company	Catalog Number
Human Epidermal Keratinocytes, neonatal	Life Technologies	#C-001-5C
Keratinocyte Serum Free Medium (KSFM)	Gibco	#10724011
penicillin–streptomycin	Gibco	
Amphotericin-B	Gibco	
Soybean Trypsin Inhibitor	Thermo Scientific	#17075029
1X PBS	Invitrogen	#00-3000
0.25 %Trypsin-EDTA	Gibco	

1- Prepare a solution of 99% Keratinocyte-SFM medium (#10724-011, Gibco), 1% penicillin–streptomycin, and 0.01% Amphotericin-B.
2- Rinse the cells in the T-75 flask with PBS.
3- Add 3 ml trypsin to T-75 flask and leave the flask in room temperature for 5 min.
4- Add 9 ml of trypsin inhibitor to the cells and pipet that up and down gently few times.
5- Pipet the whole solution in a 50 ml C-tube and centrifuge for 7 min in 180 g.
6- Take the supernatant out and add 3ml KSFM medium and re suspend the cells pellet gently.
7- Count the cells with hemocytometer and Plate keratinocyte with the desired cells density.

Fixing the samples:

Materials:

Table C.4. Materials needle for fixing the cells

Name	Company	Catalog Number
Methanol	-	-
4% Paraformaldehyde (PFA)	-	-
PBS	-	-

1- In order to stain keratin intermediate filaments, or desmoplakin in keratinocytes it is better to fix the samples with methanol, in other cases use PFA
2- Prepare 100% methanol cooled down to -20^{o}C, or 4% PFA in room temperature.
3- Pipet off the culture medium from the keratinocyte and replace it with PBS.
4- Remove the PBS and replace it with cold methanol. Incubate in freezer for about 10 min. in case of using PFA incubate the sample on room temperature for 1 hr.
5- Remove Methanol/PFA and replace with fresh PBS.
6- What the samples again with PBS.
7- Store at 4 ^{o}C.

Immunofluorescent Staining

Materials:

Table C.5. Other reagent needed for immunofluorescent staining of the cell

Name	Company	Catalog Number
Normal Donkey Serum	abcam	#ab7475
Normal Goat Serum	abcam	#ab7481
Prolong Gold Antifade Mountant with DAPI	Life Technologies	P36935
Prolong Dimond Antifade Mountant	Life Technologies	P36962
PBS	Gibco	

Table C.6. List of primary antibodies

Name	Company	Product Number	Concentration
Anti-Desmoplakin I+II	abcam	ab16434	1/100
Anti-E Cadherin	abcam	EP700Y	1/100
Integrin Beta 1	Santa Cruz Biotechnology	sc-6622	1/100
Anti-Human CD 104	BD Pharmingen	555722	1/100
Anti-Cytokeratin	Biomedical Technologies	BT-571	1/100
Anti-Actin	Millipore	MAB1501	1/100
Anti-Involucrin	abcam	[SY5] ab68	1/500
Cytokeratin 5 (A-16)	Santa Cruz Biotechnology	sc-17090	1/100
Keratin 14	Biolegend	PRB-155P	1/1000(?)
Anti Yap/Taz (63.7)	Santa Cruz Biotechnology	sc-101199	1/50
Anti Yap (H-9)	Santa Cruz Biotechnology	sc-271134	
Keratin 10 (DE-K10)	Thermo Fisher	MA5-13705	1/100
Laminin 332	From another Lab		1/100
Myosin, Light chain (MY-21)	Thermo Fisher	MA1-24940	1/100
Phospho-MYL1 (Ser20) l	Thermo Fisher	PA1-26470	1/100
Alexa Fluor® 594 Phalloidin	Life Technologies	A12381	1/40

Table C.7. List of secondary antibodies

Secondary Antibodies	Company	Product Number	Concentration
Alexa Flour 488 goat anti rabbit	Thermo Fisher	A11034	1/100
Alexa Flour 568 goat anti mouse	Thermo Fisher	A11031	1/100
Alexa Flour 350 goat anti mouse	Thermo Fisher	A21049	1/100
Alexa Flour 546 donkey anti mouse	Thermo Fisher	A10036	1/100
Alexa Flour 546 donkey anti Rabbit	Thermo Fisher	A10040	1/100
Alexa Flour 680 goat anti Rabbit	Thermo Fisher	A21076	1/100
Alexa Flour 488 Donkey anti goat	abcam	ab150129	1/100

1. Permeablized the cells with 0.5% Triton-X for 5 min.
2. Rinse them in PBS for 10 min
3. Block the samples for 30 min 37 °C with either 10% normal goat serum or 10% normal donkey serum, depending on the secondary antibody that you use.
4. Incubate the samples for 1:30 hr at 37 °C with anti- body combinations in table …
5. Rinse the sample with PBS three times each tome for 1:30” min.
6. Again Block the samples for 30 min 37 °C with either 10% normal goat serum or 10% normal donkey serum
7. Incubate the samples for 30 min at 37 °C with secondary antibody combinations in table …
8. Rinse the samples three times each time for 1:30” min.
9. Mount the samples with mounting media on microscope cover glass.
10. In staining with phalloidin omit the blocking and secondary antibody step.
11. If fixed by methanol, you can skip permeabilization step.

Fractionation of normal human keratinocyte cultures into stem-cell, transit-amplifying cell- and terminally differentiated

Materials

Table C.8. Collagen type IV

Name	Company	Catalog Number
Collagen from human Placenta (Collagen Type 4)	Sigma	#C5522

1. Coat a 100 mm dish with human placenta type 4 collagen.
2. Trypsinize the cell.
3. Filter the cell suspension once trough a 70µm strainer (BD Falcon) prior to centrifugation.
4. Plate the cells on the collagen type 4 coated petri dish and let the cells adhere for 20 min in 37ºC, 5%CO_2 incubator. The cells that attach to the plate within this 20 min could be stem-cell.
5. Plate the supernatant, containing the non-adherent cells on another collagen type coated petri dish and incubate that for 1.5 hr in 37 ºC, at 5% CO_2 incubator. The cells attached in this period would be transit-amplifying cells.
6. The rest of the cells left in supernatant would be differentiated keratinocytes.